

Frequency Adapted Crossover of Susceptibility in Coupled Dipolar System

By
Nilangshu K Das

ENGG02201104014

Indira Gandhi Centre for Atomic Research
Kalpakkam-603102
India

*A thesis submitted to the
Board of Studies in Engineering Sciences*

*In partial fulfillment of requirements
for the Degree of*

DOCTOR OF PHILOSOPHY

of

HOMI BHABHA NATIONAL INSTITUTE



July, 2015

Homi Bhabha National Institute

Recommendations of the Viva Voce Board

As members of the Viva Voce Board, we certify that we have read the dissertation prepared by **Nilangshu K Das** entitled "**Frequency Adapted Crossover of Susceptibility in Coupled Dipolar System**" and recommend that it may be accepted as fulfilling the dissertation requirement for the Degree of Doctor of Philosophy.

_____ **Date:**

Chairman - **Dr. B. K. Panigrahi**

_____ **Date:**

Guide/Convener - **Dr. T. Jayakumar**

_____ **Date:**

Member - **Dr. P. Barat**

_____ **Date:**

Member - **Dr. K. Laha**

_____ **Date:**

External Examiner - **Dr. Indrani Bose**

Final approval and acceptance of this dissertation is contingent upon the candidate's submission of the final copies of the dissertation to HBNI.

Date:

Place: Kalpakkam

T. Jayakumar

CERTIFICATE

I hereby certify that I have read this dissertation prepared under my direction and recommend that it may be accepted as fulfilling the dissertation requirement.

Guide-

T. Jayakumar

Date:

Place: Kalpakkam

STATEMENT BY AUTHOR

This dissertation has been submitted in partial fulfillment of requirements for an advanced degree at Homi Bhabha National Institute (HBNI) and is deposited in the Library to be made available to borrowers under rules of the HBNI.

Brief quotations from this dissertation are allowable without special permission, provided that accurate acknowledgment of source is made. Requests for permission for extended quotation from or reproduction of this manuscript in whole or in part may be granted by the Competent Authority of HBNI when in his judgment the proposed use of the material is in the interests of scholarship. In all other instances, however, permission must be obtained from the author.

(Nilangshu K Das)

Date:

Place: Kalpakkam

DECLARATION

I, hereby declare that the investigation presented in the thesis entitled "**Frequency Adapted Crossover of Susceptibility in Coupled Dipolar System**" submitted to **Homi Bhabha National Institute (HBNI)**, Mumbai, India, for the award of **Doctor of Philosophy in Engineering Sciences** is the record of work carried out by me under the guidance of **Dr. T. Jayakumar**, Director, Metallurgy and Materials Group, Indira Gandhi Centre for Atomic Research, Kalpakkam, India. The work is original and has not been submitted earlier as a whole or in part for a degree / diploma at this or any other Institution / University.

(Nilangshu K Das)

Date:

Place: Kalpakkam

DEDICATIONS

Solely Dedicated to My Parents

ACKNOWLEDGMENTS

The research included in this dissertation could not have been performed if not for the assistance, patience, and support of many individuals. I would like to extend my deep sense of gratitude first and foremost to my research supervisor and mentor **Dr. T. Jayakumar**, Director, Metallurgy and Materials Group (MMG), Indira Gandhi Center for Atomic Research (IGCAR) for his whole hearted support, encouragement, guidance and patience during the course of my research work. Without his untiring mentorship, constant inspiration, valuable discussions and suggestions, this thesis would not have been possible. I cannot think of a better supervisor to have.

I would additionally thank **Dr. P. Barat**, former Head, Material Science Section, Variable Energy Cyclotron Centre (VECC) for his whole hearted support in both the research and especially the revision process that has led to this document. His knowledge and understanding of physics and mathematics has allowed me to fully express the concepts behind this research. He has helped me through extremely difficult times over the course of the analysis and the writing of the dissertation and for that I sincerely thank him for his confidence in me. I am truly thankful for his steadfast integrity, and selfless dedication to both my personal and academic development. Dr. Barat is a dedicated teacher, from whom I have learnt the vital skill of disciplined critical thinking. His forensic scrutiny of my technical writing has been invaluable. I appreciate him for critically going through the draft of my thesis and research papers that have been published. He has always found the time to propose consistently excellent improvements. He has helped me in many of my personal difficulties that I have faced during this research work. I owe a great debt of gratitude to Dr. P. Barat.

I would also like to extend my appreciation to **Dr. B. K. Panigrahi** chairman of doctoral committee who has served as a voice of quiet wisdom in matters ranging from the most basic aspects of the experiment, to the theoretical understanding that many of my doubts have eventually got cleared. He has spent time with me in the starting from synopsis to thesis writing.

I sincerely mention, during the evolutionary process of my research work, I have received many useful tips and valuable suggestions from **Dr. K. Laha**. I extend my gratitude to Dr. Laha, for his comments on the draft of my thesis.

My sincere thanks also goes to **Dr. P. Gangopadhyay** for his meticulously word-by-word corrections of the thesis. I appreciate him for critically going through the draft of my thesis.

My sincere thanks to my doctoral committee chairman **Dr. B. K. Panigrahi**, and members **Dr. P. Barat** and **Dr. K. Laha** for regularly evaluating the progress of the work and giving many useful suggestions.

I am grateful to Director, IGCAR, **Dr. P. R. Vasudev Rao** for providing me permission and encouragement to pursue this work. I am grateful to Head, NDED, **Dr. B. P. C. Rao** for providing valuable suggestions while writing my thesis. I am thankful to Head, EMSIS, **Dr. C. K. Mukhopadhya** for providing me permission and inspiration to pursue this work.

This research would not have been possible without the assistance of **Mr. Anirban Bagchi**, Student of Jadavpur University who helped me to get the nano-composite sample, **Mr. Sounak Dey**, Student of Indian Statistical Institute who helped me to construct the experimental apparatus and build the foundations for the data analysis. A special mention of **Dr. Sarbajit Pal** and **Dr. Pande** of VECC for their technical support and participation in some critical experiments. In particular, I would like to thank **Mr. Kanchan Majumder** and **Mr. Khare**

of VECC, Kolkata for their support in the mechanical design and coil design in the experimental setup. I am thankful to **Dr. Amal Giri, Santu Dey, Dr. Gayatri N. Banerjee** and **Mishreyee Bhattacharya** for their open discussion to clear some of my doubts.

I have to salute my twin Fujitsu Servers, **CELSIUS-R930** for their 24×7 service to generate the valuable data during the research.

Finally I would like to extend my deepest gratitude to my parents **Sri Nirmal Chandra Das** and **Mira Das** without whose love, inspiration and blessings I could never have completed this doctoral degree.

I am lucky to have a son, **Shounak**, the sweet boy who has a very big contribution in this thesis. Several drawings and graphs in this thesis are prepared by him. I always appreciate his innocent concern in my research work.

Last, but not least, I would like to thank my wife **Sharmistha** for her love and constant support, for all the late nights and early mornings, and for keeping me sane over the past several months. Thank you for being my muse, editor and proofreader. But most of all, thank you for being my best friend. I owe you everything.

Above all, I owe it all to almighty God, **Lord Jagannatha** for granting me wisdom, strength, and health to undertake this research work and enabling me to take it to completion.

Contents

1	Introduction	1
1.1	Literature Survey	4
1.2	Thesis Outline	11
1.3	Thesis Contributions	11
2	Problem Definition	15
2.1	Harmonic Oscillator	17
2.2	Non-linear Oscillators	20
2.3	System of Limit Cycle Oscillators	22
2.4	N-body Limit Cycle Oscillators Poses A New Problem	23
3	Susceptibility of Chaotic Oscillators System	25
3.1	Interacting System of Oscillators	27
3.2	Magnetic Needle, a Huge Dipole	29
3.3	A Dipole Oscillator in Double Well Potential	30
3.4	Dynamics of Coupled System	33

3.5	Numerical Analysis	35
3.6	Conclusion	37
4	Crossover of Susceptibility: Simulation Studies	39
4.1	Single Domain Magnetic Islands : Superparamagnetism	41
4.2	Model and Simulation	42
4.3	Simulation Code flowchart	49
4.3.1	Step 1:Setting Simulation Parameters	50
4.3.2	Step 2: System Initialization	51
4.3.3	Step 3: External Field Applied	52
4.3.4	Step 4: Main Loop	52
4.3.5	Step 5: Calculatate Susceptibility	53
4.4	Simulation Results	54
4.5	Comments on Simulation Results	56
4.6	Conclusion	60
5	Crossover of Susceptibility: Experimental Verification	62
5.1	Sample Preparation : sol-gel process	63
5.2	Sample Characterization	66
5.3	Susceptometer Development	69
5.3.1	Self-inductance type Susceptometer: Working Principle	70
5.3.2	Measurement Methodology	72

5.3.3	Design of Coil : Field Uniformity	75
5.3.4	Analog Circuit Details	84
5.3.5	Validation of Susceptometer	85
5.4	Experiment with Nano-magnetic Samples and Results	86
5.5	Conclusion	89
6	Summary and Outlook	93
6.1	Summary	94
6.2	Future Outlook	97
Appendix A Fish School approaching towards a predator		100
Appendix B Differential Equation : Dynamics of interacting Dipoles under external perturbation in a dissipative double well potential		102
Appendix C Dipole-Dipole Interaction Potential		104
Appendix D Rodrigues' rotation formula		107
Appendix E Direction of magnetic moment after turning at an angle ψ from easy axis		109
Appendix F Angular Dependence of Energy Equation		112
Appendix G Stoichiometric Calculations for Ni-silica nano-composites		114
Appendix H M-H Curve Co-silica nanocomposite		116

Appendix I Low frequency susceptibility plot from simulation data 118

Appendix J Low frequency susceptibility plot from experimental data 120

List of Figures

2.1	Mechanical model of Duffing oscillator, with double well potential developed by the pair of N-poles.	21
3.1	An ensemble of $71 \times 71 \times 71$ dipoles in a three dimensional lattice is arranged in an anti-ferromagnetic ordering. The dipole-dipole interaction field along the central line of the ensemble is plotted.	28
3.2	Compass needle in a uniform magnetic oscillating field.	30
3.3	Arrangement of coupled dipoles in an array.	31
3.4	Functional representation of the double well potential due to various applied field strength.	32
3.5	Under-damped oscillation of a dipole, restricted within the two minima at $\theta = 0$ and π	33
3.6	Dynamics of dipole attractor at the two minima indicating suppression of chaos by weak damping.	34
3.7	For various γ values phase lag of the system is demonstrated. Phase lag of the system exceed 90° for some definite frequency ranges only. .	36

3.8	The phase lag with respect to the applied field is position dependent. Dipoles at the ends (blue) have phase lag less than the dipoles at the center (red).	37
4.1	Easy axis of an uniaxial anisotropy crystal (black broken line) Magnetic moment is shifted away from easy axis by an angle ψ when a field H is applied along Z -axis.	44
4.2	The volume susceptibility of cobalt-silica nano-particles against frequency of the applied field obtained from the simulation of 15x15x15 nano-magnetic assembly	55
4.3	The observed magnetization of the ensemble of the nano magnets due to the application of sinusoidal magnetic field of low frequency $t_r < T/4$ as observed in the simulation results. The overall magnetization is paramagnetic at low frequency.	58
4.4	The observed magnetization of the ensemble of the nano magnets due to the application of sinusoidal magnetic field of high frequency $t_r > T/4$ as observed in the simulation results. The overall magnetization is diamagnetic at high frequency.	59
5.1	Schematic representation of sample preparation of magnetic nano-composite.	67
5.2	FESEM micrographs reveal the topographic details of the powdered nano-composites developed by sol-gel technique. These micrographs are the silica flakes embedded with Co or Ni nano-particles. The structure and size determination of these metal nano-particles are carried out by HRTEM.	68

5.3	HRTEM micrographs reveal average size and separation of the nano-magnets inside the powdered nano-composites as synthesized by sol-gel technique.	68
5.4	$V_0 e^{i\omega t}$ is the voltage applied to the LR circuit, and there is a phase lag (θ) between the voltage source and the current passing through the circuit.	71
5.5	Block diagram of analog circuit	73
5.6	Block diagram of computational flow.	74
5.7	Axial and radial components of magnetic field due to a single circular current loop of radius R_i and carrying current I_i	76
5.8	Combined representation of discrete step bobbin and shape modified bobbin. M is the field concentrated region for the discrete coil design. The profile of the shape modified bobbin, for the left half of its length, is defined by the generalized logistic function. The profile of the rest half is the mirror image of the former. $\theta = \tan^{-1} B \frac{R_f - R_0}{4}$ for the shape modified bobbin.	77
5.9	Flow chart for the optimization of the parameters R_f and C	79
5.10	Axial field distribution and the optimum profile of the bobbin obtained by GA using MATLAB. The absica is in terms of the width (0.152 mm) of the wire (38 SWG). The values $R_f = 8.28 \text{ mm}$ and $C = 15.4$ as obtained by GA optimization.	80
5.11	FEMM plot demonstrates uniformity of magnetic field at 600KHz.	81
5.12	Axial homogeneity of the magnetic field obtained from FEMM simulation.	81

5.13	Experimental setup to measure the axial field distribution by SPECTRAN Analyzer. Inset of the figure shows the bobbin (at the left top corner).	82
5.14	The axial field distribution obtained from the experimental setup shown in the Fig. 5.13.	83
5.15	Network analyzer data shows that the solenoid coil is used below its resonance frequency.	84
5.16	The variation of volume susceptibility of Ni-silica nano-composites against frequency of the applied field at $77^{\circ}K$ from the experimental data.	88
5.17	The variation of volume susceptibility of Ni-silica nano-composites against frequency of the applied field at $300^{\circ}K$ from the experimental data. Inset shows the negative susceptibility data.	88
5.18	The variation of volume susceptibility of 20% Co-silica nano-composites against frequency of the applied field at $77^{\circ}K$ and $300^{\circ}K$ from the experimental data.	89
A.1	Sailfish attacks Sardines in all directions. Sardines often come pretty close to the Sailfish for protection. There are incidences when we see the Sardines are heading towards the Sailfish which is very unlikely in nature. This is a condition where the system is susceptible to the external perturbation but opposing the perturbation. This is called diamagnetic susceptibility.	101
C.1	Dipole dipole interaction.	105

D.1	Rotation about a general axis through the origin, showing the axis of rotation and plane of rotation. Two dimensional basis of the plane of rotation.	108
E.1	Direction of magnetic moment after turning at an angle ψ from easy axis.	110
F.1	Energy plots of various γ_0 values	113
H.1	M-H curve of 20%Co-silica nano-composite at room temperature. Remanence (M_r) is 0.5432 e.m.u per gm and coercivity is 0.00678 T . .	117
I.1	χ_{ac} of Co-silica nanocomposites at 300K	119
J.1	Real χ_{ac} of Co-silica nanocomposites at 300K	121
J.2	Imaginary χ_{ac} of Co-silica nanocomposites	122

List of Tables

4.1	Conditions at which negative susceptibility has been observed of an ensemble of cobalt nano-magnets	56
5.1	Error estimation in the measurement of change in inductance ΔL . . .	85
5.2	Error estimation in the measurement phase	85
5.3	Constant of proportionality of the susceptometer	86
5.4	Comparison with known materials	86
5.5	Experimental Results of nano-composites Co-silica and Ni-silica . . .	90

List of Symbols

ω	Angular frequency
ϕ	Average phase
θ	Phase angle
γ	Intensity of dissipation
ω_0	Natural frequency
K	Anisotropy constant
Γ	Torque
μ	Magnetic moment, dipole moment
μ_0	Permeability of free space
H_0	Peak external field
H	Applied field
I	Moment of inertia
J	Angular Momentum
κ	Depth of potential well
β	Damping coefficient
α	$\frac{\mu H_0}{I}$
T	Time period, Temperature in Kelvin
N	Number of particles
E	Energy
V	Volume

τ	Relaxation time
τ_0	Pre-exponential factor
τ_{-+}	Relaxation time for -1 to +1 state
τ_{+-}	Relaxation time for +1 to -1 state
k_B	Boltzmann constant
ψ	Angular deviation from easy-axis
γ_0	Direction cosine of easy-axis from z-axis
ξ	Reduced energy
M_s	Saturation of Magnetization
f	Frequency
S	State (± 1)
$J(r, r')$	Coupling coefficient between r and r' element
P	Switching probability
h_{dd}	Dipole-dipole interaction field
h	$\frac{M_s H}{2K}$
h_T	Dipolar field plus applied field
L	Length of solenoid
δ	Diameter of coil
δt	Time resolution of simulation
I_0	Peak magnetizing current
B_0	Field inside susceptometer

E_d	Dipole interaction energy
T_0	Critical Temperature
M_z	Magnetization in z-direction
D_{pts}	Number of data points
χ	Susceptibility
Ψ	Magnetic flux

List of abbreviations

FEMM	Finite Element Method Magnetics
KM	Kuramoto Model
MRI	Magneto Resonance Imaging
GA	Genetic Algorithm
ODE	Ordinary Differential Equation
TEOS	Tetraethyl orthosilicate
TMOS	Tetramethyl orthosilicate
SEM	Scanning electron microscopy
TEM	Transmission electron microscopy
HRTEM	High resolution TEM
FESEM	Field emission SEM
RMS	Root mean square
SWG	Standard Wire Gauge
SAD	Selected Area Defraction
L-R	Inductance and resistance

Chapter 1

Introduction

Jonathan Bird, an American Photographer heads down to Cancun in Mexico on an expedition to film one of the world's fastest fish - the sailfish! He gets in the water with a school of sailfish zooming around hunting sardines. As the sailfish shows up, the sardines form a bait ball to confuse the predator. In that video, the sailfish (predator) is attacking repeatedly the bait ball from various directions and a situation is spotted where the sardines are approaching towards the sailfish instead of moving away from the predator. This unusual movement of the sardines indicates that the school of sardines (system) under certain conditions is negatively susceptible to the predator (external perturbation) when the bait ball acts as a system of hydro-dynamically coupled dipoles. The occurrence of negative susceptibility for a system of dipoles under the influence of external perturbation is explained in this thesis and a similar phenomenon is simulated on an ensemble of superparamagnetic particles and verified experimentally on magnetic nano-composites.

A bait ball is a swarm of small fishes in a tightly packed spherical formation with a common center and it acts as a system. Systems of various types are classified

in physics *viz.*, open system, closed system, isolated system *etc.* An open system can exchange both matter and energy with its surroundings. On the contrary, an isolated system does not interact with its surroundings so that the mass and energy of the system do not change with time. In reality, systems are never isolated, they are coupled with the neighboring systems and their environment. Two systems are coupled if information from one is transmitted to, and alters the behavior of, the other. If the information exchange is bidirectional and periodic, the system is called an oscillator and the time evolution of such dynamical system is represented by second order differential equation. In the case of coupled systems, the dynamics is governed by coupled differential equations. The behavioral patterns of coupled systems corroborate many natural phenomena. Hence, the study of time evolution of the dynamical process of coupled system through in-silico experiments has attracted many researchers. Coupled differential equations can be formed but the solutions of those differential equations are not straight forward. It becomes more complex when the coupled system interacts with the time varying environment.

Examples of systems of coupled oscillators are numerous as they are ubiquitous in nature as well as in man-made world. The familiar systems of coupled oscillators are coupled either by linear deformations or torsion of springs, or it may be the case of electrical devices, *e.g.*, coupled LC circuits. The canonical example consists of two pendula horizontally connected with a weak spring whose relaxed length is restricted by the distance between the bobs of the pendula [1] [2]. Number of mass-points interconnected by co-linear springs in three dimensional matrix is a useful model to study the oscillations of molecules in crystals [1] [3]. The vibrational solution of coupled oscillators is expressed in terms of the normal modes and these normal modes certainly have importance in the understanding of many physical phenomena.

Symmetry and pattern formation is another interesting topic where integrated

studies of system of coupled oscillators and its environment reveal certain complex patterns [4] and those patterns do not evolve when an oscillator and its environment are studied individually. In general, these patterns are observed in the environment that changes periodically. It is usual that a periodic external perturbation compels the coupled system to follow its own pace and the overall system dynamics will have a phase lag with respect to the perturbation. This phase lag is the consequence of intrinsic parameters of the system and it also depends on both frequency and amplitude of the perturbation. The phase lag is an important property that increases with frequency and simultaneously there is a variation of extent of oscillation or amplitude.

The physical properties of coupled systems are often described either by intensive or by extensive properties. An intensive property is a bulk property of a system that does not depend on the system size. An extensive property is a physical quantity which is the sum of the properties of noninteracting subsystems that compose the entire system. There is a complex parameter to define the collective response of the oscillators under external perturbation, called susceptibility of the system. More general, a susceptibility, χ is a quantification for the change of an extensive property under the variation of an intensive property. It is a dimensionless proportionality constant that indicates the degree of polarization in the system in response to an external perturbation. Susceptibility is frequency dependent and it develops due to the interactions among the constituent subunits in the system. If the subunits of the system are oscillators, the susceptibility of the system of oscillators depends on the extent of oscillation (amplitude). χ becomes non-linear for large oscillations, and the higher order terms in the expression of χ appear significant when the system experiences external perturbations of large magnitude. This nonlinearity introduces phase lag between the collective system dynamics and the external perturbation. As a result, there is a possibility of change of gross dynamical properties in the system of coupled oscillators.

If this phase lag exceeds 90° with respect to the external perturbation, the susceptibility becomes negative and the system intrinsically opposes the perturbation *i.e.*, a diamagnetic susceptibility in the system. This is uncommon in nature. Is there any possibility where the dynamics of the coupled oscillators system goes more than 90° out of phase of the external perturbation? This thesis reveals a possibility of such crossover of susceptibility in a coupled dipolar system under certain conditions and it has also been established experimentally in an ensemble of interacting superparamagnetic particles in nano-composites.

Many researchers have contributed to the field of coupled systems and a large volumes of reported works is available in various literature but only a few works have been done on susceptibility of coupled dipole oscillator system so far [5].

1.1 Literature Survey

The problem addressed in this thesis is solved classically by computer simulation. Very few relevant works have been reported in the past but the model studied in this work is related to several models available in the literature. Although dynamics of dipoles under periodic external perturbations have been reported adequately, dynamic patterns formation particularly in coupled dipolar systems has been observed in a few occasions only [6].

There are several kinds of dipole formations in nature, for example electric dipole, magnetic dipole, flow dipole, vortex dipole, etc. All these dipoles interact among themselves by a long range interaction and this interaction influences the dynamics of the dipolar systems when they are allowed to rotate about their axis. There is a complex parameter to define the collective responsiveness of the dipoles under external perturbation *i.e.*, susceptibility of the system. In 1994, Nikazima *et al.* have presented a microscopic theory to study the two-dimensional orientational phase

transition of the interacting dipolar system and its dynamic susceptibility in the para electric phase [7]. On the basis of a classical mechanical model, they have carried out the statistical mechanical calculations in the framework of the molecular field approximation and linear response theory. In their studies, an orientational phase transition and its dynamic susceptibility have been reported.

A single dipole is too small in dimension to carry out some physical experiment in the laboratory. Macroscopically, a magnetic needle is a representation of a large dipole. Meissner and Schmidt have carried out simple experiments on a magnetic needle to study the transition from normal modes of vibration to chaotic vibration under oscillatory external field [8]. Magnetic needle in external magnetic field is a non linear dynamical system where angular displacement is large and it also exhibits periodic behavior under certain conditions. The period of such system is related to the external driving force and inertia of the needle.

There are physical systems that are modeled as an array of interacting oscillators based on Kuramoto model [9]. Dynamics of N-body oscillator system possesses unique normal modes of oscillation limited by the number of degrees of freedom [10]. Simplest model of this kind is the spring coupled mass system that resonates at the frequencies of its normal modes. These normal modes depend upon the intrinsic parameters of the system. The dynamics of the system can be appreciated only when the oscillators are in a collective motion. In this collective motion, an order parameter has to be identified to characterize the dynamics. Relative phase among the oscillators can be an order parameter as it characterizes the modes of coordination [11]. Kuramoto has suggested a model to understand the complex dynamics of coupled oscillator system. Later Sakaguchi has extended Kuramoto (KM) model in the presence of external periodic field [12],[13]. The order parameter is defined as $r(t)e^{i(\omega t + \phi)} = \frac{1}{N} \sum_{j=1}^N e^{i\theta_j}$ [13] where $r(t)$ with $0 \leq r(t) \leq 1$ measures the phase coherence of the oscillators, ϕ measures the average phase lag with respect

to the external field, θ_j is the phase of the j^{th} oscillator and ω is the frequency of the external periodic field. Oleh *et al.* has investigated the transition to synchrony in a system of phase oscillators that are globally coupled with a phase lag using Sakaguchi-KM model [14]. They have shown some unusual types of synchronization transitions for certain frequency distributions.

Normally, this phase lag of the system relative to the external field increases to 90° as the frequency of the external wave reaches the frequencies of the normal modes and it exceeds 90° as the external frequency goes beyond the normal modes of oscillations [10]. This holds good for oscillators performing small oscillations in linear response domain but the scenario becomes different if the oscillators are nonlinear and coupled. The variation of this phase lag with the frequency of the external wave is entirely different in comparison to the linear case. The dynamics of such coupled system depends upon the instantaneous relative position of the subunits in the phase space. In this thesis related study, subunits are dipole oscillators. The parameters governing the differential equation of the dipole oscillator define whether the dynamics to be chaotic or non-chaotic under the influence of an external periodic field [6]. The coupled oscillations of N number of nonlinear non-chaotic dipoles show an interesting feature. It is capable to oscillate collectively at a common frequency or phase, irrespective of the intrinsic natural frequencies or initial phases of the individual oscillators [10]. This phenomenon in the field of coupled system is termed as synchronization. Synchronization, a prominent and well-studied topic of coupled systems, is the phenomenon observed everywhere in nature and finding several applications in engineering and physics. In 1973, Huygens may have reported synchronous motion first in the literature [15]. Later, in recent decades, the subject of synchronization has attracted many researchers. For example, arrays of chaotic systems are studied in [16, 17, 18, 19]. For coupled nonlinear oscillators, a seminal study to understand synchronization was done by Kuramoto [9]; the work is reviewed in [20, 21]. Synchronization of phase and suppression of chaos of the nonlinear

oscillators are the two significant criteria when the system is periodically driven. Some times small damping is applied to the system to control chaos [22] and a periodic stable state of the system can be achieved.

The dynamics of the N-body oscillator system become more realistic if the coupling of the subunit (dipole oscillator) is considered to be of long range. Due to the long range interaction, the behavior of the subunits located in the core of the array differs considerably with respect to those located in the periphery. There exists a possibility of occurrence of cooperative phenomenon among the subunits as observed in the nature e.g., in the fish schooling dynamics [23]. The existence of this type of cooperative phenomenon has been established analytically by Sakaguchi [13]. This cooperative phenomenon in the array of coupled systems depends strongly on the type and the strength of interaction among the subunits. In this work, the dynamics of a system of coupled dipoles oscillating in a dissipative medium subjected to an external periodic field has been studied. It is observed that the phase lag of the system exceeds 90° at a frequency of the external field lower than the frequencies of normal modes of the system. This type of phenomenon is new in classical system and it has been observed experimentally in nano-magnetic composites [24]. This dynamical phenomenon is rare to observe because the parameter values of the governing differential equation are very critical for its occurrences. This model is useful in the simulation of cluster of nano-magnets, fish-schooling dynamics or in the development of high sensitive nano-magnetic detectors. Magnetic nano-composites consist of a collection of superparamagnetic particles. If the average distance of separation between the superparamagnetic particles is comparable to the particle dimensions, then the interaction between the particles becomes significant and the system acts as a coupled dipole system.

The nano-magnetic ensemble appears in many contexts and several theories have been suggested to understand its behavior due to applied magnetic field [25]-[29].

The deviation of the behavioral patterns of interacting nano-magnetic particles from the models of Stoner-Wohlfarth [30] and Neel-Brown [31] are accredited to dipolar interaction and applied magnetic field. In the nano-magnetic particle system, dipolar interaction is ubiquitous due to the long range interactions and manifests many exotic physical phenomena [32]. The dynamic magnetization of a dipolar nano-magnetic ensemble due to the applied magnetic field is influenced by anisotropic energy, dipolar interaction energy and Zeeman energy. In most of the earlier studies, the dynamics of the nano-magnets have been studied while the Zeeman energy supersedes the other two forms of energies [33, 34]. However, to appreciate the synergetic effect of these three energies their magnitudes should be comparable. The relaxation time of non-interacting nano-magnetic particles depends on the anisotropic energy barrier only, however the presence of long range dipolar interaction has a predominant influence in determining the relaxation time and has been addressed extensively at several theoretical [35] and experimental studies [36]. The theoretical approaches are primarily based on the mean field theory, where a localized interaction field appears to be responsible for the observed effects [37] and demands analytical solutions. Traditional mean field theories overlook local fluctuations due to dipolar interaction. The mean field approach is limited in its effort to explain the exact behavioral pattern of magnetization for an applied magnetic field on a finite assembly of nano-magnetic particles. In the interacting nano-magnetic particle system the local interaction field brings the system into a stable minimum energy state [38, 39, 40]. External magnetic field acts as a perturbation to this interacting particle system and disturbs the magnetic ordering and the stability in turn [25]. The system will try intrinsically to oppose the applied field, the cause of its instability. This leads to a new concept of diamagnetism in the interacting nano-magnetic ensemble.

For experimental verification of frequency adapted crossover of magnetism in nano-magnetic ensembles, a susceptometer is developed and susceptibility of the

magnetic nano-composites is measured. Susceptibility measurement setups are predominantly non contact type and based on the comparison of unequal mutual inductance technique. This technique has its own advantages and has been proposed by Hartshorn [41]. An AC magnetic field is applied by a primary coil and the electro motive force induced in the gradiometer coil is used to measure the magnetic susceptibility [42] [43] of samples. The sensitivity of the susceptometer has been increased by modern low noise electronic components [44]. Principle of measurement remains the same. Many researchers have started developing miniature susceptometer [45] [46]. Some of them use Superconductor Quantum Interference Device [47] for small samples at low temperature and at low magnetic field measurements. AC source, precision sensing coils and high-sensitive lock-in amplifier are the major components to measure in- and out-of-phase susceptibility. Sensing coils are even replaced by a toroid with a thin cut as proposed by Fannin *et al.* [48]. Short circuit and open circuit transmission line technique has been used for the measurement of complex susceptibility in microwave region [49]. Park *et al.* have developed a compact AC susceptometer for ferrofluids in a very low magnetic field ($10\mu T$) [50]. Another technique exists that is absolute coil self-inductance method to measure magnetic susceptibility where, the accuracy depends on the precise measurement of inductance. Hence, design of such type of susceptometers encounters several practical difficulties associated with many limitations. Primarily, the complex impedance sources *viz.*, inter-turn capacitance, line capacitance, coil-resistance *etc.* of a coil varies with temperature and frequency. These factors limit the upper cut-off frequency in the measurement of the AC susceptometer. Secondly, due to the use of smaller dimension of the self-inductance coil, the magnetic field is non-uniform over the sample. However, uniformity of the field is necessary and the uniform field is very much obtainable in long solenoid. The limitations mentioned above do not restrict the use of self-inductance type susceptometer in the measurement of absolute susceptibility as proposed by Dho [51]. In- and out-of-phase components of

complex susceptibility can be derived from the phase associated with the sample, where the phase is measured using a high frequency digital lock-in amplifier. Lock-in amplifier in the range of MHz is very costly. So the phase measurement without lock-in amplifier as proposed by Das *et al.* [52] is a very simple analog technique and can replace the high cost lock-in amplifier for normal laboratory use. In this susceptometer development, the small coils have been wound on a specially shaped bobbin to avoid the non-homogeneity of the magnetic field [53].

Magnetic coils are usually cylindrical inductive coils to produce magnetic field for various engineering and scientific applications [54, 55, 56, 57]. Susceptometer demands uniformity of the magnetic field within a volume of interest. Infinite solenoid produces uniform magnetic field but in reality, magnetic field uniformity is a challenging task especially for the solenoids used in the nano- or bio-electromagnetic experiments [57]. Helmholtz coil system [57] is used in laboratory for the generation of uniform magnetic field in smaller volume of interest. Merritt and Ruben coil systems are implemented where large volume of uniform magnetic field is required [55, 56]. However, a Ruben coil system is more difficult to build [58]. Specific applications like calorimetric measurements of nano-particles, cancer therapy, eddy current probes, etc. demand uniformity of magnetic field generated by solenoid of smaller dimensions than that are being used in Magnetic Resonance Imaging (MRI) [59] systems. Some researchers have attempted to build minimum volume coil configurations using a linear-programming technique [60] or finite-element method (FEM) [58] to produce uniform magnetic field. The magnetic field strength is maximum at the center of a finite solenoid and it reduces towards the ends. Improvement of uniformity of magnetic field inside a solenoid is realized with the help of structural modifications along with the magnetic flux concentrator rings at the coil ends [57]. Two-dimensional finite element analysis simulation software *e.g.*, FEMM [61] is usually used to validate the design. In this thesis, the principle, design methodology and performance of a kind of miniature solenoid which can be used for development

of self-inductive type susceptometer have been described. A typical shape of the winding surface has been arrived at which would achieve the required uniformity of magnetic field of the solenoid has been arrived. In engineering shape design, there are various methods. An optimization technique using non-dominated sorting genetic algorithm (GA) has been adopted, which is a multi-objective optimization method in real engineering problems [62, 63]. In this case, the required region and extent of uniformity of the magnetic field within the solenoid has been identified and the design was optimized by using GA, as explained in the Chapter 5.

1.2 Thesis Outline

The main body of the thesis consists of the following chapters.

- Introduction (Chapter 1)
- Problem Definition (Chapter 2)
- Susceptibility of Chaotic System of Oscillators (Chapter 3)
- Crossover of Susceptibility: Simulation Studies (Chapter 4)
- Crossover of Susceptibility: Experimental Verification (Chapter 5)
- Summary and Outlook (Chapter 6)

1.3 Thesis Contributions

The major focus of the thesis is to demonstrate the occurrence of negative AC susceptibility in an assembly of interacting magnetic dipoles placed in an external magnetic field which is a periodic function of time. The result is established by

carrying out exhaustive computer simulation as well as through the designing and setting up of an experimental arrangement involving magnetic nano-composites. To explain the genesis of the idea, the example of a fish population with predator-prey type situation is invoked which exhibits a negative susceptibility-like phenomenon with the prey population (sardines) moving towards the predator (sailfish) when attacked from various directions. Chapter 1 and 2 of the thesis introduce the basic concepts associated with the problem studied in the thesis along with a literature survey. The dynamics of both linear and nonlinear oscillators driven by a periodic external force are discussed. The discussion is extended to a system of coupled nonlinear oscillators, e.g., the Kuramoto model which exhibits the phenomenon of synchronization. The possibility of a system of coupled limit cycle oscillators (limit cycle behaviour is obtained in a dissipative system) under a periodic driving force exhibiting diamagnetic susceptibility is also pointed out. Chapter 3 and 4 describe the theoretical studies, namely, the numerical computations carried out in the thesis to demonstrate the crossover of the susceptibility from the paramagnetic (positive susceptibility) to the diamagnetic (negative susceptibility) regime. The type of oscillator considered is represented by a magnetic dipole originating from either a magnetic needle (Chapter 3) or a single domain nano-magnet (Chapter 4). The dynamics of a magnetic needle in a magnetic field that varies sinusoidally with time include chaotic behaviour which is obtained as the limiting result of a cascade of period doubling bifurcations as the external magnetic field strength is varied. In the case of a coupled dipolar system, synchronization and chaos suppression are achieved by introducing damping in the dipolar dynamics. The dipolar dynamics is further subjected to a double well potential with the minima of the potential representing the two favourable orientation of a dipole, indicative of the presence of considerable magnetic anisotropy in the dipolar system. The dipoles further interact via long range interaction with the interaction strength inversely proportional to the cube of the distance separating the dipoles. The full differential equation

developed in the thesis governs the dynamics of interacting dipoles in a time periodic external magnetic field in dissipative double well potential. In the thesis, the number of dipoles in the coupled system (the dipoles arranged in one dimensional array) is $N=91$. Three parameters, namely, α (external perturbation), β (damping) and γ (interaction strength) govern the system dynamics. The 91 coupled differential equations are solved numerically using fourth order Runge Kutta method. The average phase lag of the dipolar system with respect to that of the magnetic field is controlled by the parameter γ . The average phase lag has to exceed the value $\pi/2$ for obtaining negative susceptibility. The computations carried out on the one dimensional system provide conclusive evidence of negative susceptibility in certain frequency ranges of the external magnetic field. In Chapter 4 and 5 of the thesis, the bulk of the evidence towards the crossover of susceptibility in a coupled dipolar system is presented. In Chapter 4, simulation studies are carried out on a collective system of N magnetic dipole oscillators interacting via long range interactions and subjected to an oscillating magnetic field. The magnetic dipole originates from a single domain nano-magnet, i.e., a superparamagnetic particle. The dipoles are arranged a three dimensional array. A magnetic moment has certain possible orientations (easy axes), parallel or anti-parallel to easy axis, thus it can be represented as an Ising variable. The Hamiltonian describing the system of interacting dipoles is an Ising-type Hamiltonian with long range interactions. The mean field approximation is made in the treatment of the Hamiltonian. An exhaustive simulation study of the dipolar system is undertaken to provide the evidence of a crossover to the diamagnetic phase, characterised by a negative susceptibility. How the crossover occurs with the changes of frequency is described using figures. In tabular form, a summary of the conditions for the observance of the negative susceptibility is also presented. The dependence of the crossover frequency on various parameters like particle size, particle spacing, field strength, temperature and system size is broughtout in the simulation study. Chapter 5 provides an experimental demon-

stration of the phenomenon of susceptibility crossover. Magnetic nano-composites constitute an experimental realization of the system of interacting dipoles. The experimental arrangement devised in the thesis for the measurement of susceptibility meets the twin challenges of weak field and high frequency measurements. A self-inductance type susceptometer is designed, as part of the thesis investigation, to demonstrate the susceptibility crossover. The experimental results provide clear evidence of frequency-dependent susceptibility crossover. In summery, the thesis makes an important contribution in demonstrating the exsistance of a susceptibility crossover from para-to-dia regime in a coupled dipolar system by an oscillating magnetic field. The most important thing in this thesis is experimental verification of the results in simulations. The study further elucidates a physical mechanism for the occurrence of negative susceptibility.

Chapter 2

Problem Definition

Resonance and vibration in normal modes are the classical phenomena, they are detected in driven and coupled linear harmonic oscillators and they have relevance in all the natural sciences and in engineering. Linearity of oscillators is considered for small parametric approximations. Real life oscillators are nonlinear and the system of coupled oscillators can in general be of very complex dynamics. The associated equations of motion are not exactly integrable. Hence, numerical integration is required. Any small inaccuracy in the prescription of the initial state may build up an exponential divergence of nearby trajectories and this extreme sensitiveness of the system turns it chaotic. Large amplitude oscillation, large driving force or coupling between the oscillators leads non-linear oscillator to chaotic oscillator. Now-a-days, the study of chaotic oscillators has emerged as an object of interest in physics, mathematics and engineering. The classical results of the dynamics of driven, or coupled harmonic oscillators, are important because these results reveal the question of which phenomena emerge when chaotic oscillators are coupled or somehow driven or perturbed. The most relevant phenomena studied theoretically or experimentally until now are the synchronization and the suppression of chaos in the dynamics of the chaotic systems driven by weak external periodic force.

The periodic force driving the oscillator is characterized by its amplitude, and its frequency, f . The phase of the force at any instant t is simply $2\pi ft$. The dynamics of the chaotic coupled oscillators follows the pace of the periodically driven force. The phase of the oscillator gets modified to follow the driving force, called phase synchronization. This is a fundamental phenomenon which appears in many situations found in science and engineering. An incoherent collective behavior appears in the dynamics of an ensemble made of similar, but not identical chaotic oscillators. In some of the experiments, a weak external applied force may be introduced where certain coherence in the collective behavior emerges due to the phenomenon of phase synchronization. For example, circadian rhythm is a biological oscillation. These rhythms are due to a circadian clock, and they have been widely observed in plants, animals, fungi, and cyanobacteria. The chaotic synchronization is useful in biology to understand the development of externally imposed circadian rhythms [65]. In another example in electrical engineering, the integration of multiple elements in a single unit requires the dynamics of the different elements to be paced. This occurs particularly in multichannel chaotic communications [66].

A second phenomenon that has been observed in the study of chaotic oscillators driven by a periodic force is the suppression of chaos under weak applied forces. This suppression of chaos draws the interest of many researchers because the knowledge of this phenomenon reveals the understanding of the physics on nonlinear systems. It has vast applications not only in applied sciences but in technology as well. There are many systems in the natural sciences that are driven by periodic perturbations; *e.g.*, the climate system and the living organisms which are acted on by daily, monthly and yearly basis perturbations. The understanding of many phenomena in climatology and biology require to take into account of this suppression of chaos. In many technical systems, chaos is harmful; this occurs in confined plasma used in thermonuclear fusion, as well as in mechanical, electrical and optical systems. With a little modification of the system, chaos can be eliminated and it has got a lot of

practical interest.

For linear oscillators, analytical solutions are available whereas, for non-linear oscillators, there is no straight forward solution. The analytical solutions of simple harmonic oscillators under dissipative or forced (or combination of both) have been used in the explanation of many physical phenomena. The results are certain and well known. Although non-linear oscillators have explained many physical phenomena, still there are immense possibilities to get many interesting results that may not have been explored so far. Following sections will explain a new problem that emerges when there is a mutual synchronization among dissipative coupled non-linear oscillators under periodic force.

2.1 Harmonic Oscillator

When a system is a free harmonic oscillator, the time evolution of the state of the system is given by Eq. (2.1)

$$x(t) = A \sin(\omega_0 t + \delta) \quad (2.1)$$

This simple harmonic oscillation describes a variety of practical instances. The dynamical behavior of the harmonic oscillator is studied by means of simple pendulum in the gravitational field under free small oscillations. According to Newton's laws of motion, $x(t)$ has to obey the dynamical law Eq. (2.2)

$$\frac{d^2 x}{dt^2} + \omega_0^2 x = 0, \quad (2.2)$$

whose general solution is Eq. (2.1) and ω_0 is the natural frequency of the oscillator. An element which is relevant in most practical cases is dissipation. Dissipation is meant as an effect which opposes to the change of x , and it is assumed that it

behaves like a friction force proportional to \dot{x} . In this approximation, the differential equation for the dynamical variable, $x(t)$, of the harmonic oscillator becomes

$$\frac{d^2x}{dt^2} + 2\gamma\frac{dx}{dt} + \omega_0^2x = 0, \quad (2.3)$$

where the new positive parameter, γ , measures the intensity of the dissipation. The general solution of this dynamical equation [67] depends on the relation between γ and ω_0 , as stated by the following expressions:

$$\begin{aligned} x(t) &= Ae^{-\gamma t} \cos(\omega_\gamma t + \delta), \text{ for } \omega_0^2 > \gamma^2; \\ x(t) &= (C_1 + C_2)e^{-\gamma t}, \text{ for } \omega_0^2 = \gamma^2; \\ x(t) &= C_1e^{+\gamma t} + C_2e^{-\gamma t}, \text{ for } \omega_0^2 < \gamma^2; \end{aligned} \quad (2.4)$$

A damped oscillation of angular frequency ω_γ evolves in underdamped condition ($\omega_0^2 > \gamma^2$). An important property of the harmonic oscillator is linearity. This means that the dynamical equations are such that if $x_1(t)$ and $x_2(t)$ are two independent solutions of Eq. (2.2) or (2.3), then any linear combination of them $x(t) = c_1x_1(t) + c_2x_2(t)$, with c_1 and c_2 real numbers is also a solution. This property is used in the theory of linear ordinary differential equations to get the solution.

A simple but interesting case, is when there is a periodic external driving force. That is, the case of a damped harmonic oscillator driven by an external periodic force, whose dynamical behavior, $x(t)$, is described by the linear second order differential equation

$$\frac{d^2x}{dt^2} + 2\gamma\frac{dx}{dt} + \omega_0^2x = F \sin \omega t, \quad (2.5)$$

where the term in the right hand side of Eq. (2.5) is the external periodic force. The general solution of Eq. (2.5) is given as

$$x(t) = x_0(t) + \frac{F \sin(\omega t + \phi)}{\sqrt{(\omega_0^2 - \omega^2)^2 + (2\gamma\omega)^2}}, \quad (2.6)$$

with $\phi = -\tan^{-1} \frac{2\gamma\omega}{\omega_0^2 - \omega^2}$, and $x_0(t)$ is given by Eq. (2.4). In Eq. (2.6), $x_0(t)$ is transient part of the dynamics.

When systems of interest are made of two or more oscillators and they interact weakly among them, the dynamics of such systems is complex. The results on the dynamics of coupled harmonic oscillators can be obtained by the consideration of two identical free oscillators mutually coupled. The coupled dynamics of these systems are given by

$$\begin{aligned} \frac{d^2 x_1}{dt^2} + \omega_0^2 x_1 + \kappa^2 (x_1 - x_2) &= 0, \\ \frac{d^2 x_2}{dt^2} + \omega_0^2 x_2 + \kappa^2 (x_2 - x_1) &= 0, \end{aligned} \quad (2.7)$$

where the two oscillators are labeled 1 and 2, respectively, and κ^2 is a measure of the strength of the coupling. The condition of weak coupling is expressed by the condition $\kappa < \omega_0$. The time evolution of this coupled system, obtained by the application of the standard techniques for the solution of systems of ordinary linear differential equations, is then given by

$$\begin{aligned} x_1(t) &= A_1 \sin(\omega_1 t + \delta_1) + A_2 \sin(\omega_2 t + \delta_2), \\ x_2(t) &= -A_1 \sin(\omega_1 t + \delta_1) + A_2 \sin(\omega_2 t + \delta_2) \end{aligned} \quad (2.8)$$

All the linear oscillators, as discussed above, illustrate some of the important properties. These include

- oscillations around stable equilibrium,
- dissipation leads to equilibrium state,

- loss of memory of initial conditions,
- external forces combined with dissipation allows sustained oscillations that are independent of the initial conditions.

Linear oscillators should have a single frequency but they are not linear in strict sense. A pendulum is not a simple oscillator, but rather a non-linear one, with the frequency decreasing with increased amplitude. The effect of non-linearity becomes significant for larger amplitudes. The frequency changes with amplitude make interesting responses when the system is driven at different amplitudes.

2.2 Non-linear Oscillators

So long, linear oscillator systems have been discussed, but in practice, nonlinearity is the reality, it is significant and relevant. A non-conservative system in which energy is added to and subtracted from the system, results a periodic motion called a limit cycle. In mathematics, non-linear oscillator is a very significant type of oscillator that exhibits limit cycle oscillation. By the limit cycle oscillator, we mean a mathematical object whose parameters evolve in time and periodically return to their initial values after a threshold is crossed. In the study of collective dynamical systems with two-dimensional phase space, a limit cycle is a closed trajectory in phase space having the property that at least another trajectory spirals into it in asymptotic time. Such behavior is exhibited in some nonlinear systems. Limit cycles have been used to model the behavior of many real world oscillatory systems. The study of limit cycles was initiated by Henri Poincare (1854-1912) [64]. The equation of motion of general form of nonlinear dynamical system is

$$\frac{d^2x}{dt^2} + f\left(x, \frac{dx}{dt}\right) + \frac{dV(x)}{dx} = A_0 \sin \omega t \quad (2.9)$$

where $V(x)$ is the potential function (having at least one stable equilibrium or minima), and $f(x, \dot{x})$ is a damping term, may not be linearly varying with the velocity. F. C. Moon has experimentally realized this model by means of a simple magneto-mechanical system [68]. This is made up of a vertical magnetic flexible beam fixed at its upper end to a vibrating support which provides the chaos enhancing force $A_0 \sin \omega t$ (as shown in Fig 2.1). The wire is acted on at the lower free end by two North-pole magnets that create two equilibrium points, and then the double-well potential, $V(x)$. Eq. (2.9) allows many different and interesting realizations, which include the Duffing equations, and others such as the equations of the motion of a driven pendulum undergoing large amplitude oscillations. The differential equation of these cases may be expressed in the form of Eq. (2.10).

$$\frac{d^2x}{dt^2} + 2\gamma \frac{dx}{dt} + \omega_0^2 \sin x = A_0 \cos \omega t. \quad (2.10)$$

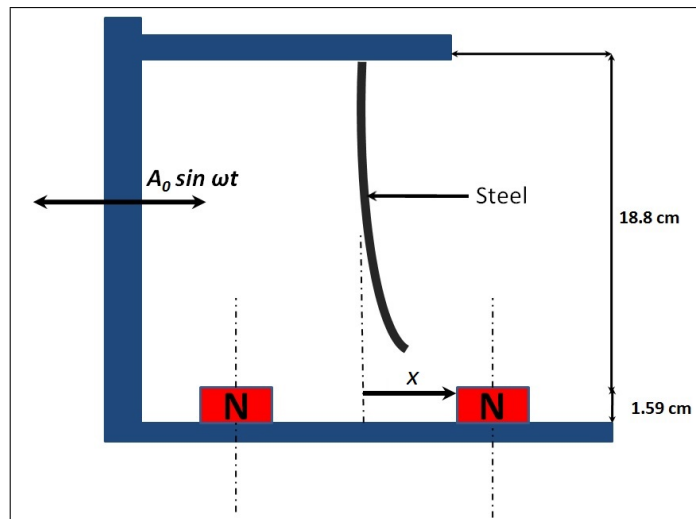


Figure 2.1: Mechanical model of Duffing oscillator, with double well potential developed by the pair of N-poles.

The dynamical properties with linear oscillators summarized in the previous page hold for nonlinear oscillators too. Nonlinearity has additional significance on the dynamical behaviors and hence nonlinear systems allow new kinds of solutions for the oscillations around the equilibrium. These solutions have been named as aperiodic

solutions. The time evolution of the system observable, $x(t)$, when an aperiodic (or transient) solution vanishes with time, oscillates around the equilibrium; however, there is no definite form of the function $x(t)$, limited to a finite time interval that repeats itself. Moreover, the phase space plots of such systems do not converge to closed curves nor approaches to the equilibrium, instead, they trace cloudy entangled trajectories that never repeat themselves.

Nonlinear systems can be modeled by means of nonlinear differential equations, like Eq. (2.9). There is no general method to solve nonlinear equations like the one that is employed to obtain the motions of the several types of harmonic oscillators [69] studied above. In general, and especially when aperiodic solutions are involved, the motion of the oscillator in phase space has to be obtained by means of one or more of the numerical methods that have been developed to solve differential equations [70]. Although there are analytical tools to deal with nonlinear systems [71], computational methods play an important role in the study of nonlinear dynamical systems.

The following section describes the dynamics of large number of coupled systems, they are called collective systems.

2.3 System of Limit Cycle Oscillators

Studying dynamics of collective behavior is of great interest for the scientists from different disciplines for a quite long time. The most interesting thing observed in collective systems composed of many dynamical components is synchronization. The occurrence of synchronization occurs in systems composed of limit cycle oscillators has been described by a simple model proposed by Yoshiki Kuramoto [72]. According

to the model, Kuramoto proposed a simple coupled equation given in Eq. (2.11).

$$\dot{\theta}_i = \omega_i - \frac{K}{N} \sum_{j=1}^N \sin(\theta_i - \theta_j), \quad (2.11)$$

where θ_i represents the phase of the i^{th} oscillator, and N the total number of the oscillators. Kuramoto model [9] provides quantitative measures by which we can study the phenomenon of synchronization at the steady state of the system or while the system is evolving into the steady state. Sakaguchi has extended the model for periodic external force given in Eq. (2.12) [13].

$$\dot{\theta}_i = \omega_i - \frac{K}{N} \sum_{j=1}^N \sin(\theta_i - \theta_j) - B \sin(\theta_i - \omega t). \quad (2.12)$$

In this collective motion of the oscillators, an order parameter has to be identified to characterize the dynamics. Relative phase among the oscillators is an order parameter as it characterizes the modes of coordination [73]. In this model, the order parameter (ϕ) is defined as $r(t)e^{i(\omega t + \phi)} = \frac{1}{N} \sum_{j=1}^N e^{i\theta_j}$ where $r(t)$ with $0 \leq r(t) \leq 1$ measures the phase coherence, and ϕ is the average phase. Sometimes these oscillators are called phase oscillators.

2.4 N-body Limit Cycle Oscillators Poses A New Problem

The ordinary differential equation Eq. (2.5) represents the damped harmonic oscillator under external periodic force and its phase (ϕ) is equal to $-\tan^{-1} \frac{2\gamma\omega}{\omega_0^2 - \omega^2}$. The phase lag depends upon the strength of dissipation (γ) and frequency of external force (ω). Here, the negative sign indicates lag and ϕ is higher for higher damping strength and frequency. The phase lag also increases as ω approaches towards ω_0 .

Therefore, for all possible values of ω , phase lag cannot exceed 90° . This holds good not only for an isolated harmonic oscillator but also for an oscillator in a coupled system because the dynamics follow Eq.(2.6). In collective system, the phase of individual limit cycle oscillators does not exceed 90° hence, the average phase ϕ of Eq.(2.12) apparently cannot exceed 90° .

Some interesting questions that come up in this context are:

- What is the maximum possible phase lag of a limit cycle oscillator when it is sitting in a system?
- Is it possible that the average phase lag exceeds 90° in the system of N-body limit cycle oscillators? In that case, the dynamics of the oscillators is such that the system opposes the external field, resulting in a diamagnetic state of the system.

Now the problem is defined as :

- Is there any possibility that the phase lag of the system exceeds 90° for $\omega < \omega_0$?
- Is there any possibility that a system of oscillators can show a negative (diamagnetic) susceptibility at a frequency lower than the natural frequency of the oscillators?
- How and at what conditions the phase of the collective motion demonstrate diamagnetic susceptibility?

This problem cannot be solved by any generalized approach or by any standard models rather it requires more specific formulation of the system dynamics. This brings in the possibility for a new concept of negatively susceptible system excited by periodic perturbation. The following chapters will validate the above statement by numerical simulation and by verifying experimentally using nano-magnetic composites.

Chapter 3

Susceptibility of Chaotic Oscillators System

The problem defined in Chapter 2 has originated from a natural phenomenon, the predator-prey interaction of school of fishes. When a predator shows up, a disorganized school of fishes regroup and swim closer together with coordinated movements. Someone in the school spots a predator and starts to take some sort of evasive action, all fellow fishes also respond [74]. Prey grouping and predator confusion have been studied and simulated by many researchers [75] providing a more quantitative view of the evolved grouping strategies considering nearest neighbor distance and degree of coordination. In the case of moving or stationary group of fishes, there is a tendency that denser groups (having a smaller distance of separation between the neighbors) offer greater safety in terms of the confusing the predator. This was proposed by Kunz [75] and practically demonstrated in several Youtube videos *e.g.*, School of Fish! [76]. Because of their immense size, school of fishes often confuses predators, making it difficult for the predator to single out one individual prey. Polarization or coordinated movement is seen when they are at closer distance. Tsang *et al.* have suggested fish motion as a moving dipole in a doubly periodic domain

[77]. Dipolar interaction is the cause of their coordinated movement.

Dipole formations in nature are of various types, e.g., electric dipole, magnetic dipole, flow dipole, vortex dipole, etc. An electric dipole is a small separation of equal positive and negative charges. A magnetic dipole is a tiny magnet of microscopic size, equivalent to a flow of electric charge around a loop. A flow dipole is also formed by the separation of a sink and a source in the flow. Vortex dipole is formed around the object in the flowing fluid. Equal and opposite vortices are developed at the head and tail of a fish when it swims, as if fish is a floating dipole in water. The dynamics of school of fishes is considered to be a collection of dipoles in an unbounded viscous fluid that captures long range hydrodynamic interaction. Fish swims preferentially parallel or anti-parallel to the flow of water. Therefore, the flow of water imposes a double well potential on the collective dynamics of the fishes. Similar to electrical dipoles, fish schooling dynamics is also modeled considering dipole-dipole interaction [78]. All these dipoles experience long range interaction and this interaction influences the dynamics of the dipolar systems. In some occasions (Jonathan Bird's Blue World: Sailfish!) [79], it is seen that a predator deviates the collective movement of the fishes by attacking them. The predator can deflect the fishes who are heading the school. Sudden appearance of a predator initiates a cooperative turning in the school and the school is still continues to turn in the opposite direction of the predator even when the predator at that instant may have moved away from the school. In the video, produced by Jonathan [79], it is seen that a situation arises when the fishes are approaching towards the predator instead of moving away from the predator and this is due to the repeated attack of the predator alternately from upstream and downstream directions (*vide* Appendix A). Thus, the group of fishes shows a negatively susceptible system against the external perturbation of the predator. From the above discussions, following conclusions are drawn.

- Fish in a stream acts as vortex dipole [77].
- Fish-dipoles are in a double well potential [77].
- School of fishes shows a high degree of polarization among themselves [74].
- Degree of coordination among the fishes increases with the narrowing of the separating distance among the neighbors [74].
- The predator gets confused for higher degree of coordination in the school of fishes [75].
- The predator attacks alternately from different directions. But, it is seen that the fishes are heading towards the predator instead of fleeing away (Appendix A). This means that the system is opposing the external perturbation [79] and that is a negatively susceptible system [24].

In this chapter, feasibility of a negatively susceptible system is demonstrated considering a collection of dipole oscillators under a periodic perturbation. To realize negative susceptibility, an array of interacting dipoles is considered as oscillators. Here the dipoles oscillate about the axis by the influence of an external magnetic field.

3.1 Interacting System of Oscillators

Interaction between the oscillators may be between the nearest neighbors or of long range. The dynamics of collective system becomes more realistic if the coupling of the oscillators is considered to be of long range instead of nearest neighbor coupling. When oscillators of similar type are spatially distributed, essentially they occupy a volume. For long range interaction, the strength of interaction is a function of distance (r) between the oscillators (typically proportional to r^{-n}); n is a real number.

Due to this varied strength of interaction, the behavior of the oscillators located in the central part of the occupied volume differs considerably with respect to those located at the surface. The strength of interaction field is shown in Fig. 3.1. This figure illustrates that the oscillators in the central region are strongly coupled than the oscillators located at the surface. Although the oscillators are similar yet due to long range interaction, the Hamiltonians of the oscillators are different. Therefore, the relative phase of the oscillators at the central region is more than those located at the surface. In a coupled system, there exists always a possibility of occurrence of cooperative phenomenon among the oscillators due to presence of external perturbation as observed in the nature [23]. The existence of this type of cooperative phenomenon has been established analytically by Sakaguchi [13]. This cooperative phenomena in the assembly of coupled systems primarily depends on the type and the strength of interaction among the oscillators. Since the external perturbation is the primary cause of the cooperative phenomenon in the limit cycle oscillator system. So, there must be a time lag between the effect and it's cause. This delay predominantly depends on the strength of interaction, intensity of dissipation, and many other parameters of the system.

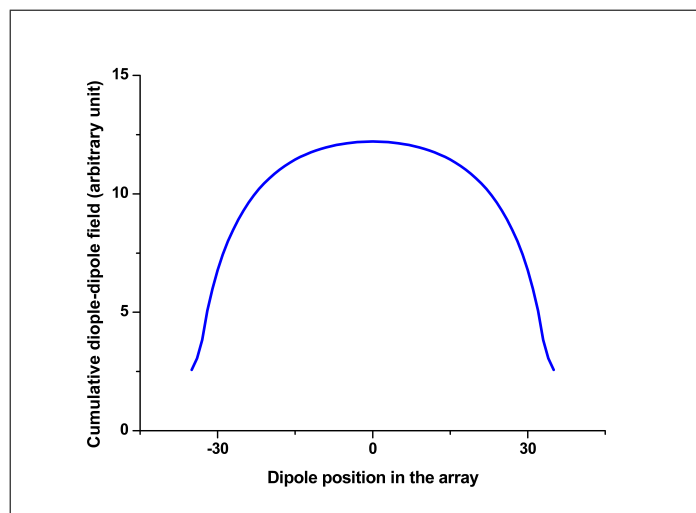


Figure 3.1: An ensemble of $71 \times 71 \times 71$ dipoles in a three dimensional lattice is arranged in an anti-ferromagnetic ordering. The dipole-dipole interaction field along the central line of the ensemble is plotted.

The topic discussed in this thesis is the susceptibility of a system of coupled dipoles. If the dipoles are fixed at its center of mass and free to rotate, the dipoles act as a phase oscillator. The angular displacement with respect to the periodic field is measured. Practically working with dipoles is difficult but magnetic needle is a good approximation of a big dipole. A magnetic needle acts as an oscillator and the dynamics of the needle becomes chaotic under certain conditions. This phenomenon is discussed in the following section.

3.2 Magnetic Needle, a Huge Dipole

The basic building block in the system of coupled oscillators is dipole. Magnetic needle is equivalent to a dipole other than the dimension. The dynamics of a spinning compass needle in a magnetic field that varies sinusoidally with time is studied in this section to understand the basic characteristics of the dynamics of the dipoles. Meissner and Schmidt have performed a simple experiment to study the transition of order to chaos in a magnetic needle as shown in Fig. 3.2 [8]. The electromagnets are generating time varying uniform magnetic field $H = H_0 \sin \omega t$. If the angle between the compass needle of moment m and the magnetic field direction θ , the torque exerted on the needle is $\Gamma = \vec{\mu} \times \vec{H} = \mu H \sin \theta \hat{n}$. The equation of motion is written as,

$$I \frac{d^2 \theta}{dt^2} = \mu H_0 \sin \omega t \sin \theta, \quad (3.1)$$

where I is the moment of inertia of the needle. This simple Eq. (3.1) is non-integrable just like multi-body problem.

The total energy (Hamiltonian) of the mechanical system may be written as given in Eq. (3.2).

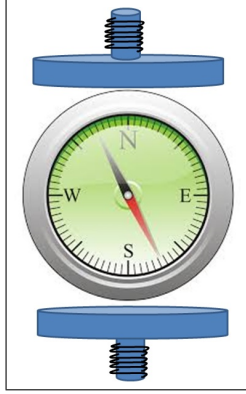


Figure 3.2: Compass needle in a uniform magnetic oscillating field.

$$H(\theta, J, t) = \frac{J^2}{2I} + \mu H_0 \sin \omega t \cos \theta, \quad (3.2)$$

Initially, the system is periodic with time and by gradually increasing a parameter (say H_0) causes a fixed point to bifurcate by period doubling, e.g., it becomes a periodic orbit of period 2, further increase of H_0 results in another bifurcation to period 4 and so on to period 2^n . When $n \rightarrow \infty$, the system becomes chaotic.

3.3 A Dipole Oscillator in Double Well Potential

In this coupled dynamical system, dipole oscillators are the limit cycle oscillators in the system. Dipole is a pair of equal and opposite strength ($\pm\mu$) points separated by a finite distance as shown in Fig. 3.3. Each dipole is fixed at the middle and rotates on the plane about an axis passing through the center of mass of the dipole and perpendicular to its length. These dipoles are placed with a regular spacing in a straight line and all experience an external periodic field $H_0 \sin \omega t$ as shown in the Fig. 3.3. The dynamics of the dipoles is constrained by double well potential and dipped in a viscous medium.

To understand the coupled dynamics, it is essential to look into the uncoupled motion of the dipoles. In the case of a freely rotating dipole under periodic field, the

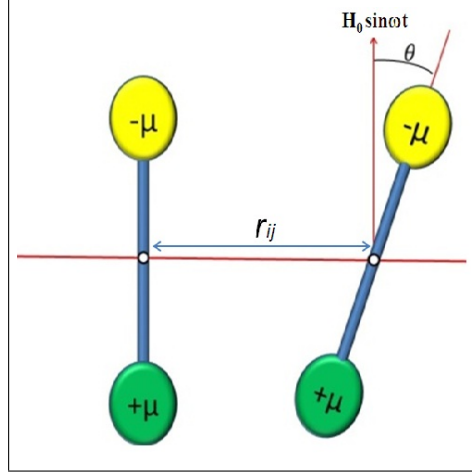


Figure 3.3: Arrangement of coupled dipoles in an array.

dynamics is represented by the ordinary differential equation (ODE) (3.1). Dipole behaves chaotic when $\omega < \sqrt{\frac{2\mu H_0}{I}}$ and non-chaotic when $\omega > \sqrt{\frac{2\mu H_0}{I}}$ [8]. This criterion does not follow when the motion of the dipole is restrained by some potential well.

If the dipoles are associated with a pair of favorable axes, its motion is biased by a double well potential and these two favorable orientations of the dipoles are separated by an energy barrier of height κ . The double well potential used in this study is represented by the function $-\kappa \cos^2 \theta$ which has two minima at $2n\pi$ and $(2n + 1)\pi$ respectively, as shown in Fig.3.4. This is a standard potential function used in magnetic anisotropy [30]. The shape of the potential well gets modified by the external field as $-\kappa \cos^2 \theta + \mu H_0 \cos \theta \sin \omega t$ and is shown in Fig.3.4 for different strength H_0 of applied magnetic field.

If $\mu H_0 \sin \omega t$, the energy imparted to the dipoles by the external field, does not exceed 2κ , the dipole may not flip to the other minima and the motion of the dipole will always be restricted within a particular well. The dynamics of such dipole will follow the ODE as given in Eq.(3.3) derived from the Hamiltonian of the dipole oscillator (Appendix B), where β is the damping coefficient, $\alpha = \frac{\mu H_0}{I}$ and $\omega_0 = \sqrt{\frac{\kappa}{I}}$. These four parameters ω_0 , α , β , ω govern the dynamics of the dipoles.

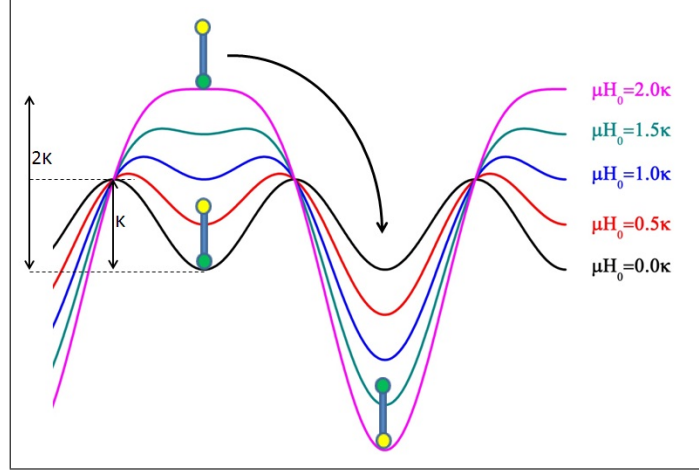


Figure 3.4: Functional representation of the double well potential due to various applied field strength.

$$\frac{d^2\theta}{dt^2} = -\omega_0^2 \sin 2\theta + \alpha \sin \omega t \sin \theta - \beta \dot{\theta} \quad (3.3)$$

The prime interest is to study the dynamics of the dipoles when the dipoles toggle between the two minima in a non chaotic manner. This can be achieved when the dynamics satisfies two criteria. The first criterion is μH_0 should be more than 2κ (i.e., $\alpha > 2\omega_0^2$). To satisfy this criterion, the system becomes prone to energy blow-up and chaotic, because there is a constant supply of energy to the system by the driving agent. To avoid this, damping is introduced in the dynamics of the system [22]. The second criterion is that the system has to settle at the minima alternately for each half cycle of the driving force. Hence, the damping coefficient β should be optimized to make the settling time less than $\frac{T}{2}$, where T is the time period of the external wave. By adjusting suitable values of β , the settling time is made to less than $\frac{T}{2}$ and the numerical solution of Eq.(3.3) is shown in Fig. 3.5. This figure shows that the dipole toggles from one minimum to the other when the external field changes its polarity and it undulates about the minima and settles to equilibrium. The dynamics of these non-interacting dipoles in the dissipative medium is projected in the domain of the angular position (rads) vs. angular velocity (rads/sec), as shown

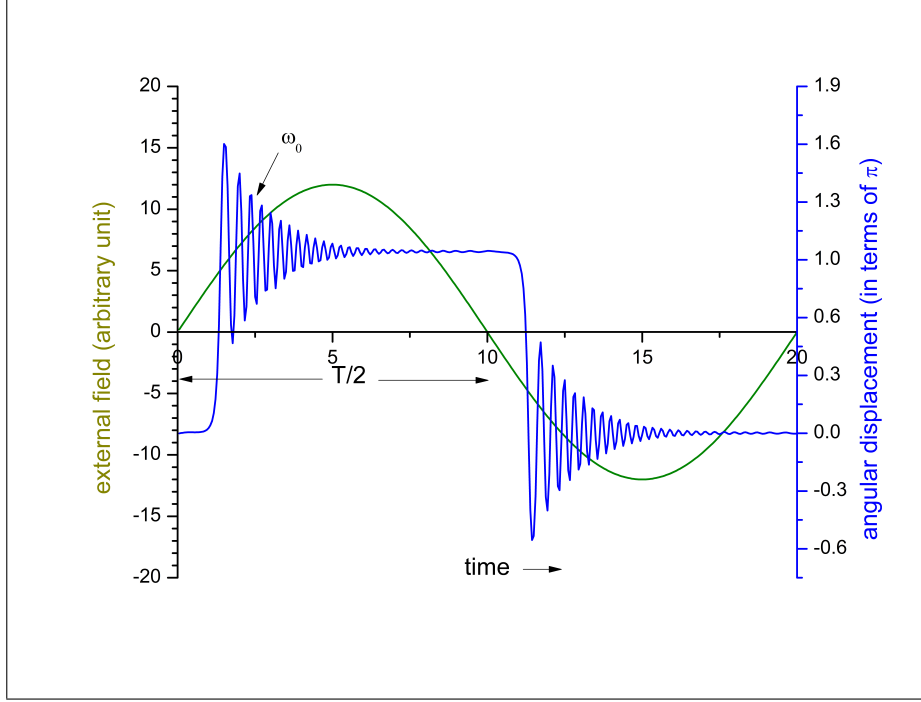


Figure 3.5: Under-damped oscillation of a dipole, restricted within the two minima at $\theta = 0$ and π .

in Fig. 3.6 and it looks like a fixed point attractor and the system tend towards 0 or π alternately. The behavior of the dipole oscillator as shown in Fig. 3.5 is similar to an under-damped oscillator. The oscillations of the dipoles before settling to 0 or π are damped depending upon the values of β . In the next section, coupled dynamics of the dipoles is discussed.

3.4 Dynamics of Coupled System

According to the Caldeira-Leggett model, one can establish a minimal Hamiltonian model of a coupled system to replicate the realistic physical phenomenon and can be solved numerically [81]. If J is the angular momentum of the dipoles and r_{ij} represents distance between the i^{th} and j^{th} dipoles, the Hamiltonian of i^{th} dipole in coupled condition is given by the following Eq. (3.4). Here the \sum term arises due to collective dipolar interactions.

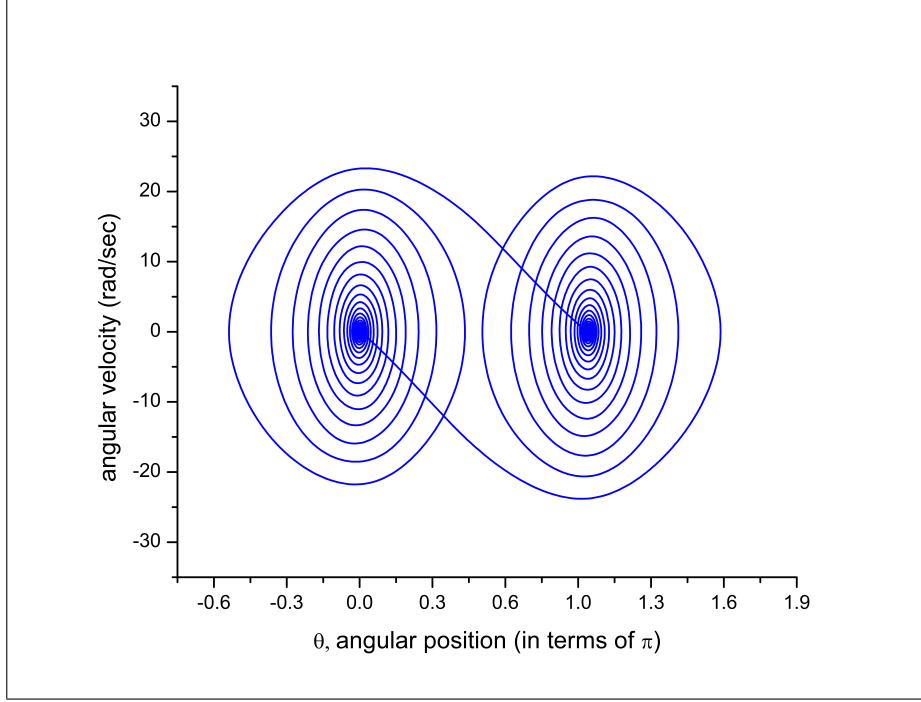


Figure 3.6: Dynamics of dipole attractor at the two minima indicating suppression of chaos by weak damping.

$$\begin{aligned}
 H_i = & J^2/2I - \kappa \cos^2 \theta_i + \mu H_0 \sin \omega t \cos \theta_i - \beta \dot{\theta}_i \\
 & + \mu^2 \sum_{j=1(i \neq j)}^N \frac{1}{r_{ij}^3} (-2 \cos \theta_i \cos \theta_j + \sin \theta_i \sin \theta_j)
 \end{aligned} \tag{3.4}$$

From this Hamiltonian the dynamics of the individual dipoles in the coupled system is derived (Appendix B) as in the Eq.(3.5).

$$\begin{aligned}
 \frac{d^2 \theta}{dt^2} = & -\omega_0^2 \sin 2\theta + \alpha \sin \omega t \sin \theta - \beta \dot{\theta} \\
 & + \gamma \sum_{j=1(i \neq j)}^N \frac{1}{r_{ij}^3} (2 \sin \theta_i \sin \theta_j + \cos \theta_i \cos \theta_j)
 \end{aligned} \tag{3.5}$$

The ODE described in Eq.(3.5) has three critical parameters α (external perturbation), β (damping) and γ (strength of interaction, $\gamma = \frac{\mu^2}{I}$) that governs the dynamics of the system. If α is very large compared to β and γ , the dynamics of the system is dominated by the external field. The following section explains the

numerical solutions of the coupled ODE, as given in Eq.(3.5).

3.5 Numerical Analysis

In the model of the coupled system, $N=91$ dipoles are considered and 91 coupled equations are solved numerically using 4th order Runge-Kutta method. The natural frequency, ω_0 of the dipoles is chosen to be 2π per second. α and β are chosen to be $18\omega_0^2$ and $0.3\omega_0^2$ respectively so that the overshoot of oscillation dies down to prevent chaos. γ is varied from $0.5\omega_0^2$ to $3.0\omega_0^2$ to understand the nature of the dynamics when α and β remain constant. For $\gamma = 0$, all the dipoles are non-interacting and follow the external field with a constant phase lag less than 20° , as shown in Fig. 3.5. For $\gamma \neq 0$, additional phase lag with respect to the external field develops in the system and it increases with higher values of γ . Fig. 3.7 shows various combinations of the parameters for which the coupled system demonstrates the average phase lag more than 90° for a limited range of frequencies of the external field. For lower values of $\gamma (< 0.5\omega_0^2)$, the average phase lag never exceeds 90° . For $\gamma = \omega_0^2$, the phase lag of the system exceeds 90° between the applied frequency 3.8 rad/sec to 6.4 rad/sec. Further increase in γ value, the phase lag exceeds 90° at lower frequency range. For $\gamma = 3\omega_0^2$, the phase lag of the system is above 90° between the frequency range 0.1 rad/sec to 1.8 rad/sec, otherwise the system is chaotic. This indicates that the strength of interaction is the prime cause of this phenomenon. It is also important to note that the phase lag is not same for all the dipoles in the system. In Fig. 3.8, the variation of the phase lag among the dipoles is shown separately. The dipoles in the core has phase lag more than the dipoles located at the ends. The dynamics of the coupled oscillators can be explained physically based on the results obtained from numerical computation.

A continual counteraction between the external field and dipolar interaction gov-

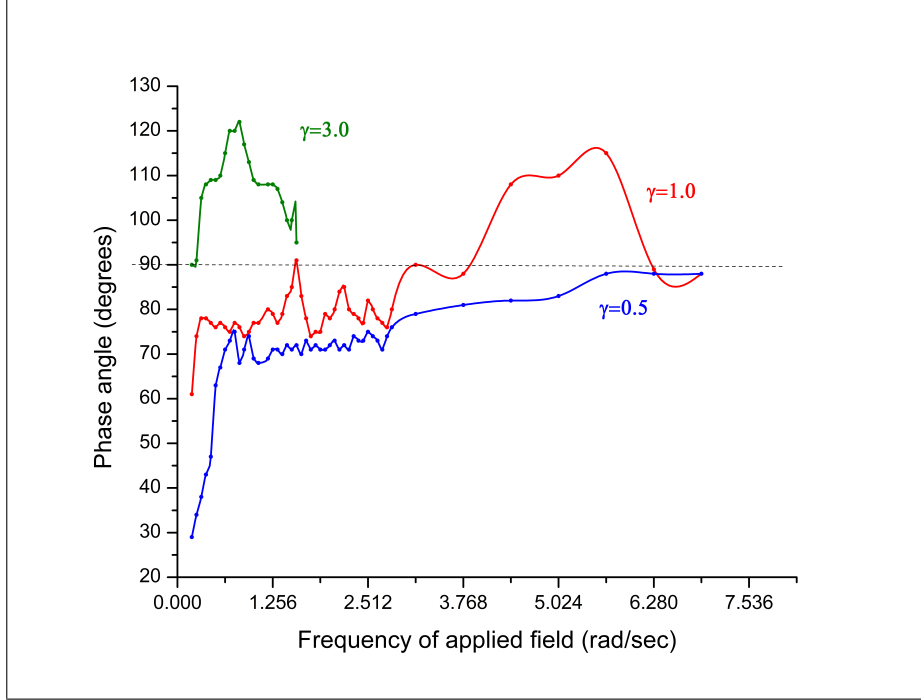


Figure 3.7: For various γ values phase lag of the system is demonstrated. Phase lag of the system exceed 90° for some definite frequency ranges only.

erns the dynamics of the system. When the external field surpasses the dipolar interaction, the phase lag is less than 90° but for certain combination of the parameters, dipolar interaction overcomes the external field and the phase lag becomes greater than 90° . Due to the long range interaction, dipoles located at the ends are loosely coupled and hence the system initiates to respond to the external field at either ends of the array. This turning of the dipoles at the ends, sets off a series of sequential turnings in the array due to the sudden change in the interaction field caused by the neighbor reversal [13], [82]. This makes the dipolar orientation in the outer region aligned with respect to the applied field whereas the core remains in opposition to the applied field. Thus the dipoles in the core experience a field generated collectively by the dipoles at the ends. The opposing field created by the dipoles at the ends becomes adequately high to turn a large number of dipoles in the core which can be looked as a cooperative switching. Due to this cooperative switching, majority of the dipoles in the array oppose the applied field by more than 90° . The interesting thing in the observation is that the phase of the system lags

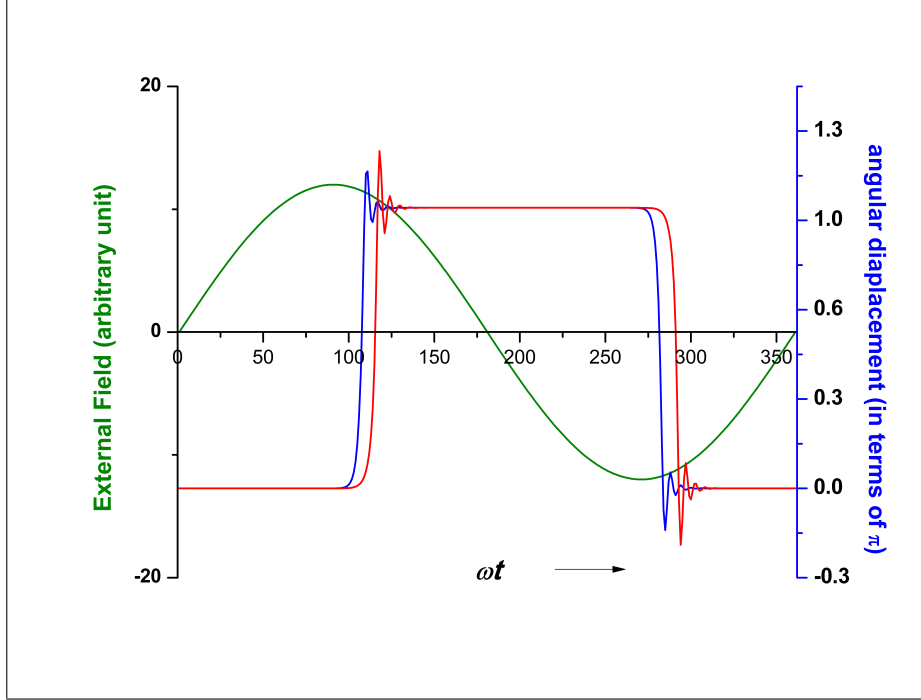


Figure 3.8: The phase lag with respect to the applied field is position dependent. Dipoles at the ends (blue) have phase lag less than the dipoles at the center (red).

more than 90° to 110° when the external frequency is much less than the resonating frequency of the system. Thus, it originates a new concept of negative susceptibility in the system of coupled nonlinear oscillators. In the next chapter, a more specific simulation on nano-magnetic ensembles is presented.

3.6 Conclusion

This chapter has explained the term susceptibility *i.e.*, susceptibility of collective oscillators system subjected to an external perturbation. As magnetic needle is the gross representation of a dipole, the historical experiment done by Meissner and Schmidt is explained here to understand how the dynamics of the needle becomes chaotic. Ordinary differential equation is derived from the Hamiltonian of the dipole oscillator to analyze the dynamics of the magnetic needle. The synchronization and chaos suppression is achieved by introducing damping in the dynamics

of the dipoles. A simulation result of 91 dipoles arranged in an one dimensional array is presented in this chapter where an extra summation term called interaction potential is added with the coupled equations of motion of the dipoles. The coupled differential equations are solved by Runge-Kutta method and the solution shows negative susceptibility at some frequencies of the applied field.

Chapter 4

Crossover of Susceptibility: Simulation Studies

Classical thermodynamics describes macroscopic properties in terms of a few variables: temperature, pressure and volume; but this is the thermal average of microscopic states of the constituent subunits. If it is assumed that the system is made up of a set of identical subunits and average over all of the subunits then this system is called a statistical ensemble. Here, identical subunits means they are all in the same thermodynamic state. The most common statistical ensembles are micro-canonical, canonical and grand canonical ensembles. Micro-canonical ensemble is a concept used to describe the thermodynamic properties of an isolated system. Possible states of the system have the same energy and the probability for the system to be at any given state is the same. Therefore, it describes a system with a fixed number of particles (N), a fixed volume (V), and a fixed energy (E). Canonical ensemble describes a system where the number of particles (N) and the volume (V) are constant, and it has a well defined temperature (T), which specifies fluctuation of energy. Grand canonical ensemble describes a system with fixed volume (V) and temperature (T), but to specify the fluctuation of the number of

particles, it introduces chemical potential. In this thesis, the so called identical sub-units are dipole oscillators. They are fixed in numbers (N) and occupy a constant volume (V) at temperature T . It is known that the varieties of collective behavior appear in the dynamics of an ensemble made by similar, but non-identical limit cycle oscillators [83]. The simplest way to consider the coupling in the collective system is the nearest neighbor interaction as seen in Ising model where phase transition in one dimension is not possible. But it has been proved that there is a phase transition in one-dimensional Dyson model for an infinite linear chain of spins with $\frac{1}{r^\alpha}$ as coefficient of interaction potential [84], [85] when $1 < \alpha < 2$. Here, an ensemble of superparamagnetic particles has been considered. Assuming those single domain particles as dipoles and the dipoles are coupled with each other with long range interaction, crossover of susceptibility has been established.

A single domain nano-magnet acts as a magnetic dipole. In addition, it switches or oscillates its magnetization about the easy axis depending upon its size, temperature and anisotropy. In a grand canonical ensemble of nano-magnets, dipolar interaction potential varies spatially within the ensemble because a long-range type of interaction exists between the dipoles (Fig. 3.1). So, dipole-dipole interaction alters the relaxation time of the nano-magnets in the ensemble. The relaxation time of the interacting nano-magnets depends upon the average separation among the nano-magnets and the total number of nano-magnets present in the ensemble. Hence, the aggregation of interacting nano-magnetic dipoles demonstrates both experimentally and theoretically as a model system to detect intriguing co-operative physical phenomena. A crossover from paramagnetic to diamagnetic phase due to the variation of frequency of the applied sinusoidal magnetic field of a nano-magnetic ensemble is presented in this chapter. This interesting phenomenon may be significant on the design and development of magnetic devices. The simulation of the system is in good agreement with the experimental results and those results will be explained in chapter 5.

4.1 Single Domain Magnetic Islands : Superparamagnetism

The magnetization reversal of a single domain superparamagnetic particle is due to the applied magnetic fields and thermal agitation. In 1948, Stoner and Wohlfarth (SW) [30] have first given the theoretical description of the magnetic switching of a single domain (diameter $< 10\text{ nm}$) nano-magnets. It has been assumed that due to strong exchange coupling between the atomic spins, all the atoms always remain in a single domain state. Hence, during reversal process, all the spins reverse simultaneously as a single domain. Therefore, a single domain of N atomic magnetic spins (moment = μ_{at}) is described as a giant moment $\mu = \sum \mu_{at}$ of the particle. In magnetically ordered material, there are certain preferred orientation(s) of the magnetization. These preferential directions are called easy axes. The magnetic moment, μ of the single domain nano-magnet prefers to stabilize in the easy axes only. Due to thermal agitation, polarity of μ (± 1) changes with time, and the average time of switching of magnetization is called *superparamagnetic relaxation time* (τ). The reversal of magnetization follows Arrhenius Law as given in Eq. (4.1):

$$\tau = \tau_0 \exp \frac{KV}{k_B T}, \quad (4.1)$$

τ_0 is called pre-exponential factor (10^{-9} sec to millions of years), V is the volume of the particle, k_B is Boltzmann constant, K is the anisotropy energy per volume and T is temperature. The state (orientation) of each nano-magnet about the easy axis is ± 1 and they can flip between the states due to thermal agitation or external fields. This single domain nano-magnet acts as a switching dipole and the rate of transition between the states ± 1 about the easy axis depends upon temperature and anisotropy, as per Eq. (4.1). Because of this anisotropy, the magnetic dipoles cannot freely follow the external applied field and hence a counter action exists between the

applied field and the dynamics of the magnetic dipoles. As a result, a diamagnetic susceptibility evolves in the ensemble of superparamagnetic particles. Following section provides the derivation for the condition of para-to-diamagnetic crossover of susceptibility by periodic external magnetic field in an ensemble of nano-magnets.

4.2 Model and Simulation

In this thesis, exciting results of simulation are presented by computing the dynamic evolution of magnetization of an ensemble of nano-magnets under the influence of spatial variation of interaction energy along with temporal variation of Zeeman energy. A three-dimensional Ising-like model with cobalt nano-magnets is considered at various lattice points of a simple cube. On this account $7 \times 7 \times 7$, $11 \times 11 \times 11$ and $15 \times 15 \times 15$ Ising-like cobalt nano-particles of dimension 6.5 to 7.5 nm are arranged in a cubic array of lattice constant 8.8 to 15 nm. The easy axes of the nano-magnets are chosen to be at some random angle with respect to the z-axis. The magnetic field $H = H_0 \sin(\omega t)$ is applied along the z-axis. The ensembles of the nano-magnets are kept at various temperatures 77K and 300K respectively, which are well below the magnetic ordering temperature [38] so initially the assembly of nano-magnets will be in the anti-ferromagnetic ordering. Therefore, in the simulation, the initial ordered state is taken to be anti-ferromagnetic [40]. In this computation, the duration of switching is assumed to be instantaneous and the stable state of the magnetic moment of the nano-magnets is taken to be either parallel or anti-parallel to easy-axis, energy minima of the nano-magnet. The size of the nano-magnetic particles, lattice constant and applied magnetic field are so chosen that the three forms (anisotropy, Zeeman and dipole-interaction) of energies are of the same order.

If $K_{Co} = 4.1 \times 10^5 J/m^3$, $V = 2.21 \times 10^{-25} m^3$ (diameter, $d = 7.5 nm$), $T = 300K$, Boltmann constant $k = 1.3806488 \times 10^{-23} m^2 kg s^{-2} K^{-1}$. Here, Thermal energy, $kT =$

4.14×10^{-21} Joules and anisotropy energy, $K_C V = 9.06 \times 10^{-22}$ Joules. Here, thermal energy is 4.56 times the anisotropy energy. So, the blocking temperature of the magnetic nanoparticles is less than 16K. If $KV \gg kT$ thermal energy cannot switch the magnetic moment from one orientation to other.

SW model shows how the anisotropies present in a system can lead to a hysteresis, although there is no irreversible effects associated with domain wall pinning. Originally, SW model has assumed shape anisotropy, but it is widely used for the case of uniaxial magneto crystalline anisotropy. The existence of coherent rotation of the magnetization of each nano-magnet (i.e., no internal degrees of freedom) is the most important assumption in this model. The equilibrium direction of the particle magnetization vector is determined by the strength, direction of the applied magnetic field and orientation of the easy axis of anisotropy (Appendix D and E). If a magnetic field H is applied along z -axis and \hat{e} is the direction of the easy axis, the magnetization vector \hat{m} will rotate away from the easy-axis due to the applied field. The magnetization vector is rotated on the basal plane by an angle ψ , as shown in Fig. 4.1.

The total energy of the system is given by

$$E(\psi) = -KV \cos^2 \psi - M_s V H \cos(\gamma_0 - \psi), \quad (4.2)$$

where γ_0 is the direction cosine of easy-axis with respect to z -axis, K is the anisotropy constant, V the volume of the nano-magnet and M_s is the saturation magnetization of the bulk material. The Eq. (4.2) can be transformed to reduced energy form as given below.

$$\xi = \left(\frac{E}{2KV} + \frac{1}{4} \right) = -\frac{1}{4} \cos 2\psi - h \cos(\gamma_0 - \psi), \quad (4.3)$$

where $h = \frac{M_s H}{2K}$. For given values of γ_0 and h (or H), the magnetization vector will

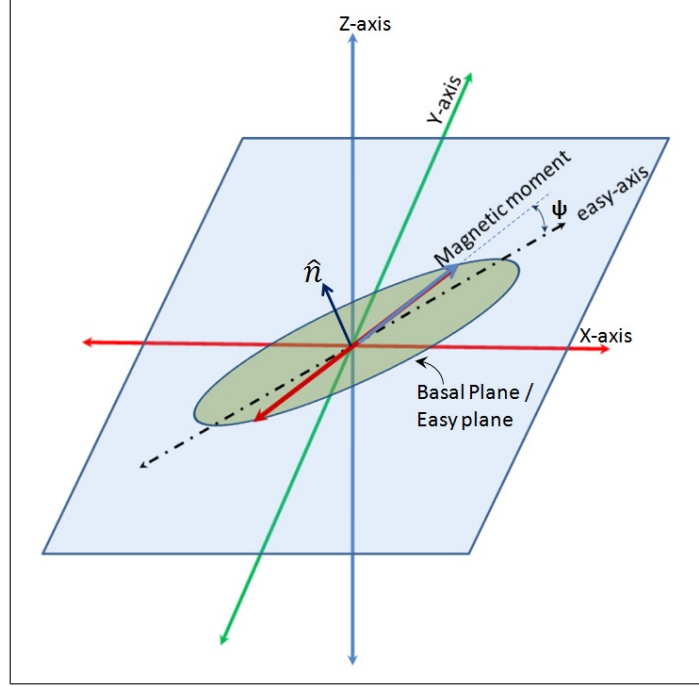


Figure 4.1: Easy axis of an uniaxial anisotropy crystal (black broken line) Magnetic moment is shifted away from easy axis by an angle ψ when a field H is applied along Z-axis.

choose ψ so that it minimizes the energy function in Eq. 4.3. Therefore, $\frac{\partial \xi}{\partial \psi} = 0$ and $\frac{\partial^2 \xi}{\partial \psi^2} > 0$.

The first condition, i.e., the equilibrium condition implies

$$\frac{\partial \xi}{\partial \psi} = \frac{1}{2} \sin 2\psi - h \sin(\gamma_0 - \psi) = 0, \quad (4.4)$$

The second condition, i.e., the condition for stability limit implies

$$\frac{\partial^2 \xi}{\partial \psi^2} = \cos 2\psi + h \cos(\gamma_0 - \psi) > 0. \quad (4.5)$$

Eq. (4.4) has multiple solutions for a given h and γ_0 and possibly more than one of these solutions represent an energy minimum. In order to get a unique solution, it is essential to specify expected value or follow the history of the value of h for each γ_0 . So, instead of analytical solution, numerical method is more suitable to find the

stable minima of ψ with respect to h . The value of ψ at which the energy minimum occurs gives the direction cosines of $\hat{m} = \cos \alpha, \cos \beta, \cos \gamma$. Thus the magnetization m_z in the direction of magnetic field is obtained.

Nano-magnets are assumed to experience same external magnetic field, $h(t) = h_0 \sin 2\pi ft$. The dynamics of the nano-magnets follows the Hamiltonian as given in Eq. (4.6) where $J(r, r')$ is the coupling coefficient and $S^r(\pm 1)$ is the state of magnetization.

$$\mathbf{H} = - \sum_{\langle r, r' \rangle}^N J(r, r') S^r S^{r'} - \sum_r^N h(t) S^r \quad (4.6)$$

At a given site r , the instantaneous magnetic field $h_T(r, t)$ experienced by a nano-magnet is the sum of applied field and the field produced by the dipoles as given by Eq. (4.7) where h_{dd} is the field produced by the nano-magnets (dipoles). h_{dd} is expressed in Eq. (4.8).

$$h_T(r, t) = h_{dd}(r, t) + h(t) \quad (4.7)$$

$$h_{dd}(r, t) = \sum_{r' (r \neq r')}^N J(r, r') S^{r'} \quad (4.8)$$

The Brownian relaxation dynamics of a clustered superparamagnetic particle system is investigated through characterization of complex magnetic susceptibility due to frequency and field strength variations. In non-equilibrium physics, the phenomenological Langevin model for the motion of a Brownian particle submitted to an external force yields correlation function which does not fulfill the sum rules of linear response theory. This means that the model can actually not be the macroscopic manifestation of an underlying microscopic dynamical model [80]. A classical

heavy particle with a path of classical independent harmonic oscillators - constitutes a special case of the Langevin model. Caldeira and Leggett proposed minimal Hamiltonian model [81]. In the system considered in this thesis work, the dynamics of nano-magnets with imposed constraint is analyzed by a minimal Hamiltonian model which mimics the realistic physical phenomenon [81]. This minimal Hamiltonian of the system of interacting nano-magnets is represented in the form of a single spin Hamiltonian as given in Eq. (4.9).

$$\mathbf{H} = -h_T(r, t)S^r = - \sum_{r'(r \neq r')}^N J(r, r')S^{r'}S^r - h(t)S^r \quad (4.9)$$

Let $P(+, t)$ and $P(-, t)$ are the probabilities that the dipole is in the state of +1 and -1 respectively at the instant of time t . We also take $1/\tau_{-+}$ and $1/\tau_{+-}$ be the transition rates of the dipole from state -1 to +1 and from state +1 to -1 respectively. The master equation of these probabilities is given in Eq. (4.10).

$$\frac{dP}{dt} = -\frac{P(+, t)}{\tau_{-+}} + \frac{P(-, t)}{\tau_{+-}} \quad (4.10)$$

We assume that the resolution of the observation time of our model $\delta t \ll \tau$. Therefore, during δt , no switching of the dipole occurs, hence $\frac{dP}{dt} = 0$ in that interval. As a result the ratio of the probabilities follow Eq. (4.11).

$$\frac{P(+, t)}{P(-, t)} = \frac{\tau_{-+}}{\tau_{+-}} \quad (4.11)$$

The applied field compels the dipoles to align in the field direction hence $P(+, t) > P(-, t)$ in the positive half cycle of the applied field and vice versa. In this case, the dipole will behave paramagnetic. This is quite usual. However, in this study an unusual occurrence of $P(+, t) < P(-, t)$ in the positive half cycle of the applied

field and vice versa is discussed. In this case only, the system of dipoles manifests diamagnetism. This diamagnetism occurs when a dipole is in opposition to the applied magnetic field. However, this opposition does not persist for more than the relaxation time, τ of the dipole and the possibility of sustained diamagnetism exists when half of the time period (T) of the applied field is less than the relaxation time of the dipole in the system. This can be easily formulated as τ_{+-} greater than τ_{-+} and at $h = h_0$ the relaxation time τ_{-+} is greater than $\frac{T}{2}(= \frac{1}{2f})$ for the positive half cycle of the field and vice versa.

The minimal Hamiltonian of the system of interacting nano-magnet is represented in the generalized form of a single spin Hamiltonian as given in Eq. (4.6) and Eq. (4.9). The same Hamiltonian is rewritten for nano-magnets in Eq. (4.12) where h_T is the field experienced by each nano-magnet consisting of the imposed field ($h_0 \sin 2\pi ft$) and dipolar magnetic field h_{dd} . If the easy axis of the nano-magnets is parallel to the z -axis, the Hamiltonian is modified with $\gamma_0 = 0^\circ$ as given in Eq. (4.13) where M_s is saturation of magnetization per unit volume (V) and K is the anisotropy constant.

$$\mathbf{H} = -S^r KV \cos^2 \psi - S^r M_s V h_T \cos(\gamma_0 - \psi) \quad (4.12)$$

$$\mathbf{H} = -S^r KV \cos^2 \psi - S^r M_s V h_T \cos \psi \quad (4.13)$$

The net magnetic field h_T in Eq. (4.13) at any arbitrary j^{th} lattice location at any instant of time t is given by Eq. (4.14) where $S^i = \pm 1$ is the state of the i^{th} nano-magnet and the other variables have their usual meaning. The expression of h_{dd} is derived in the Appendix C of this thesis.

$$h_T = h_0 \sin 2\pi ft + h_{dd}$$

$$= \{h_0 \sin 2\pi ft\} \hat{z} + M_s V \sum_{j=1(i \neq j)}^N S^i \frac{1}{r_{ij}^3} \left\{ \begin{array}{l} \frac{3(x^i - x^j)(z^i - z^j)}{r_{ij}^2} \hat{x} \\ + \left(\frac{3(y^i - y^j)(z^i - z^j)}{r_{ij}^2} \right) \hat{y} \\ + \left(\frac{3(z^i - z^j)^2}{r_{ij}^2} - 1 \right) \hat{z} \end{array} \right\} \quad (4.14)$$

For simplicity, the magnetic moments of the nano-magnets are considered in the $\pm z$ directions, the energy expression of each nano-magnet becomes independent of the transverse components of h_T and the corresponding relaxation time τ in relation with instantaneous net magnetic field is given by the Eq. (4.15) and (4.16) where $h_K = M_s/2K$ [29].

$$\tau_{+-} = \tau_0 \exp \left\{ \frac{KV}{K_B T} \left(1 + \frac{h_T}{h_K} \right)^2 \right\} \quad (4.15)$$

$$\tau_{-+} = \tau_0 \exp \left\{ \frac{KV}{K_B T} \left(1 - \frac{h_T}{h_K} \right)^2 \right\} \quad (4.16)$$

The condition of diamagnetism arises from Eq. (4.11) where τ_{+-} should be less than τ_{-+} for positive h .

$$\begin{aligned} \exp \left\{ \frac{KV}{K_B T} \left(1 + \frac{h_T}{h_K} \right)^2 \right\} &< \exp \left\{ \frac{KV}{K_B T} \left(1 - \frac{h_T}{h_K} \right)^2 \right\} \\ \Rightarrow \frac{4h_T}{h_K} &< 0 \\ \Rightarrow h_{dd}(t) + h(t) &< 0 \end{aligned} \quad (4.17)$$

Hence, from Eq. (4.17), it is clear that the diamagnetism is possible for the nano-

magnetic ensemble if the instantaneous applied field h is in opposite polarity with respect to the instantaneous interaction field h_{dd} .

The switching probability of each nano-magnet at different spatial locations in the ensemble is different and hence the overall magnetization is time varying. So the magnetization of the ensemble must have a phase lag with respect to the applied magnetic field [29]. The dipolar field at each lattice site in the ensemble depends upon the overall orientation of the nano-magnets and it changes whenever a nano-magnet switches from one state to the other. Therefore, in the process of simulation, the dipole-dipole interaction field is computed for each nano-magnet whenever switching occurs at any lattice site. The whole process is stochastic and the particle switches according to the Boltzmann probability and the time evolution of the state of the individual nano-magnets is extended from Eq. (4.11) to Eq. (4.18).

$$\frac{P(+, t)}{P(-, t)} = \frac{\tau_{-+}}{\tau_{+-}} = \exp\left(-2\frac{KV + M_s V h_T}{k_B T}\right) \quad (4.18)$$

This theoretical study is converted into a simulation code based on the flowchart given in the following section.

4.3 Simulation Code flowchart

In the simulations, it is assumed that the magnetic field is generated by a solenoid coil and the nano-magnetic ensemble is situated inside the coil. Externally, the coil is excited by sinusoidal current. The simulation code has been written in C programming language and in a sequential flow. It is started with the initializations of the system and ended with measurement of susceptibility of the system. In this section, details of the flow of the simulation are explained.

4.3.1 Step 1: Setting Simulation Parameters

All the parameters in the simulation have been set in first step.

Diameter of the nano-magnets, $d = 6.5 \text{ nm to } 7.5 \text{ nm}$ and volume, $V = \pi \frac{d^3}{6}$

System size: $N = N_x \times N_y \times N_z$ and $N_x = N_y = N_z (= 7, 9, 11, 15)$

Permeability of cobalt, $\mu_{Co} = 4.2 \times 10^{-3}$ SI unit

Magnetization per unit volume, $M_s = 1.4 \times 10^6$ SI unit

Anisotropy Energy Constant of Co, $K_{Co} = 4.1 \times 10^5 \text{ J/m}^3$

Pre-exponential factor, $\tau_0 = 10^{-9} \text{ sec}$

Parameters of the susceptometer solenoid:

Length of the solenoid, $L = 25.0 \times 10^{-3} \text{ m}$

Number of turns, $N=300$ turns

Diameter of the coil, $\delta = 5.0 \times 10^{-3} \text{ m}$

Peak magnetizing current, $I_0 = 10.0 \times 10^{-3}$ Amp to $25.0 \times 10^{-3} \text{ Amp}$

Field inside the susceptometer coil, $B_0 = \mu_{Co} \frac{NI_0}{L} \text{ Amp/m}$

Lattice distance, $l = 8.8 \times 10^{-9}$ to $15.0 \times 10^{-9} \text{ m}$

Temperature of the system, $T = 77^\circ \text{ K}$ and 300° K

Frequency of the applied field, $f = 50 \times 10^3$ to $1 \times 10^6 \text{ Hz}$

(Note: In a sample of randomly distributed magnetic nano-particles with

average moment $\mu = M_s V$ and average separation l , the dipole interaction energy $E_d \approx \frac{\mu_0 \mu^2}{4\pi l^3}$ where μ_0 is the permeability of free space. There is a critical temperature below which these magnetic nano-particles can result in ordering of the magnetic moments, the critical temperature $T_0 \approx \frac{E_d}{k_b}$.

4.3.2 Step 2: System Initialization

Before the simulation was started, the system was initialized by setting the randomly chosen easy-axis of the nano-magnets. Initial magnetic moment vectors have been defined either in state +1 where the direction cosines are $(\cos \alpha_0, \cos \beta_0$ and $\cos \gamma_0)$ or in state -1 where the direction cosines are $(\cos(180^\circ + \alpha_0), \cos(180^\circ + \beta_0)$ and $\cos(180^\circ + \gamma_0))$ so that the initial ordering of the ensemble of the nano-magnets is in anti-ferromagnetic ordering.

Set all positions [x,y,z] alternately +1 and -1

Begin loop at position [0,0,0]

Generate random number $\alpha_0 = 0^\circ$ to 180° assign direction cosine

Generate random number $\beta_0 = 0^\circ$ to 180° assign direction cosine

Generate random number $\gamma_0 = 0^\circ$ to 180° assign direction cosine

Net magnetization along z-axis, $netM_z = \sum(state) \times (direction - cosine)$

Calculate the h_{dd} at each position as given in Eq. (4.14)

End loop up to position $[N_x, N_y, N_z]$

4.3.3 Step 3: External Field Applied

As τ_0 is \approx nano-seconds, hence the time resolution (or sampling time) is measured in nano seconds. Here, the simulation is continued for the duration of 10 full cycles (*i.e.*, $\frac{10}{f}$ sec) of the applied field. Therefore, the total number of data points in nano seconds resolution are : $D_{pts} = 10 \times \frac{10^9}{f}$ and time t is ticked for every nano-sec from 0 to D_{pts} in the simulation.

For $t=0$ to D_{pts} applied field $h = h_0 \sin 2\pi ft$

4.3.4 Step 4: Main Loop

Loop start $t=0$ to $t=D_{pts}$

Catch each nano-magnet from $[0,0,0]$ of the 3-dimensional matrix

Compute dipolar field h_{dd} , Eq. (4.14)

Net magnetic field $h_T = h_0 \sin 2\pi ft + h_{dd}$

Calculate E , Eq. (4.2)

Find $E_{min1}, E_{min2}, E_{max1}, E_{max2}$

Find ψ for stable minima from E vs. ψ plot (Appendix F).

Find direction cosines $(\cos \alpha, \cos \beta, \cos \gamma)$ (Appendix E)

Find τ_{-+}, τ_{+-}

Calculate $P(+, t) = \frac{t_{noFlip}}{\tau_{-+}}, P(-, t) = \frac{t_{noFlip}}{\tau_{+-}}, t_{noFlip}$ = duration of no flip.

Decide flip or no-flip based on $P(-, t)$ and $P(+, t) \geq 1$.

Calculate $M_x = \mu \cos \alpha$, $M_y = \mu \cos \beta$, $M_z = \mu \cos \gamma$.

Complete the loop for all particles $= N_x, N_y, N_z$

Find $netMx(t) = \sum M_x$, $netMy(t) = \sum M_y$, $netMz(t) = \sum M_z$

Next increment t till $t = D_{pts}$

4.3.5 Step 5: Calculate Susceptibility

Real part of ac susceptibility is the magnetic energy stored in the sample during a cycle of applied field. Imaginary part of ac susceptibility is the energy converted into heat during one cycle of ac field. Here, 10 cycles are taken in the simulation. If time average is taken for sinusoidal magnetic field over a cycle, it becomes zero. So, it is better to take average of every half cycle. If we take full wave rectification, then this averaging issue is avoided and complete data points are integrated. Thus computation becomes simpler with very nominal error. It is straight forward and averaging is done over 10 cycles at a time.

$netM_z(t)$ and $H(t) = \sin 2\pi ft$ are now available for 10 cycles.

Apply fullwave rectification:

for $t = 0$ to $t = D_{pts}$

if $H(t) > zero$ then $H(t) = +H(t)$ and $netM_z(t) = +netM_z(t)$

if $H(t) < zero$ then $H(t) = -H(t)$ and $netM_z(t) = -netM_z(t)$

Find average field and average magnetization:

Average Field= $H(t)/D_{pts}$

$$\text{Average magnetization} = \frac{\sum netM_z}{D_{pts}}$$

Get the Susceptibility at frequency f :

$$\text{Susceptibility}(f) = \frac{\text{Average Magnetization}}{\text{Average Field}}$$

End of $t = D_{pts}$

4.4 Simulation Results

The magnetization of the ensemble is the collective effect of the state of the individual nano-magnets distributed in the ensemble. Hence, the time evolution of magnetization of the ensemble is determined by the collective state of the spin distribution determined from the evolution of the spin state of a single nano-magnet as per the Eq. (4.11). The simulation has been carried out at nano-second intervals ($\delta t = 10^{-9} \text{sec}$) for the duration of ten cycles of the external field and the average magnetization per half-cycle has been calculated from the simulation data. The susceptibility values have been obtained from the ratio of the average magnetization to the average external field. The frequency has been varied from 50 kHz to 10 MHz and the volume susceptibility of the system has been plotted with respect to the frequency, as shown in Fig.4.2. The simulation results showed that the susceptibility changes to a diamagnetic phase at and above certain frequency.

The simulation results are presented for a cluster of 3375 interacting nano-magnets arranged in a cubic lattice and a cross-over of magnetization could be seen in Fig. 4.2. From Fig. 4.2 it is seen that the frequency of crossover varies with temperature. This frequency also depends upon the particle diameter, particle separation, system size and strength of the excitation field. The variation in the crossover frequency depending upon the above parameters is presented in Table 4.1.

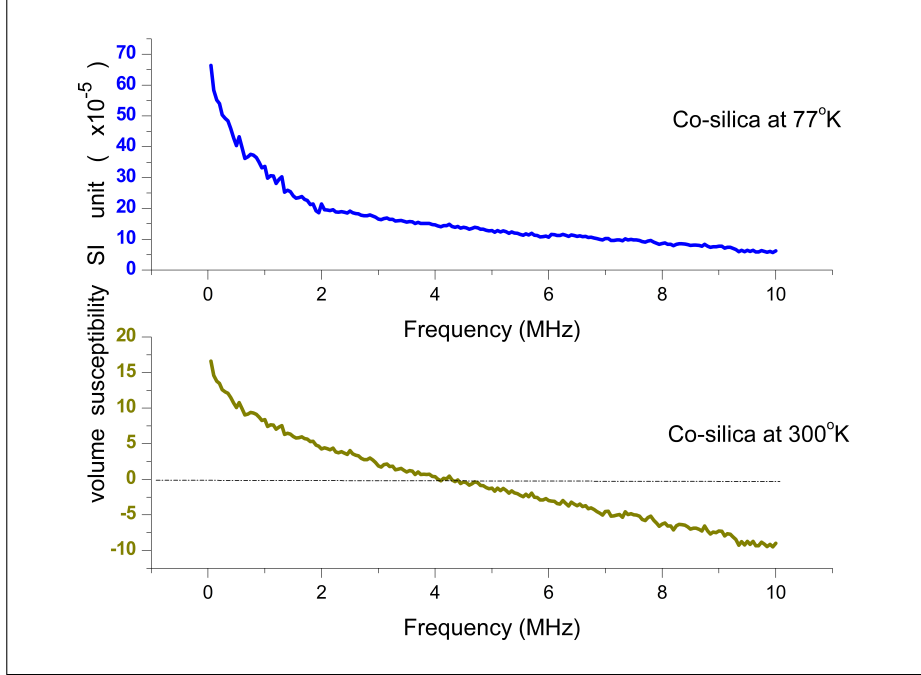


Figure 4.2: The volume susceptibility of cobalt-silica nano-particles against frequency of the applied field obtained from the simulation of $15 \times 15 \times 15$ nano-magnetic assembly

Dynamics of magnetic nano-particles in double well potential coupled to each other in a non magnetic medium is presented. These nano-particles are dipole equivalents and the interaction between the dipoles is considered to be long range and it is either attractive or repulsive based on the relative orientations of the dipoles. This dual nature of interaction is important in the occurrence of the cooperative phenomenon in the dipole system of nano-magnets. Due to the presence of oscillatory field, the system of nano-particles releases energy with a delay greater than one fourth of the time-period of the applied field. This is discussed in detail in the next section.

Table 4.1: Conditions at which negative susceptibility has been observed of an ensemble of cobalt nano-magnets

System size	Diameter of nano-magnets (nm)	Particle Separation (nm)	Magnetizing current (mAmp)	Crossover frequency (MHz)
7x7x7	6.5	8.8	10.0	10
7x7x7	7.5	10.0	12.0	10
9x9x9	6.5	10.0	17.0	25
9x9x9	7.5	10.0	17.0	13
9x9x9	7.5	11.0	13.0	13
11x11x11	7.5	10.0	18.0	13
15x15x15	7.5	10.0	20.5	20
15x15x15	7.5	11.0	19.2	10
15x15x15	7.5	15.0	11.2	8.9

4.5 Comments on Simulation Results

Observation of phase transition from para-magnetism to ferro-magnetism is quite common in literature, however the transition from para-magnetism to diamagnetism is rare [86]. We have observed a crossover from para-to-dia in an ensemble of coupled nano-magnetic dipole oscillators subjected to a periodic external magnetic field. Classically the ensemble can be looked as a coupled dynamical system with varying lags or time delays. These time delays are the relaxation times of the nano-magnets. Nano-magnetic ensemble tries to orient itself parallel to the applied magnetic field in two steps. As the dipole interaction energy of the nano-magnets at the surface is minimum the switching initiates at the surface of the ensemble. The switching of the nano-magnets at the surface sets off a series of switching in the ensemble due to the sudden change in the interaction field caused by the neighbor reversal [13][82]. Hence, this alignment process penetrates gradually into the sub-surface which makes the dipolar orientation in the outer shell aligned with respect to the applied field, whereas the core retains in its initial state. Thus, in addition to the external field, the dipoles in the core also experiences a magnetic field generated collectively by the dipoles of the shell. The thickness of the shell increases with time

and the opposing magnetic field created by the shell becomes appreciably higher to trigger a large number of nano-magnets in the core which can be looked as a cooperative switching. Initially, a small numbers n_0 of nano-magnets at the surface initiate switching. This number increases progressively with time steps to $n_1, n_2, n_3, \dots, n_c$. At the time of cooperative switching n_c becomes relatively large. The net magnetization M of the ensemble of nano-magnets under the oscillatory magnetic field $h_0 e^{i2\pi ft}$ is the superposition of the individual oscillators as given in the Eq. (4.19). Here n_0, n_1, \dots, n_c depend on the geometry and size of the ensemble and $\theta_0, \theta_1, \dots, \theta_c$ are the corresponding phase lags of those oscillators.

$$M e^{i(2\pi ft + \theta_r)} = M_s V (n_0 e^{i(2\pi ft + \theta_0)} + n_1 e^{i(2\pi ft + \theta_1)} + n_2 e^{i(2\pi ft + \theta_2)} + \dots + n_c e^{i(2\pi ft + \theta_c)}) \quad (4.19)$$

The phase θ_r associated with the net magnetization M with respect to the applied magnetic field predominantly depends upon θ_c because n_c is very large compared to $n_0, n_1, \dots, etc.$ and the phase is given in Eq. (4.20).

$$\theta_r = \tan^{-1} \frac{n_0 \sin \theta_0 + n_1 \sin \theta_1 + \dots + n_c \cos \theta_c}{n_0 \cos \theta_0 + n_1 \cos \theta_1 + \dots + n_c \cos \theta_c} \quad (4.20)$$

When θ_r is greater than $\pi/2$, the system exhibits diamagnetism in the interacting dipolar system, provided the energy of interaction is comparable to the Zeeman energy and anisotropy energy of the nano-magnets. This phenomena is observed in Ni-silica, Co-silica nano-magnetic ensembles at lower temperatures like $77K$ also. At liquid Nitrogen temperature, the frequency of the crossover is reduced by several kilo Hertz compared to room temperature. This is because the relaxation time reduces at lower temperatures and the cooperative switching gets delayed. The temporal location of this cooperative switching with respect to the applied field determines

the degree of paramagnetism or diamagnetism of the ensemble, as shown in Fig. 4.3 and Fig. 4.4.

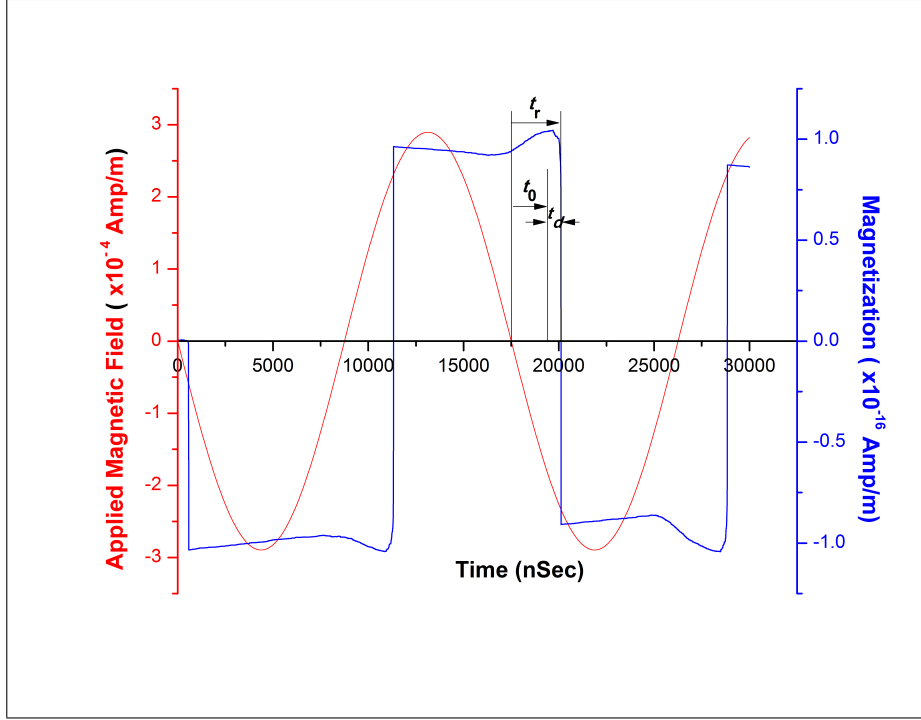


Figure 4.3: The observed magnetization of the ensemble of the nano magnets due to the application of sinusoidal magnetic field of low frequency $t_r < T/4$ as observed in the simulation results. The overall magnetization is paramagnetic at low frequency.

After a time gap of t_0 , the reversal of magnetization creeps into the sub-surface of the ensemble until a critical shell thickness develops to initiate the cooperative switching in the core. The system inherently takes time, $t_d (= t_1 + t_2 + \dots + t_c)$ to develop the critical shell thickness. As a result, the cooperative switching is further delayed by t_d over t_0 , where t_d depends on relaxation time of the nano-magnets. The transition time of total reversal of population of nano-magnets, $t_r = t_0 + t_d$. This t_r is the governing factor of the state of the overall magnetization. The maximum value of t_0 is $T/4$ when $h_0 = (h_K - h_{dd}(0))$, where $h_{dd}(0)$ is the dipolar interaction field at the surface. In that case, t_r is always greater than $T/4$ and the ensemble should show diamagnetism for all frequencies. If h_0 is greater than $(h_K - h_{dd}(0))$, t_0 is less than $T/4$, and the contribution of t_d becomes important to make t_r greater

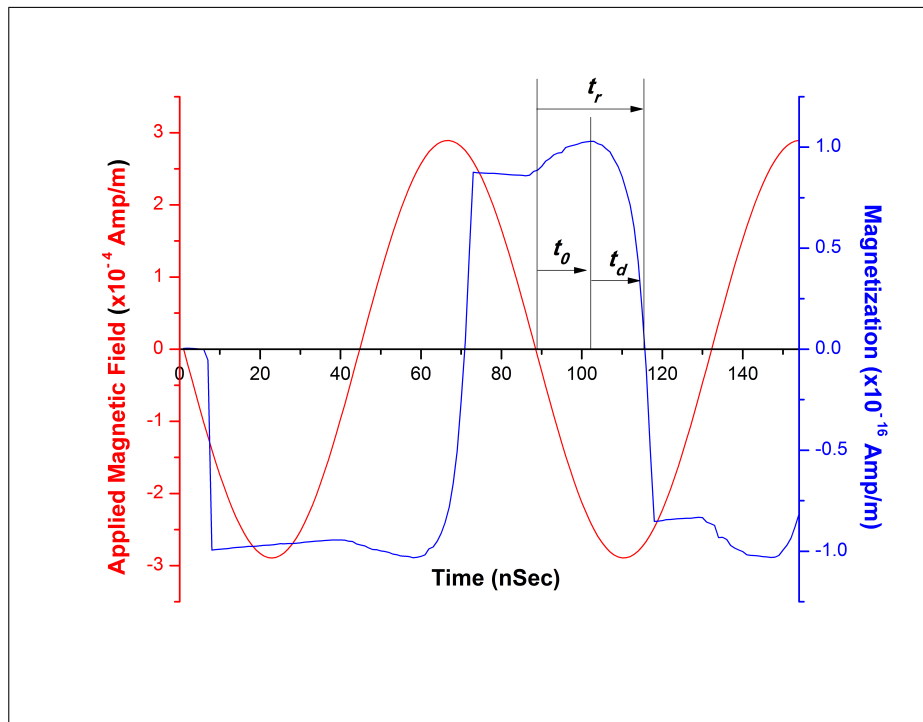


Figure 4.4: The observed magnetization of the ensemble of the nano magnets due to the application of sinusoidal magnetic field of high frequency $t_r > T/4$ as observed in the simulation results. The overall magnetization is diamagnetic at high frequency.

than $T/4$. This can be achieved by increasing the frequency or by increasing the relaxation time of the nano-magnets or the combination of both.

4.6 Conclusion

The results presented in Table: 4.1 and in Fig. 4.2 has been analyzed and presented in this section. Comparison of simulation results of cobalt superparamagnetic particles is given below to sum-up the variations of crossover frequency with particle size, particle spacing, field strength, temperature and system size.

1. Effect of particle size: Larger particle size of the nano-particles results in higher magnetic moment of the dipole and longer relaxation time. Therefore, crossover frequency will be lower for bigger particle size. In Table: 4.1, $9 \times 9 \times 9$ system, 6.5 nm particle size shows crossover frequency of 25 MHz and 7.5 nm particle size shows 13 MHz.
2. Effect of field strength: For higher field strength (200 Amp/m and above), when Zeeman energy is more than twice the anisotropy energy (2κ), this crossover cannot be observed because the dipoles will be forced to follow the external field. The system is simply continues to be paramagnetic.
3. Effect of temperature: Simulation is done at 300°K and 77°K temperatures. The crossover frequency reduces with reduction in temperature. This is because; the relaxation frequency is less at low temperature according to Neel relaxation expression.
4. Particle spacing: The crossover frequency reduces with larger spacing because interaction potential is less for larger separations.
5. Effect of array size of the system: Smaller than $7 \times 7 \times 7$ of the system is fully paramagnetic and no diamagnetism is observed. This phenomenon of para-to-

dia susceptibility takes place in the array due to a cooperative switching. If the size of the array does not exceed a minimum value, cooperative phenomenon does not occur and system continuously behaves as paramagnetic.

Chapter 5

Crossover of Susceptibility: Experimental Verification

Crossover of susceptibility in frequency domain is established in the previous chapters. Experimental verification of this finding is essential to establish its importance in real life applications. Various types of dipoles are available in nature as explained in the introductory section of the chapter 1. Two types of simulations are carried out in this work. In chapter 3, magnetic needle type dipole oscillators are simulated and in chapter 4, nano-magnets are simulated under external field. In both the simulations, the oscillating objects (magnetic needles or nanomagnets) are able to oscillate about its centre. The dipoles are immobilized in the array, but allowed to oscillate. To do a similar arrangement in the experimental setup, Ni-silica and Co-silica nano-composites are experimented separately. Here, nano sized magnetic particles are embedded in the silica matrix and undisturbed magnetic moments are aligned in their respective easy axis. These nano-composites are equivalent to the simulation arrangements. In powdered form, these metal nano-composites are tested in the AC susceptometer. The size of the nano-composite powder is in the order of microns. Therefore, a single nano-composite powder is equivalent to a cluster

of nano-magnets fixed in the silica matrix. In the simulation, nano-magnets are arranged in a regular spacing but in the experiments they are randomly distributed and their easy axes are also randomly oriented. Here, the magnetic nano-composites are chosen to establish this frequency dependent crossover of susceptibility.

5.1 Sample Preparation : sol-gel process

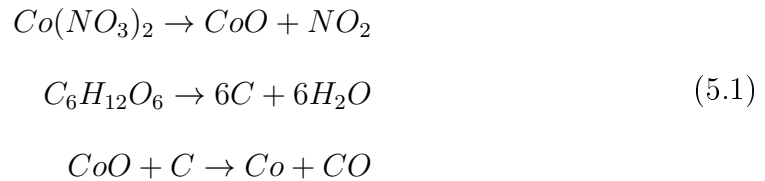
The sol-gel process [88] is a wet-chemical technique (also known as chemical solution deposition) used primarily for the synthesis of materials starting from a chemical solution, which acts as the precursor for an integrated network of either discrete particles or network polymers. The sol-gel process involves the evolution of networks, the formation of a colloidal suspension (sol) and gelation of the sol to form a network in continuous liquid phase (gel). The precursors used for synthesizing the colloids generally consist of metallic ions and ligands, which are the elements surrounded by various reactive species. Alkoxysilanes (e.g., Tetramethyl orthosilicate, TMOS and tetraethyl orthosilicate, TEOS) are the most popular precursors as they react readily with water. In general, sol-gel formation occurs in five steps: Hydrolysis, alcoholysis, Water and alcohol condensation for the Growth of particles and agglomeration of particles followed by the formation of networks throughout the liquid medium resulting in thick gel.

Several initial conditions are necessary in the process *viz.*, pH level, temperature of the reaction, reagent concentration, duration of reaction, type and concentration of catalyst, molar ratio of $H_2O : M^+$ (where M^+ is the cation), aging temperature and time of gel formation, etc. It is required to control these parameters to vary the structural, magnetic, electrical and optical properties of the derived inorganic sol-gel network. The chemistry involved in sol-gel process is important for proper preparation of the nano composites.

Tetra-ethyl ortho-silicate ($Si(OC_2H_5)_4$) [TEOS] is the source of Si for silica-gel formation and it is used as the precursor to prepare silica gel. Here, $R = -C_2H_5$ in the reaction. Subsequent condensation reactions involving silanol group (Si-OH) produce siloxane bonds (Si-O-Si) along with the by-products: water and alcohol. This gives the required sol. After condensation, the sol is aged for a certain time to form gel of long chains of siloxane bonds ($HO\cdots-Si-O-Si-O-Si-O-Si\cdots-OH$), terminated by hydroxyl groups, resulting in the thickening of the sol to form the gel. Finally, the gel is heated up in oxygen (or air) atmosphere to get SiO_2 .

5 ml of TEOS and 5 ml of ethyl alcohol have been taken in a beaker for the preparation of one solution. In another beaker, 5 ml of double distilled water, 5 ml of ethyl alcohol, required amount metallic salt nitrate (or chloride) and dextrose have been added. Both the beakers have been kept on continuous stirring at room temperature using a magnetic stirrer for about 30min. The metallic salt solution has been added drop by drop in other beaker in stirring condition. The total mixture in the first beaker has been stirred for another 30 minutes. Thereafter whole system has been left undisturbed for solidification for 2-3 weeks.

In the preparation of co-silica nano composites, dextrose is used as reducing agent and cobalt nitrate is the metallic solution and the following reactions take place.



The following is the stoichiometric calculation of 20% Co-silica nano-composite.

Molecular wt. of $Si(OC_2H_5)_4 = 208.33$ gm/mol

Molecular wt. of $SiO_2 = 60.08$ gm/mol

Molecular wt. of Co = 58.93 gm/mol

Molecular wt. of $Co(NO_3)_2 \cdot 6H_2O$ = 291.03 gm/mol

Molecular wt. of $C_6H_{12}O_6$ = 180.15 gm/mol

5 ml of TEOS and 5 ml of ethyl alcohol has been mixed throughly in a beaker. Density of TEOS is approximately 1gm/cc. Therefore, 5 gm of TEOS is taken. In another beaker, 5 ml of double distilled water with 5 ml of ethyl alcohol is mixed. In the second beaker, a measured quantity of cobalt nitrate and dextrose are also to be mixed throughly. Therefore, in the net solution ratio of $TEOS : H_2O : C_2H_5OH$ is equal to 1:1:2. The amount of cobalt nitrate and dextrose required in the preparation is calculated below for 20%wt. cobalt in SiO_2 matrix.



One mole of SiO_2 is obtained from one mole of TEOS. Therefore, 208.33 gm TEOS gives 60.08 gm SiO_2 . 5gm of TEOS is taken so, 5 gm TEOS gives $\frac{60 \times 5}{208} = 1.442$ gm SiO_2

For 20% Co in silica matrix : Amount of Co = 20wt% of SiO_2

$$= 0.20 \times 1.442 \text{ gm}$$

$$= 0.2884 \text{ gm cobalt is required.}$$

From the chemical reaction, one mole of Co comes from one mole of CoO that means 58.93 gm Co comes from 74.93 gm CoO .

As 0.2884 gm of cobalt is required then, 0.2884 gm Co comes from $\frac{0.2884 \times 74.93}{58.93} = 0.3667$ gm CoO .

Following is the calculation to find the required amount of cobalt nitrate:

74.93 gm CoO comes from 291.04 gm of $Co(NO_3)_2 \cdot 6H_2O$

0.3667 gm CoO comes from $\frac{291.04 \times 0.3667}{74.93} = 1.424$ gm of $Co(NO_3)_2 \cdot 6H_2O$. Therefore,

1.424 gm of $Co(NO_3)_2 \cdot 6H_2O$ is required in the process.

Following is the calculation for the required amount of dextrose:

In this process carbon acts as reducing agent. Dextrose is the source of required amount carbon in the reaction.

One mole (12 gm) carbon is required to reduce one mole (74.93 gm) of CoO into metallic cobalt.

Then, 0.3667 gm CoO is obtained by the reduction process of $\frac{12 \times 0.3667}{74.93} = 0.0587$ gm of carbon. Therefore, 0.0587 gm of carbon is required in the reaction.

72 gm of carbon comes from one mole (180 gm) of $C_6H_{12}O_6$

0.0587 gm of carbon comes from $\frac{180 \times 0.0587}{72} = 0.1468$ gm of $C_6H_{12}O_6$

Therefore, 0.1468 gm of dextrose is required.

The gel is put into a silica boat. The boat is inserted into the constant hot zone of a tube furnace for heat treatment. A constant flow of nitrogen is allowed through the furnace to maintain an inert atmosphere within it. The temperature of the furnace is then raised till it reaches $900^\circ C$ and is held constant at this temperature for duration of 30 minutes. Thus, cobalt nano-composite is prepared.

Similarly, in the preparation of Ni-silica nano composites, dextrose is used for reducing agent and nickel nitrate is the metallic solution and the stoichiometric calculations are given in the Appendix G.

5.2 Sample Characterization

It is important to have the knowledge of topographic details and internal details of the nano-composites developed in the sol-gel process. The morphological characterization of the magnetic nano-composites has been done by scanning electron microscope (FESEM) and high resolution transmission electron microscope (HRTEM).

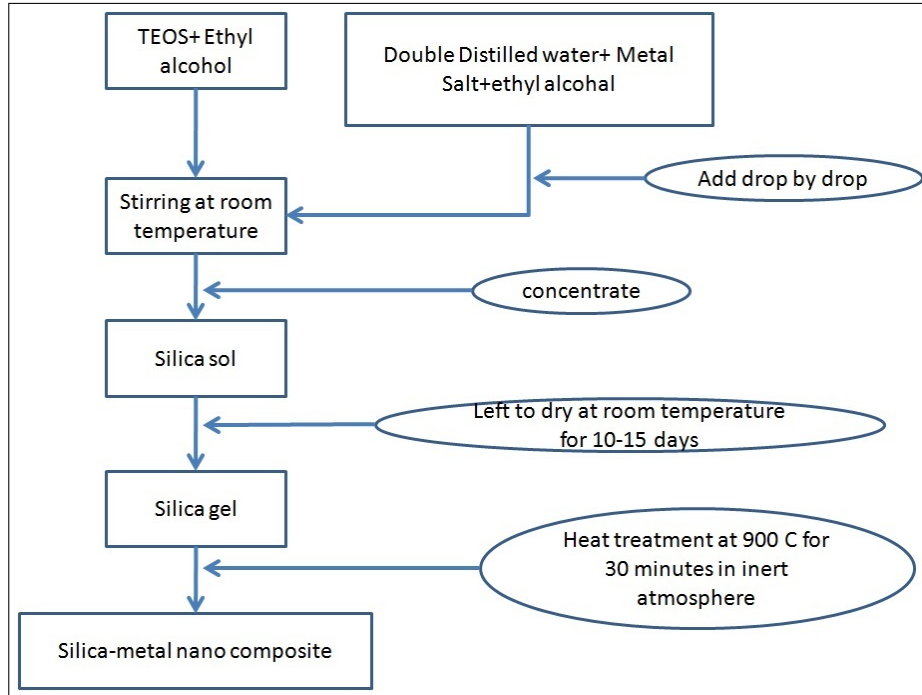
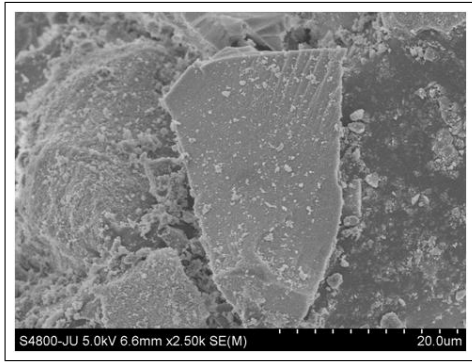


Figure 5.1: Schematic representation of sample preparation of magnetic nano-composite.

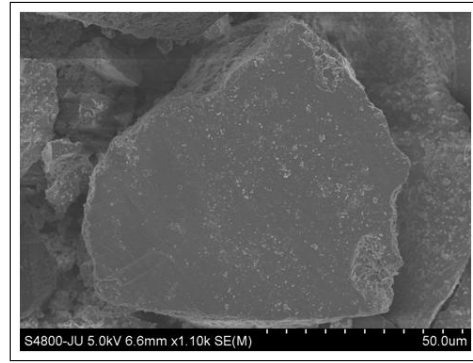
The synthesized powder sample has been placed on a conducting carbon tape, and a field emission scanning electron microscope (FESEM) (Hitachi S4800) is used to observe the morphological details of the sample. FESEM micrographs have been used to visualize very small topographic details on the surface of samples (as shown in Fig. 5.2a and 5.2b).

The existence of the crystallinity of the nano particles has been established by the selected area diffraction. From the TEM images (in Fig. 5.3) of cobalt and nickel nano-composites we conclude the average distance among the nano particles embedded in the silica matrix is around 15 *nm* and average size of the nano-magnets inside the composite are of the order of 6.5 *nm* to 7.5 *nm*.

Co-silica nano-magnetic composite in powder form has been tested to measure the susceptibility. Ac susceptibility of the samples at high frequencies have been measured by an in-house developed susceptometer. The following section describes

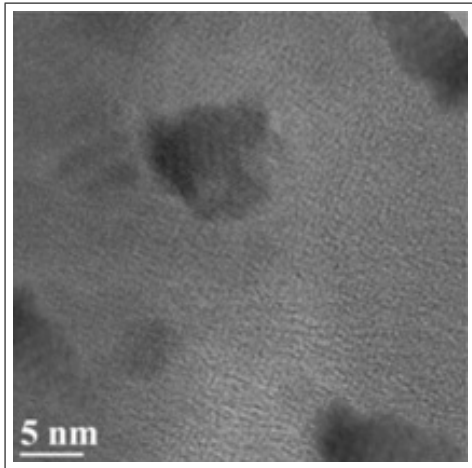


(a) FESEM Cobalt 20%.

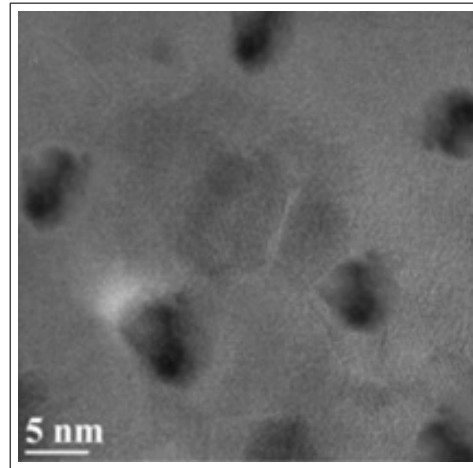


(b) FESEM Nickel 20%.

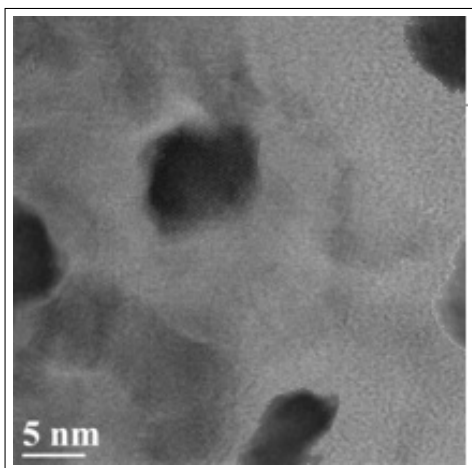
Figure 5.2: FESEM micrographs reveal the topographic details of the powdered nano-composites developed by sol-gel technique. These micrographs are the silica flakes embedded with Co or Ni nano-particles. The structure and size determination of these metal nano-particles are carried out by HRTEM.



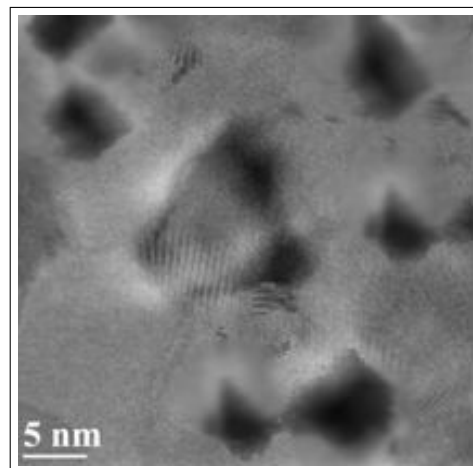
(a) Cobalt 20% HRTEM



(b) Nickel 10% HRTEM



(c) Nickel 20% HRTEM



(d) Nickel 30% HRTEM

Figure 5.3: HRTEM micrographs reveal average size and separation of the nano-magnets inside the powdered nano-composites as synthesized by sol-gel technique.

the susceptometer that has been developed as a part of this thesis work and that can also be operated in low magnetic field and at high frequencies.

5.3 Susceptometer Development

A simplified instrumentation with nominal circuitry has been developed to measure accurately, in- and out-of-phase complex magnetic susceptibility of the magnetic samples. To achieve uniform field, a shape modified absolute coil has been adopted in the measurement system. An innovative phase detection circuit has been incorporated to measure the complex susceptibility at high frequencies. In this section, design and performance of the instrumentation is described. Calibration process of the susceptometer and how to measure susceptibility of the magnetic nano-composites is also discussed here. This susceptometer is also suitable for liquid samples viz., ferro-fluids, blood samples etc.

Susceptibility measurement setups are predominantly non contact type and based on the principle of comparison of two unequal mutual inductances. The phase measurement as proposed here is a very simple analog technique, can replace the high cost lock-in amplifier for normal laboratory use. The principle and methodology to obtain the complex susceptibility of the samples without using lock-in amplifier is explained in the following sections. Small coils in the susceptometer are wound on a specially shaped bobbin to avoid the non-homogeneity of the magnetic field. This susceptometer is self-inductance type and the detail of its design is explained below.

The purpose of this susceptometer development is very significant. Low magnetic field and high frequency of operation are the two important criteria of this development. Because of low magnetic field, very weak signal will be generated in mutual inductance type susceptometer. So, self inductance type susceptometer has been

decided to develop, where large quantity of sample will be taken. Usually, samples are taken in microliter so that volume of the sample is small. Small volume ensures uniformity of magnetic field on the sample. To avoid this limitation, shape modified bobbin is used and measurable output signal is achieved in the susceptometer.

5.3.1 Self-inductance type Susceptometer: Working Principle

The differential of magnetic flux (Φ) in the solenoid with respect to the current (I) is the measure of self inductance of the coil. The flux inside a coil depends on the magnetic permeability of the core, and hence, the self inductance of the test coil, L_s is related to the magnetic properties of the sample inserted in it, given by Eq. (5.3). Here χ_{ac} is the magnetic susceptibility of the sample and other symbols have their usual meanings.

$$L_s = \mu_0(1 + \chi_{ac}) \frac{d}{dI} \int H.ds \quad (5.3)$$

In the case of air core, the self-inductance L_0 is reduced to

$$L_0 = \mu_0 \frac{d}{dI} \int H.ds \quad (5.4)$$

From Eq.(5.3) and (5.4), the change in self-inductance due to the insertion of the sample in the coil is proportional to the a.c. susceptibility [90]. Hence, χ_{ac} of the samples at different frequencies and temperatures can be obtained by a well calibrated precise inductance meter. In this instrumentation, the inductance of the coil is obtained by a formula based on the voltage drop across the inductor coil. If it is assumed that a current I_{rms} is passing through the coil and RMS voltages developed across the coil are v_{rms-0} and v_{rms-s} for air core and the core filled with sample material respectively. If r is the intrinsic resistance of the coil, then the

change in self-inductance can be represented by Eq. (5.5) which is proportional to the susceptibility of the sample. The constant of proportionality, κ depends on the coil parameters, material volume fraction, fill factor, geometrical arrangements, etc. of the sample in the coil.

$$\chi_{ac} = \kappa \Delta L = \frac{\kappa}{2\pi f} \left\{ \sqrt{\frac{v_{rms-s}^2 - r^2}{I_{rms}^2}} - \sqrt{\frac{v_{rms-0}^2 - r^2}{I_{rms}^2}} \right\} \quad (5.5)$$

For phase measurement, let us assume $V_0 e^{i\omega t}$ is the voltage applied to the L-R circuit (shown in Fig. 5.4) and θ is the phase lag between the voltage source and the current passing through the circuit.

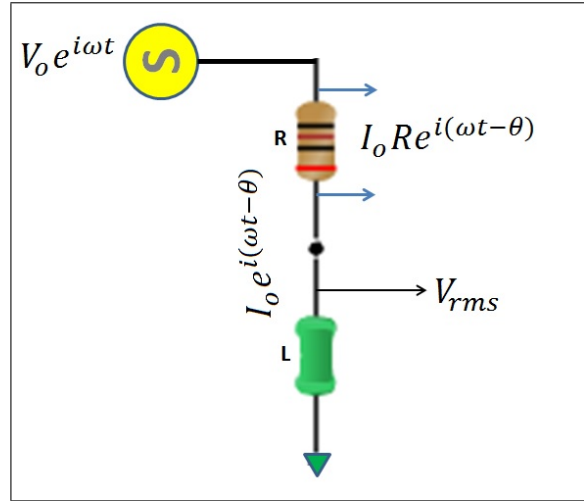


Figure 5.4: $V_0 e^{i\omega t}$ is the voltage applied to the LR circuit, and there is a phase lag (θ) between the voltage source and the current passing through the circuit.

A constant current, is maintained through the L-R circuit. $I_0 e^{i(\omega t - \theta_0)}$ is the current passing through the air-core coil, whereas $I_0 e^{i(\omega t - \theta_s)}$ is the current passing through the coil with the sample in the core. Therefore, the voltage drops across R are $I_0 R e^{i(\omega t - \theta_0)}$ and $I_0 R e^{i(\omega t - \theta_s)}$ for the air core and sample respectively. By adding these two voltages, one can get the resultant amplitude B that carries the phase $\psi = (\theta_s - \theta_0)$ linked by the sample in the coil with respect to air (θ_0), as given in Eq.(5.6).

$$\begin{aligned}
& I_0 R e^{i(\omega t - \theta_s)} + I_0 R e^{i(\omega t - \theta_0)} \\
&= 2I_0 R \cos\left(\frac{\theta_s - \theta_0}{2}\right) e^{i\left(\omega t - \frac{\theta_s + \theta_0}{2}\right)} \\
&= B e^{i\left(\omega t - \frac{\theta_s + \theta_0}{2}\right)}
\end{aligned} \tag{5.6}$$

The phase ψ is obtained from the ratio of B and the voltage drop across R (v_s or $v_0 = I_0 R$) as follows.

$$\psi = 2 \cos^{-1} \frac{B}{2v_0}. \tag{5.7}$$

From ψ the complex susceptibility is obtained as given in Eq. (5.8).

$$\chi_{real} + i\chi_{imaginary} = \chi_{ac} \cos \psi - i\chi_{ac} \sin \psi \tag{5.8}$$

5.3.2 Measurement Methodology

In this technique, susceptibility measurement is a two step process. Voltages are measured with sample and then without the sample inside the coil. This double measurement is not popular and nobody uses this method in automated measurement of susceptibility. This is a limitation of this self-inductance type measurement technique but here it is modified by using a pair of matched coils. So, instead of single source, a pair of similar sources are required as shown in Fig. 5.5. The system has been automated using a two channel arbitrary function generator (Tektronix AFG 3102), a 16-bit data acquisition module (Advantech USB-4716), an analog hardware circuit board (shown in Fig. 5.5) and a personal computer for computation, data storage and control. Two matched coils (instead of a single L-R circuit) are taken where, one coil L_0 acts as a reference with respect to the test coil L_s . The coils are excited separately by AFG 3102 through the high precision foil resistor R ($\pm 0.005\%$ tolerance, $\pm 2.0ppm/^\circ C$ temperature coefficient of resistance). These

resistors (R) act as a current to voltage converter in the circuit. The RMS voltages of v_s and v_o across these resistors are made equal by further adjusting the amplitude of the function generator of the sample coil. Now the current ($I_{rms} = v_{rms-s}/R = v_{rms-o}/R$) passing through both the coils is equal. According to Eq. (5.5), the absolute value of the ac susceptibility of the sample is obtained by the RMS voltages (V_{rms-s} and V_{rms-o}) across the coils.

The sinusoidal voltages v_s and v_o across R also carry the phase information of the individual circuits. Now these voltages are superposed by an adder circuit; the phase associated by the sample can be derived from the RMS voltage B of the adder circuit according to Eq. (5.6) and (5.7).

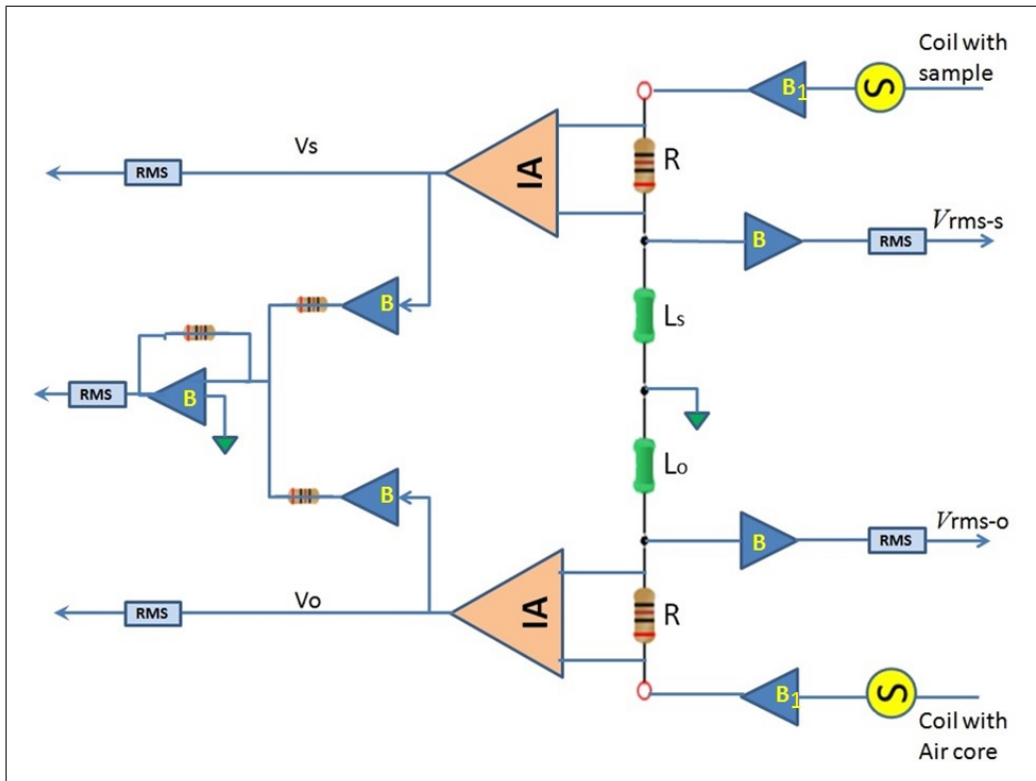


Figure 5.5: Block diagram of analog circuit

A software has been written in C programming language to interface AFG-3102, analog circuit board and USB-4716 with the computer. Computation block diagram given in the Fig. 5.6 shows the pictorial flow chart of the methodology. The starting

frequency and the amplitude are set from the graphical interface of the computer and the computer sends respective commands to either channels of the function generator. When sample is inserted inside the test coil, current imbalance occurs between the coils. The comparator C1 generates the correction factor and subsequently added to the set point. The command to the test channel of the function generator is generated according to the output of C2 and the current balance between the coils is reestablished. At this current balanced condition, v_{rms-s} and v_{rms-o} for sample and air core coils are respectively measured to compute the difference in inductance according to Eq. (5.5). This change in the inductance is proportional to the absolute susceptibility χ_{ac} of the material. The constant of proportionality, κ is derived by using a material of known susceptibility.

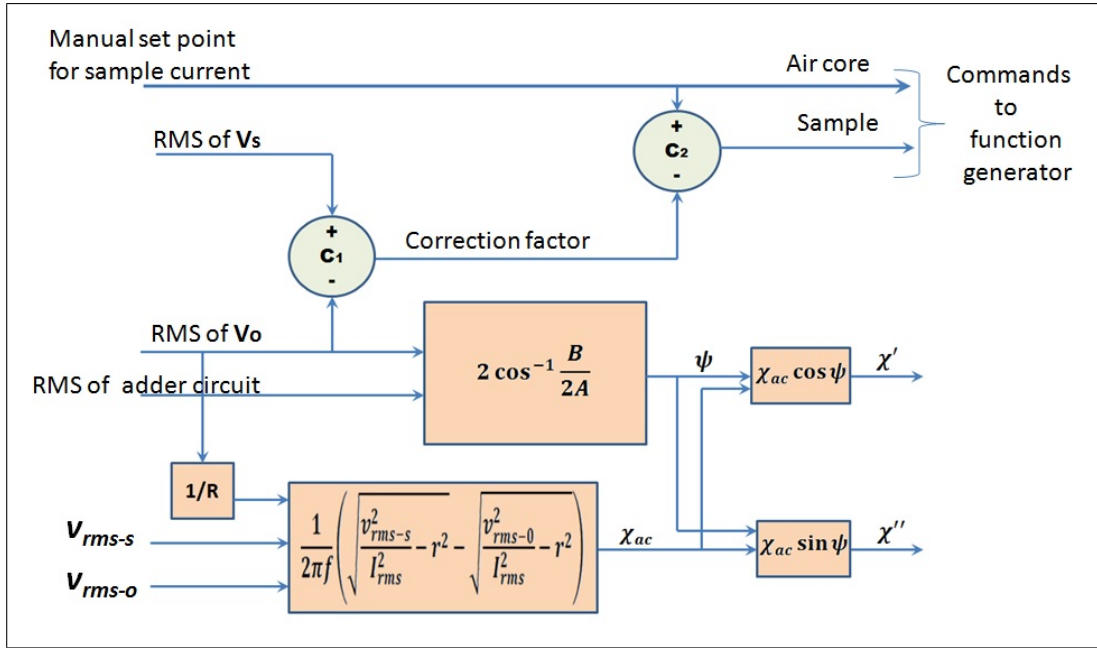


Figure 5.6: Block diagram of computational flow.

The next part of the software finds the phase associated with the sample. If the RMS voltage across R of the air-core coil is denoted by A (typically $I_0 R / \sqrt{2}$) and RMS voltage of the adder circuit is B , the phase associated by the sample is expressed by Eq. (5.8). Thus we calculate the in-phase and out-of-phase susceptibility of the sample for the set frequency given by Eq. (5.8).

The heart of the susceptometer is the solenoid coil that provides oscillatory magnetic field to the nano-composite sample. This susceptometer is self-inductance type and the coil acts as sensor to measure susceptibility. The solenoid coil is designed using genetic algorithm (GA) optimization technique as explained below.

5.3.3 Design of Coil : Field Uniformity

The uniformity of the magnetic field within a specified region of interest is defined as the measure of the maximum deviation of the magnitude of the magnetic field in relation to the average value within the specified domain [91]. Thus, the magnetic field uniformity, η is expressed in Eq. (5.9) where B_{max} , B_{min} and B_{avg} are the maximum, minimum and average values of the magnetic field within the working volume respectively.

$$\eta = 1 - \frac{B_{max} - B_{min}}{B_{avg}} \quad (5.9)$$

The magnetic field components (Fig. 5.7) produced at any arbitrary location (r, z) by an infinitely thin circular current loop of radius R_i carrying current I_i located at position Z_i , is given by Eq. (5.10) [93] where $\alpha = r/R_i$, $\beta = (z - Z_i)/R_i$, $\gamma = (z - Z_i)/r$, $Q = [(1 + \alpha)^2 + \beta^2]$, $k = (4\alpha/Q)^{1/2}$ and $K(k)$ and $E(k)$ are the complete elliptical integral functions of first and second kind respectively. The field, B_0 at the center of the coil is $\mu_0 I_i / 2R_i$. $B_z^i(r, z)$ and $B_r^i(r, z)$ are the axial and radial components of the magnetic field respectively.

$$\begin{aligned} B_z^i(r, z) &= \frac{B_0}{\pi\sqrt{Q}} \left[E(k) \frac{1-\alpha^2-\beta^2}{Q-4a} + K(k) \right] \\ B_r^i(r, z) &= \frac{B_0\gamma}{\pi\sqrt{Q}} \left[E(k) \frac{1+\alpha^2+\beta^2}{Q-4a} - K(k) \right] \end{aligned} \quad (5.10)$$

The total magnetic field of a solenoid of N_{turns} at a location (r, z) is given in

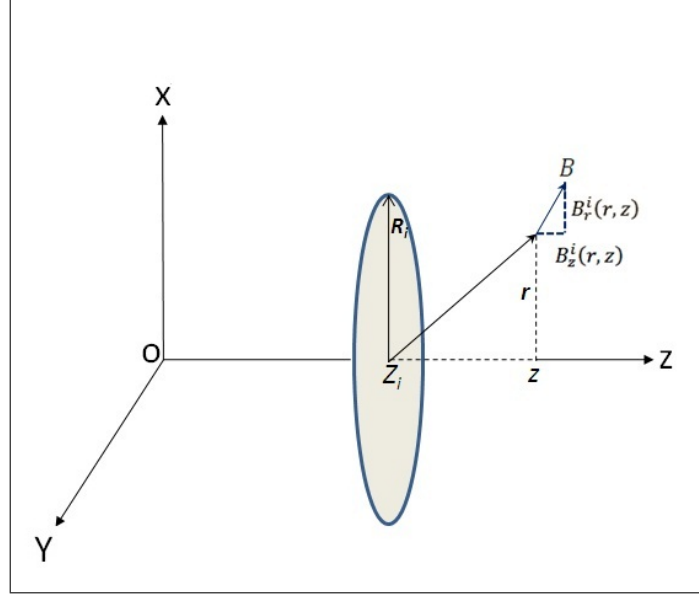


Figure 5.7: Axial and radial components of magnetic field due to a single circular current loop of radius R_i and carrying current I_i

Eq.(5.11). For uniformity of the magnetic field, $B_z(r, z)$ and $B_r(r, z)$ should be better than a specified η value for certain volume of interest.

$$\begin{aligned}
 B_z(r, z) &= \sum_{i=1}^{N_{turns}} B_z^i(r, z) \\
 B_r(r, z) &= \sum_{i=1}^{N_{turns}} B_r^i(r, z)
 \end{aligned}
 \tag{5.11}$$

It can be observed in Eq.(5.10) and (5.11) that the radial and axial magnetic field components inside the solenoid depend on the diameter of the current loops. Therefore, it is possible to change the strength of the magnetic field inside a solenoid by varying R along the axis of the coil. This is the motivation behind the shape modification of the coil to achieve field uniformity. Based on this understanding, many geometrical shapes are possible. Discrete changes of R with z have been suggested by Takahiro in large coil systems [92]. In the case of small coil, the discrete changes of radius of the bobbin in the form of collars impose discontinuities on the mechanical winding as well as the magnetic field distribution. This constraint has been eliminated in our design by a gradual variation of R with z . The basic

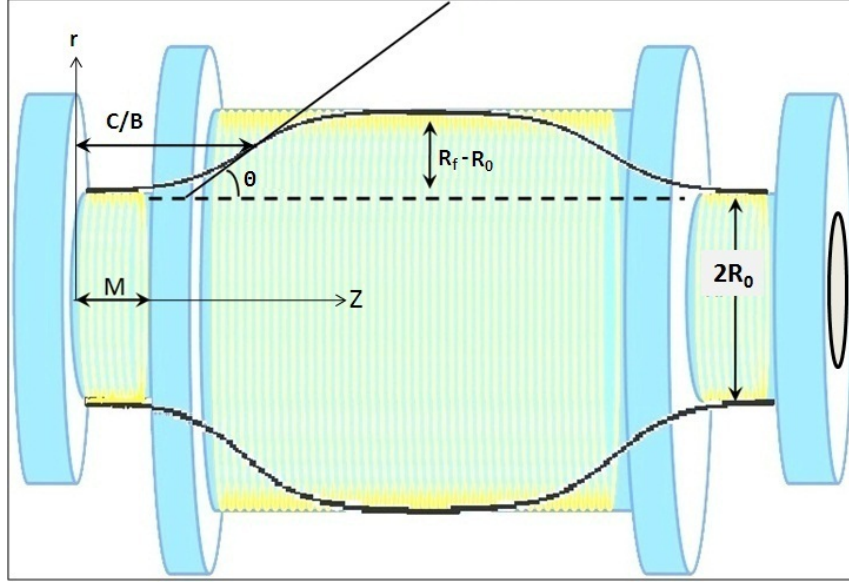


Figure 5.8: Combined representation of discrete step bobbin and shape modified bobbin. M is the field concentrated region for the discrete coil design. The profile of the shape modified bobbin, for the left half of its length, is defined by the generalized logistic function. The profile of the rest half is the mirror image of the former. $\theta = \tan^{-1} B \frac{R_f - R_0}{4}$ for the shape modified bobbin.

design criterion to make a uniform magnetic field inside a solenoid is to concentrate the magnetic field strength at the ends in the form of a field concentrator by reducing the radius of the bobbin compared to that at the center. Thus, sigmoid curve can be assumed to be a better replacement of discrete steps for the profile of the bobbin (see Fig. 5.8). The windings made on the curved surface of the bobbin will have a tendency to slip off the surface. Therefore, the frictional force between the bobbin and the windings should be sufficient to hold the windings in their position. Thus, the slope of the sigmoid curve at any location should not be more than the co-efficient of static friction (μ) between the windings of the coil and the bobbin surface. It is better to use glue after winding of the coil for rugged usage.

The silhouette of the bobbin is determined by the generalized logistic function as given in Eq. (5.12).

$$R(z) = R_0 + \frac{R_f - R_0}{1 + \exp(C - Bz)} \quad (5.12)$$

In the above equation, the lower asymptote, R_0 is the minimum radius at the ends of the bobbin. The upper asymptote, R_f determines the maximum allowable radius of the bobbin at the center. R_0 is one of the design parameters of the coil. Here C and B determine the location of the maximum growth rate of $R(z)$. The growth rate of the logistic curve $\frac{dR}{dz} = \frac{B(R_f - R_0)\exp(C - Bz)}{[1 + \exp(C - Bz)]^2}$ is slow initially and it increases to the maximum at the point where $z = \frac{C}{B}$, and $R = \frac{R_f + R_0}{2}$. Hence, $\tan \theta = \left(\frac{dR}{dz}\right)_{max} = B\frac{(R_f - R_0)}{4}$ should not exceed μ for the mechanical stability of the windings. Therefore, B is restricted by the coefficient of static friction μ as given in Eq. (5.13). The end field concentrator region of this solenoid is from $\frac{C}{B}$ to 0 as $\frac{dR}{dz}$ reduces at that region.

$$B = 4\frac{\mu}{R_f - R_0} \quad (5.13)$$

The basic parameters for any engineering design evolves from the requirement specifications. In this case, R_0 , μ , η (desired) and L (length of the solenoid) are the fundamental required parameters for the design of the miniature solenoid. Based on this input parameters, our aim is to find suitable values of R_f and C to achieve the desired η . Using the logistic function from Eq.(5.11) pare-to-optimal situation can be achieved. Keeping in mind the feasibility of windings over the bobbin and the dimensions of miniature coil, the optimization of R_f and C is obtained from the objective function. GA algorithm is inspired by the mechanisms of the natural evolution and they are usually effective in rapidly searching of the global optimum when a number of design variables need to be adjusted. Here R_f and C are taken from random pool of variables and their ranges are judiciously chosen. B is calculated from Eq.(5.13) which in turn provides the profile of the bobbin and the effective

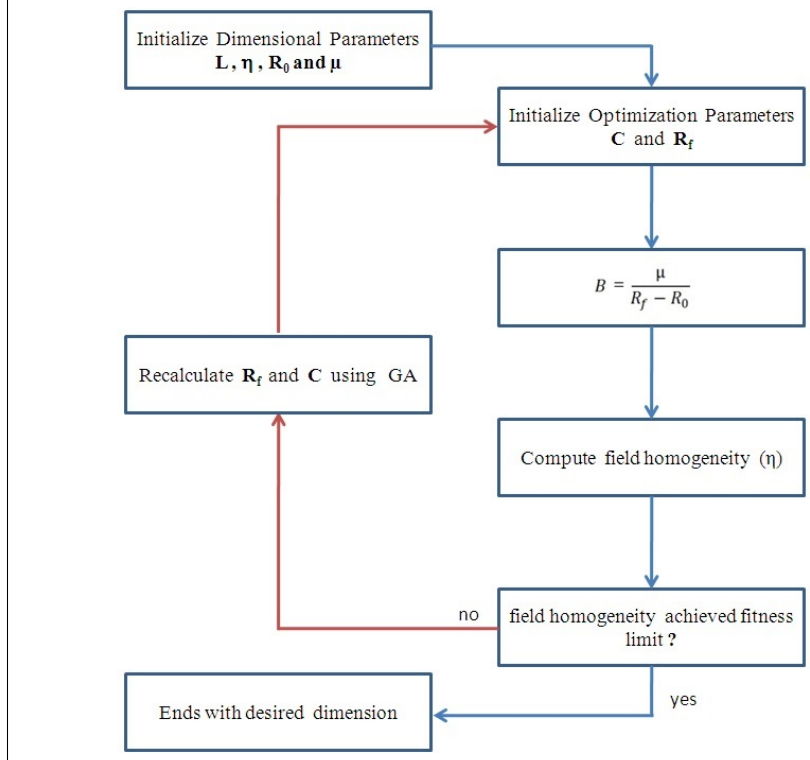


Figure 5.9: Flow chart for the optimization of the parameters R_f and C

length L_e of the curved profile is obtained from equation Eq. (5.14).

$$L_e = 2 \int_0^{\frac{L}{2}} \sqrt{1 + \left(\frac{dR}{dz}\right)^2} dz \quad (5.14)$$

The number of turns N_{turns} is equal to L_e/d of the coil where d is the diameter of the wire used to wound the coil. A simplified flow chart for GA computation is given in the Fig. 5.9. From the generated profile, the η is calculated from equation (5.9). This process is iterated to arrive at the desired η . Fig. 5.10 shows the axial field distribution and the optimum profile of the bobbin obtained by GA using MATLAB.

A miniature solenoid coil of length of 25 mm and $R_0 = 5$ mm has been constructed. If the ratio of the diameter (d) of the wire to the coil-diameter (D) is of the order of 10^{-3} then it can safely be considered that d is infinitesimal small. The

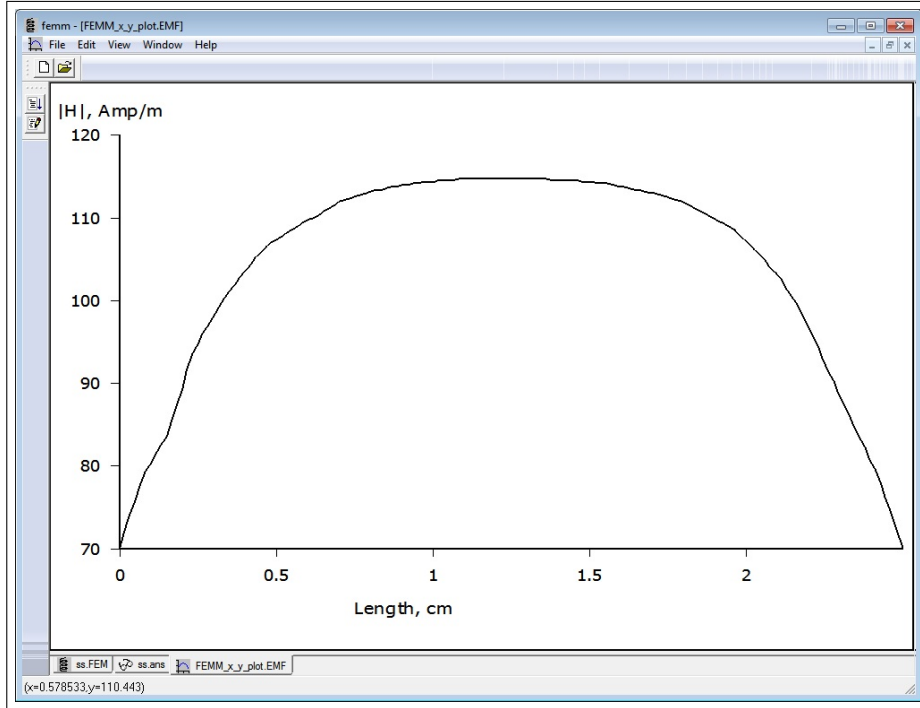


Figure 5.10: Axial field distribution and the optimum profile of the bobbin obtained by GA using MATLAB. The abscissa is in terms of the width (0.152 mm) of the wire (38 SWG). The values $R_f = 8.28 \text{ mm}$ and $C = 15.4$ as obtained by GA optimization.

coil has (38 SWG) 164 numbers of turns, the resistance of the coil is 34.5 Ohms and $\frac{d}{D} = 15.2 \times 10^{-3}$. The GA optimization technique has estimated the parameters $R_f = 8.28 \text{ mm}$ and $C = 15.4$ respectively. FEMM (Finite Element Modeling Method) simulation of the coil results in $\eta = 88\%$ when volume of interest is 80% of total volume. η improves reasonably (around 97%) if the volume of interest to be 60% of the total volume is considered. The designed parameters have been validated before fabrication of the bobbin by finite element method [61]. Axis symmetric modeling has been done considering the estimated dimension of the bobbin. The uniformity of the magnetic field from finite element simulation is shown in pseudo color in Fig. 5.11. In Fig. 5.12 it is shown the axial uniformity of field inside the coil as derived from the simulation. The figure indicates the uniformity of the field in the central part of the coil.

The uniformity of the magnetic field for the constructed coil has also been ver-

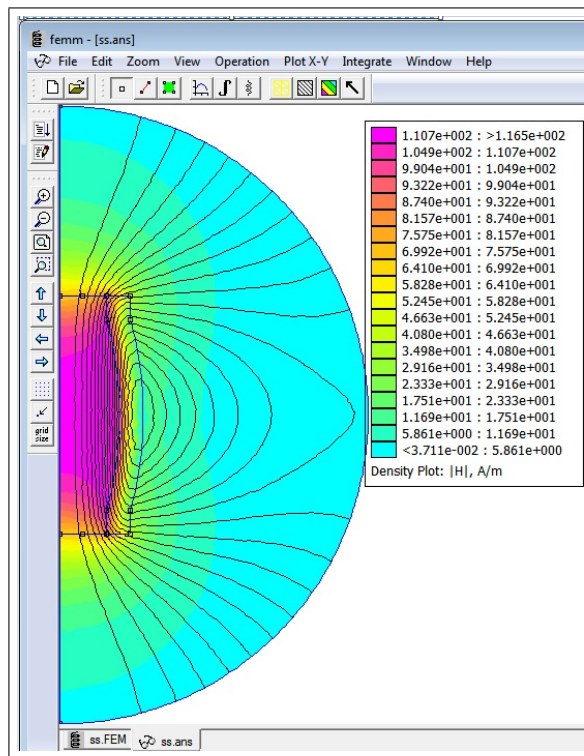


Figure 5.11: FEMM plot demonstrates uniformity of magnetic field at 600KHz.

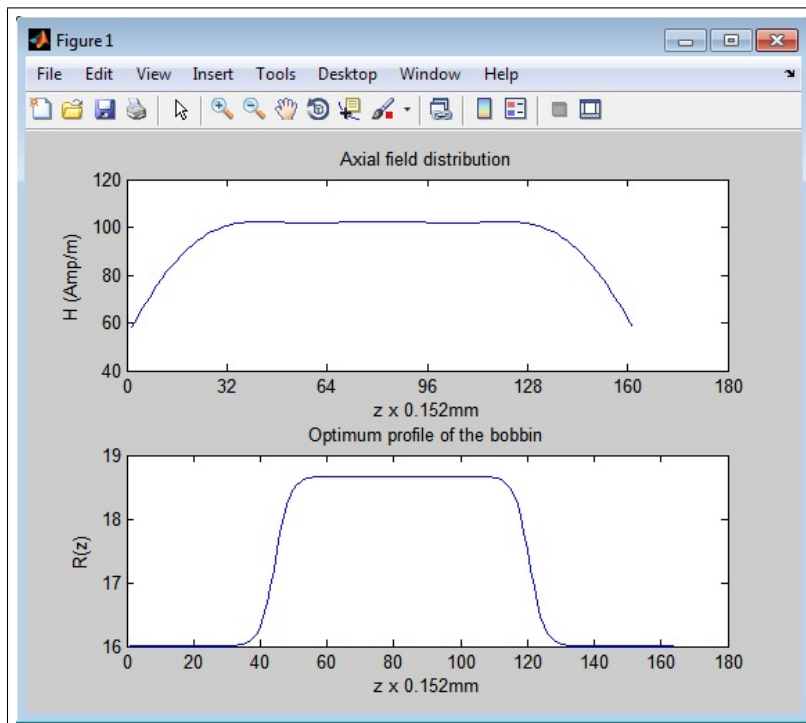


Figure 5.12: Axial homogeneity of the magnetic field obtained from FEMM simulation.

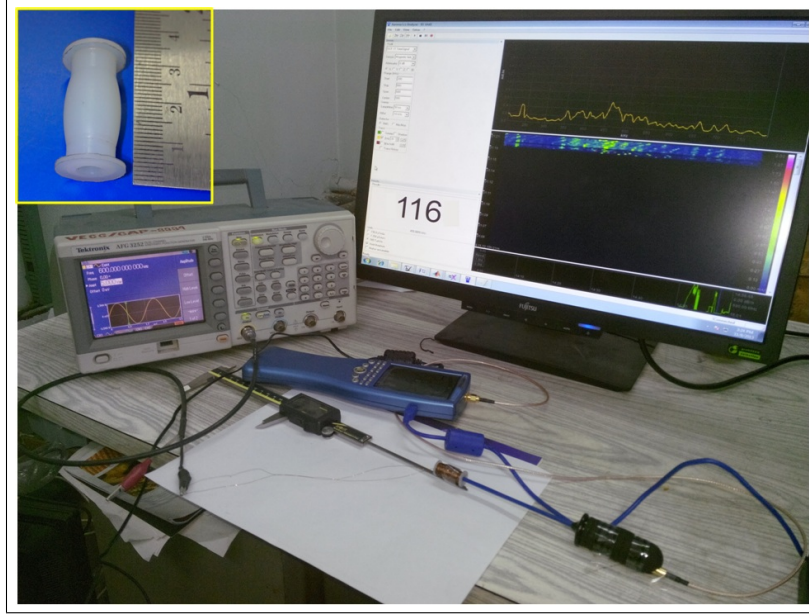


Figure 5.13: Experimental setup to measure the axial field distribution by SPECTRAN Analyzer. Inset of the figure shows the bobbin (at the left top corner).

ified by measuring axial magnetic field by a magnetic field sniffer-set (Model No. SPECTRAN NF5035 manufactured by Aaronia AG, Germany). The coil has been excited by alternating current of 10 mA at a frequency 600 kHz . The measurements made by the magnetic field probe has been compared with the computed results. To measure the axial field, the probe was positioned along the z -axis of the coil using a solid non-magnetic fixture outside the coil. The probe was inserted from one end into its central hole to the other end along the axis of the solenoid with the help of a slide caliper. The field was measured throughout the length of the coil axis by shifting the fixture along the axis in 1 mm increments. Fig. 5.13 shows the complete experimental setup used and the fabricated bobbin for the construction of the miniature solenoid. Fig. 5.14 shows the experimental results obtained from this setup.

The inductance of a coil is usually very precise at low frequencies but it varies non-linearly at higher frequencies. A pair of matched coils has been used, so that the noise picked-up by the pair of coils is nullified by subtraction. The frequency

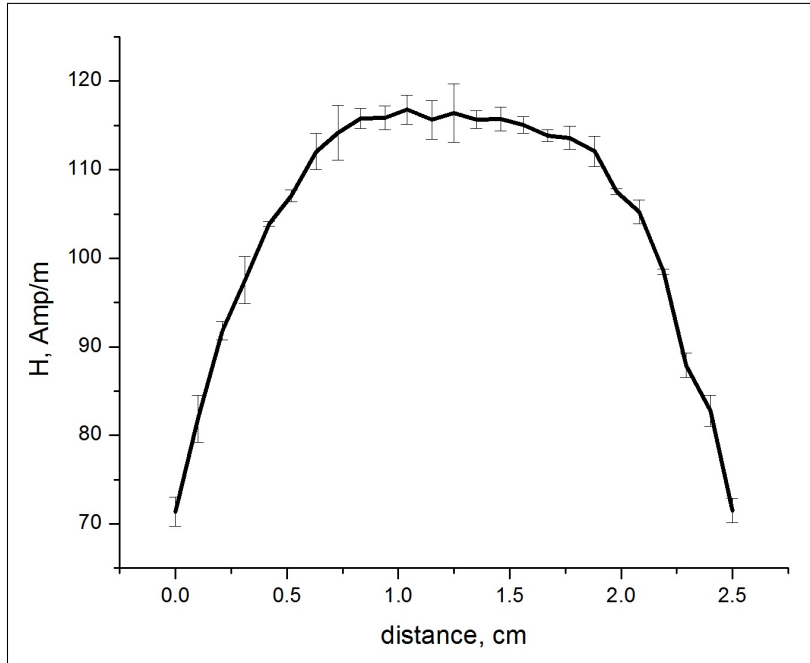


Figure 5.14: The axial field distribution obtained from the experimental setup shown in the Fig. 5.13.

response of the coils has been verified by a vector network analyzer (Agilent, Model No. N5239A). The s_{21} network analyzer data has been converted into impedance plot as shown in Fig. 5.15. The figure shows that the coil has a resonance at around 800 kHz. A generalized design procedure for generation of uniform magnetic field inside a miniature cylindrical coil is presented. Optimization technique of the design process is addressed in detail. Central field uniformity and low stray field have been achieved inside the coil. η has been improved to 97% if 60% volume of interest is considered. The presented procedure is useful in the development of any small magnetic gadgets and it supplements the concept of concentrator coils. For example, in tiny eddy current probe design, ferrite cores are used to focus the field lines. In that case, the probe becomes non-linear over frequency range due to the presence of ferrite core. A shape modified coil based on the above procedure has been used in the table top susceptometer for the measurement of susceptibility of nano-magnetic composites.

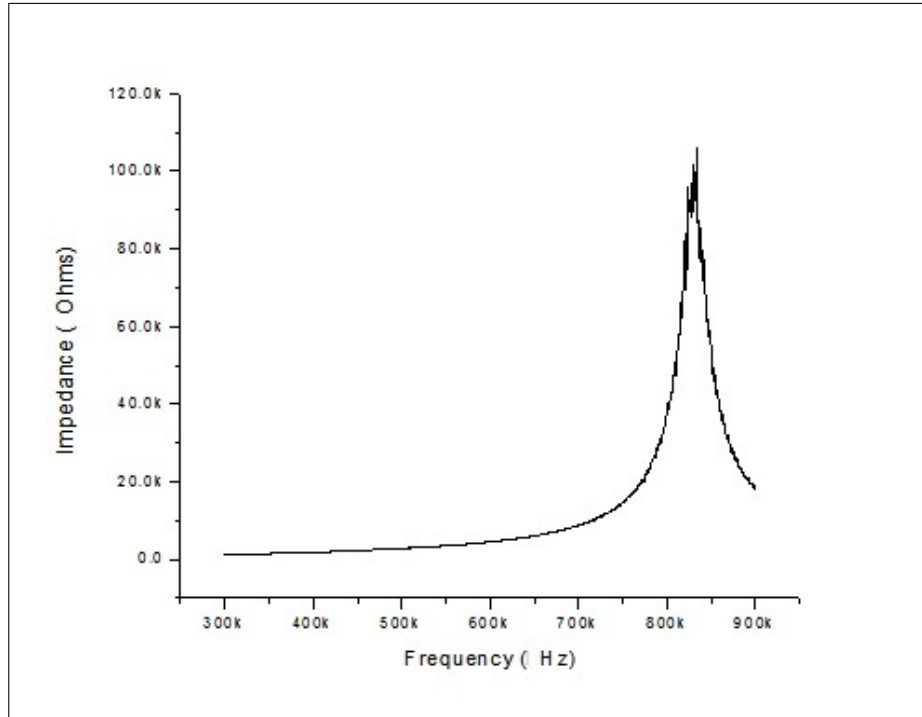


Figure 5.15: Network analyzer data shows that the solenoid coil is used below its resonance frequency.

5.3.4 Analog Circuit Details

An analog circuit has been designed and fabricated using current feedback type operational amplifier AD811. All the four buffers (B), two instrumentation amplifiers (IA) and the adder circuit have been designed by using AD811. For current feedback amplifiers, the closed-loop bandwidth depends on the value of the feedback resistor. A supply voltage $\pm 10 V$ and resistors of 649Ω have been used in the analog adder circuit along with a unity gain instrumentation amplifier. The coils have been excited by digital function generator through a pair of high power buffers BUF634 (B1 in the Fig. 5.5). AD637 has been used for RMS to dc conversion. In RMS circuit, averaging error capacitor has very important role in the accuracy of the circuit and the output dc level varies proportionally. But it is essential to note that always the ratio of two RMS is taken to find phase and hence the accuracy is enhanced.

5.3.5 Validation of Susceptometer

This susceptometer has been validated electronically. A standard L-C-R meter (Fluke PM6304, accuracy $0.05\% \pm 1$ digit, maximum resolution $0.01\mu H$) has been used to test the inductances at different frequencies using the designed measurement system. The error in the measurement has been calculated and shown in Table 5.1 and 5.2. The phase measurement error with frequency has been estimated by introducing a known phase to the function generator in one of the coil and finding the phase by the above method. The voltage drop across the inductor is more for higher frequencies therefore, the measurement error is less at higher frequencies as compared to lower frequencies (vide Table 5.1 and Table 5.2). The proportionality constant (κ) has been measured using different materials of known susceptibility by the test coil with the same fill factor and ΔL is measured. The average of the proportionality constant is found to be 10.32 (in Table 5.3). This susceptometer is also validated with the samples of known susceptibilities assuming κ to be 10.32 (as given in Table 5.3).

Table 5.1: Error estimation in the measurement of change in inductance ΔL

Freq (kHz)	L_0 (air core) standard	L_s (sample in core) standard	ΔL standard	ΔL measured	Error (%)
10	$962.55\mu H$	$966.62\mu H$	$4.07\mu H$	$4.096\mu H$	+0.64
100	$0.96623mH$	$0.96752mH$	$1.29\mu H$	$1.285\mu H$	-0.39

Table 5.2: Error estimation in the measurement phase

Freq (kHz)	Standard θ in $^\circ$ is introduced between the channels of function generator	θ in $^\circ$ is measured by the system	Error (%)
10	0.2	0.2033	+1.65
100	0.2	0.2017	+0.85

This AC susceptometer is novel in coil design and phase measurement. The sensing part of this technique is small compared to the mutual inductance type and hence

Table 5.3: Constant of proportionality of the susceptometer

Test Material	Weight (gm)	ΔL (μH)	Proportionality constant (κ)
<i>CuSO₄, 5H₂O</i>	0.3954	2.2538	9.7690
<i>FeO</i>	0.5298	6.3078	11.9822
<i>NiCl₂, 6H₂O</i>	0.5938	6.8732	9.2135

Table 5.4: Comparison with known materials

Test Material	Weight (gm)	Susceptibility ($\text{cm}^3\text{mol}^{-1}$)	Measured Susceptibility ($\text{cm}^3\text{mol}^{-1}$)
<i>Aluminum Powder</i>	0.4133	1.60×10^{-5}	1.73×10^{-5}
<i>Mn₂O₃</i>	0.9312	1.41×10^{-2}	1.48×10^{-2}
<i>NiCl₂, 6H₂O</i>	0.3048	1.52×10^{-2}	1.47×10^{-2}

the cryostat can be smaller in size and it can also be adopted in superconductors, ferro-fluids, biological samples etc. In this development, advantages of both self-inductance type and mutual inductance type susceptometers have been exploited. The measurement of RMS voltages at five different locations in the analog circuit enables measurement of complex susceptibility of the samples. The uncertainties of the measurement using this susceptometer depend on the uncertainties in the measurements of $B/2v_0$ and the five RMS voltages. To reduce the uncertainties, higher resolution Analog-to-Digital converters are needed.

5.4 Experiment with Nano-magnetic Samples and Results

The findings from the simulation study have provided the inspiration to verify experimentally the frequency dependent crossover of susceptibility. Co-silica and Ni-silica nano composites are prepared by conventional sol-gel technique. The nano composites are taken in powdered form in a glass container. The container with sample is inserted inside the susceptometer test coil and an empty container is inserted in the reference coil of the susceptometer. The SEM micrographs (Fig. 5.2) reveal the size

of the powdered nano composite particles are of the order of 10 to 50 μm . Nano sized metal particles (nickel or cobalt) are embedded in the composite. From TEM images (Fig. 5.3) of cobalt and nickel nano particles, it can be concluded that the average size of the nano particles embedded in the silica matrix is around 7 – 10 nm and average distance of separation among the nano-magnets is 11-15 nm .

The sample susceptibility has been measured by the self-inductance type absolute coil high frequency susceptometer at 300K [24]. The solenoid of the susceptometer has been operated below its resonant frequency. In the experiment, the strength of the applied magnetic field was around 70 Amp/m . The homogeneity of the magnetic field inside the susceptometer coil has been maintained by a special design of the coil [24] and that has been checked by magnetic field analyzer (Spectran Analyzer by Aaronia AG, Germany). The frequency of the magnetic field has been raised from 100 kHz to 800 kHz in steps of 50 kHz and the susceptibility has been measured for each step. Some experimental results are presented in Fig. 5.16, 5.17 and 5.18. A transition from paramagnetic to diamagnetic with frequency is clearly evident from the frequency verses susceptibility plot. This indicates that the sample is opposing the applied field at higher frequencies. The same experiment has been repeated by applying magnetic field strength of 200 Amp/m . In that case, the system did not show any transition to negative susceptibility with frequency. This may be explained as the Zeeman energy in the later case dominates the other two forms of energies (interaction energy and anisotropy energy) and the particles are forced to follow the applied field. Hence, the system shows only paramagnetic response for all the frequencies employed. Ni-silica nano-composite follows para-to-dia trend similar to that of 20% cobalt-silica nano-composites. The experiments have been conducted using 10%, 20% and 30% nickel in nickel-silica nano-composites. It is seen that the crossover frequency varies with percentage of nickel or cobalt in the nano-composites. This is because, the occurrence of this phenomenon is dependent on the size and separation of the nano-particles (see Table 5.5).

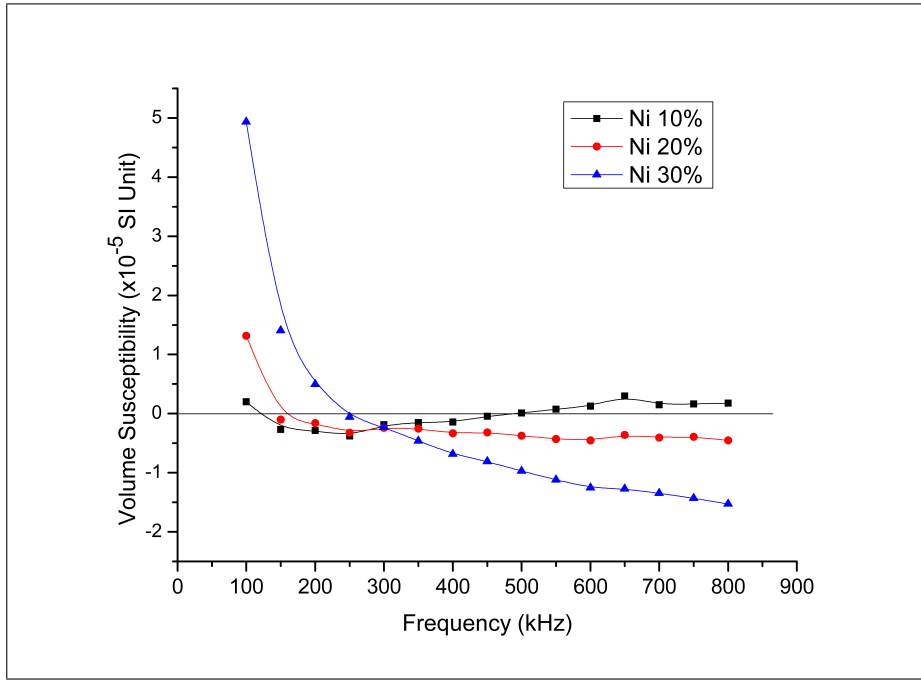


Figure 5.16: The variation of volume susceptibility of Ni-silica nano-composites against frequency of the applied field at $77^{\circ}K$ from the experimental data.

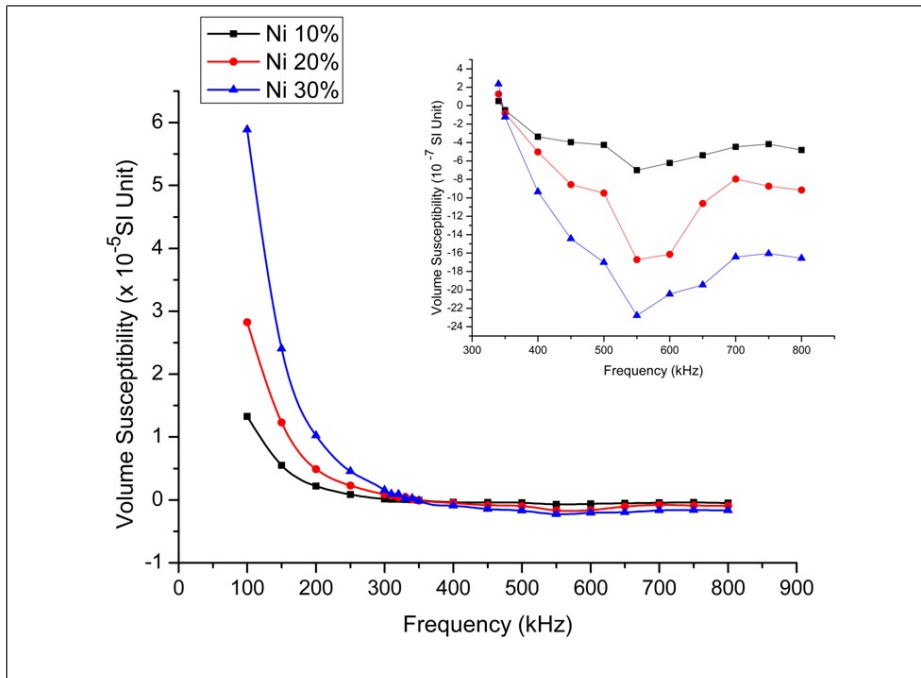


Figure 5.17: The variation of volume susceptibility of Ni-silica nano-composites against frequency of the applied field at $300^{\circ}K$ from the experimental data. Inset shows the negative susceptibility data.

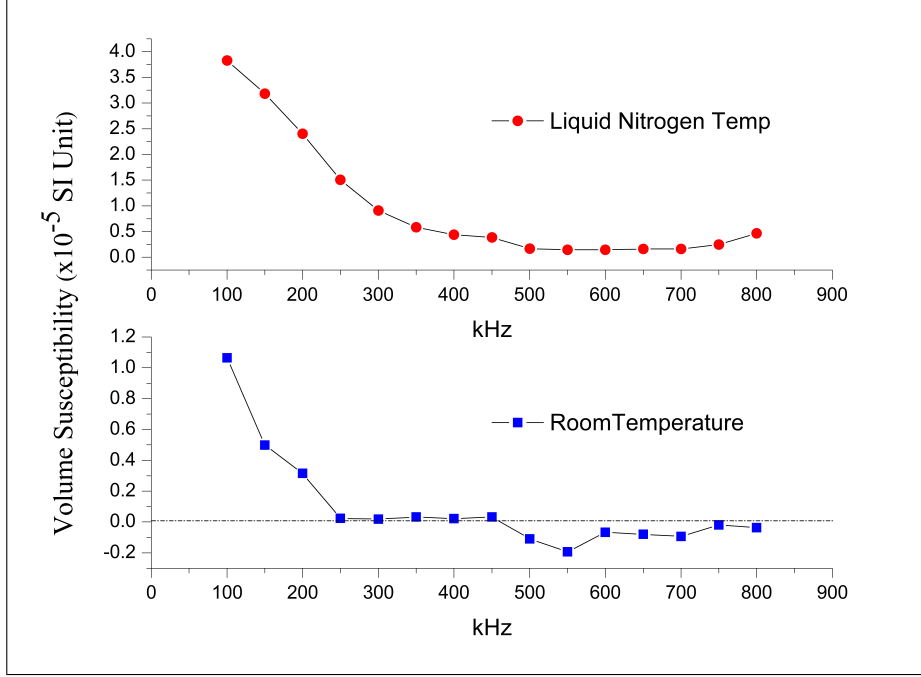


Figure 5.18: The variation of volume susceptibility of 20% Co-silica nano-composites against frequency of the applied field at $77^{\circ}K$ and $300^{\circ}K$ from the experimental data.

The simulation result is presented for a cluster of 3375 interacting nano-magnets arranged in a cubic lattice and cross-over of magnetization is shown in Fig. 4.2. But in the experiment carried out, the number of interacting nano-magnets is of the order of $10^5 - 10^6$. Here also we find experimentally similar type of transition at some frequency. The frequency response in the experimental findings is different from the simulation data. These anomalies are addressed in the discussion section. The system will try intrinsically to oppose the applied field, the cause of its instability. This originates a new concept of diamagnetism in the interacting nano-magnetic ensemble.

5.5 Conclusion

Susceptibility of magnetic nano-composites of cobalt-silica and nickel-silica have been measured and the results shown in Fig. 5.16, 5.17 and 5.18 are summarized

Table 5.5: Experimental Results of nano-composites Co-silica and Ni-silica

Nano Composite	Temperature ($^{\circ}K$)	Cross-over Frequency (kHz)
20%Co in silica	300	500
20%Co in silica	77	no diamagnetism observed
10%Ni in silica	300	350
20%Ni in silica	300	350
30%Ni in silica	300	350
10%Ni in silica	77	125
20%Ni in silica	77	175
30%Ni in silica	77	250

in Table: 5.5. The variation of susceptibility in frequency domain shows a crossover frequency, that means the susceptibility becomes negative above that frequency. The tests were carried out at room temperature and also at liquid nitrogen temperature. The size of the powdered nano-composites particles is of the order of 50-100 μm . Each particles of the nano-composites are basically a silica matrix embedded with nano-sized metal (Ni or Co) particles. These metal particles are nano-magnets, distributed randomly in the silica matrix. The average diameter of the nano-magnets is 7-10 nm . The average separation among the nano-magnets is around 11-15 nm . Samples have different percentage of metal in silica matrix (10%, 20% and 30% of metals). From Table: 5.5, the following conclusions are drawn.

1. Change of susceptibility of the nano-composites with frequency has similar trend as seen in the simulations (in Chapter 4).
2. Crossover frequency increases as the temperature of the sample increases. The reversal of magnetization follows Arrhenius Law (see Eq. (4.1)) and hence, the relaxation frequency increases with rise of sample temperature.
3. Crossover frequency of nickel-silica nano-composite at $77^{\circ}K$ is increases with higher percentage of metal in the nano-composite. From the HRTEM images, higher percentage of metal in the nano-composites indicates larger volume of the nano-magnets. Bigger nano-magnet has larger magnetic moment result-

ing in a stronger interaction potential. Stronger interaction potential means higher spring constant, in mechanical mass-spring equivalent model. Natural frequency of oscillation is more for higher spring constant. Therefore, crossover frequency is increases with the increase in the size of the nano-magnets in the composite.

4. Crossover frequency of nickel in silica nano-composite at $300^{\circ}K$ does not change for different percentages of nickel in the nano-composite. For higher volume of nano-magnets, relaxation frequency reduces and interaction potential increases. Increase in interaction potential increases frequency of oscillation. So both (relaxation frequency and normal modes of oscillations) compensate each others effect, resulting in no effective change in crossover frequency.
5. At $300^{\circ}K$ crossover in susceptibility of cobalt in silica nano-composite is observed but at $77^{\circ}K$, there is no diamagnetism observed. At low temperature relaxation frequency reduces that means weak applied field may not be able to switch the nano-magnets. Cobalt has higher saturation of magnetization (higher interaction potential) as compared to nickel, hence this weak external field is unable to initiate the cooperative switching in the core.
6. In the experimental findings, the nature of frequency response has similarity with the simulation results but the frequency at which the crossover of susceptibility takes place is one order higher in simulation than the experiment. The crossover frequency depends on the system size. The number of nano-magnets in the simulation is less than 4000 but the number of nano-magnets are more than 10^6 in the nano-composite samples. So, the simulation is done for an ensemble consisting of a very limited number of nano-magnets with the assumption that the system follows Boltzman-Gibbs extensive statistics. The exact dynamic evolution of the moments of the nano-magnets has been calculated *ab-initio* instead of using heuristic Monte-Carlo algorithm. In re-

ality, a canonical ensemble with long range interaction follows non-extensive statistics and hence the entropy of the system is not extensive. Such systems cannot be reduced to minimal Hamiltonian model to study the dynamics of the individual nano-magnets in the ensemble. The partition function of the non-extensive system of nano-magnetic ensemble will be different compared to an extensive system and hence, the crossover frequency in the simulation (in Fig. 4.2) is higher than the experimental results (in Fig. 5.16-5.18).

Chapter 6

Summary and Outlook

Understanding dynamics of interacting oscillators is an issue of interest for diverse disciplines ranging from biology to engineering. This insight helps us to interpret the behavior of many real life complex dynamical systems. A coupled system is represented by coupled differential equations or difference equations and such systems are everywhere in nature with non-linearities and complexities. These differential equations are not always integrable hence numerical solution and computer simulation is essential to analyze such systems. In this work, a special case of collective dynamics of dipoles has been investigated by computer simulation. The premise of this thesis is to understand the coupled dynamics of dipoles in a double well potential. The simulation results are also verified experimentally in magnetic nanocomposites where dipole equivalents are present. This chapter is the summery of the work carried out in this research. In addition, the outlook and future possibilities are also discussed in this concluding chapter.

6.1 Summary

In the field of magnetism, paramagnetic and diamagnetic materials do not exhibit collective magnetic interactions and they are not completely magnetically ordered. Ferromagnetic materials exhibit long-range magnetic ordering when they are below a critical temperature. This thesis does not speak about magnetism rather it tells about ordering of magnetic moments under external magnetic field. A system of oscillating dipoles behave like a paramagnetic material and the dipoles align themselves in the direction of the applied field. But the system of oscillating dipoles at some higher frequencies of the applied magnetic field shows a majority of the dipoles in the system opposing the field, as a result, a diamagnetic susceptibility is observed. This phenomenon should not be confused with magnetic phase change. That is why crossover of susceptibility is included in the title of the thesis.

In the first part of this thesis, a natural phenomenon, predator-prey interaction is introduced where a school of fishes is considered as a coupled system. Any coupled system comprises of subunits and here the subunits, the fishes are hydro dynamically interacting dipoles. They have a long range interaction and it is either attractive or repulsive depending upon their orientations. There is a synchronization and pattern formation in the fish school which is a property of chaotic coupled oscillator system.

With some pedagogical approach, the second chapter introduces the harmonic oscillator. In this context, some of the features like resonance, normal modes of oscillation of linear and non-linear oscillator are also explained. Phase of a linear oscillator with respect to the external force varies with the frequency of the applied force but how this phase lag develops between the applied force and the dynamics of the oscillator is discussed in this chapter. Oscillators no longer endure linearity if the extent of oscillation or strength of applied force is large but due to some parametric variations, the dynamics of the non-linear oscillators sometimes becomes highly dependent on initial conditions which results in a chaotic oscillation. Syn-

chronization and suppression of chaos are the two topics in externally perturbed non-linear oscillators system that are pointed out in this chapter because they are relevant in the simulation work. Additionally, some salient properties of coupled non-linear oscillators are also described here. Dynamics of oscillating dipoles in a double well potential is the main focus of the work that has been carried out in this thesis. For that reason, a mechanical model of double well potential as proposed by F. C. Moon has been explained in this chapter. All the dipoles in the potential well are coupled and they oscillate about their axis. To understand the phase of this coupled oscillator system, a simple and most widely used model proposed by Kuramoto has been adopted. Kuramoto model introduces the concept of phase oscillators system and from this, the problem of this research work on phase variation in driven coupled oscillator system has been defined.

The third chapter has explained the term susceptibility *i.e.*, susceptibility of collective oscillators system subjected to an external perturbation. The importance of this work is to find the possibility of negative susceptibility in a coupled dipole system. As magnetic needle is the gross representation of a dipole, the historical experiment done by Meissner and Schmidt is explained in this chapter to understand how the dynamics of the needle becomes chaotic. Ordinary differential equation is derived from the Hamiltonian of the dipole oscillator to analyze the dynamics of the magnetic needle. The synchronization and chaos suppression is achieved by introducing damping in the dynamics of the dipoles. A simulation result of 91 dipoles arranged in an one dimensional array is presented in this chapter where an extra summation term called interaction potential is added with the coupled equations of motion of the dipoles. The coupled differential equations are solved by Runge-Kutta method and the solution shows negative susceptibility at some frequencies of the applied field.

Fourth chapter is the pivotal part of this thesis; it is about the simulation of an

ensemble of superparamagnetic particles under the influence of oscillatory magnetic field. In the introductory part of this chapter, an example of phase transition in one dimensional Dyson model is cited, where Dyson has considered long range interaction. It is interesting to note that Ising model with nearest neighbor interaction in one dimension does not show any phase transition. Here, a realistic example of the transition of susceptibility is established theoretically in an ensemble of superparamagnetic particles. A single domain magnetic islands have coherent switching of the spins and hence the collective spins act as a dipole. These magnetic dipoles are arranged in three dimensional array and an oscillatory external field is applied on the ensemble. The simulation results shows crossover of susceptibility depending upon the frequency of the applied field and some other parameters. Switching of the nano-magnets initiates at the outer population of the ensemble and that initiates a cooperative switching in the core of the ensemble after some delay. This delay depends upon the parameters involving the interaction potentials. If this delay is more than $\frac{T}{4}$ then the system is diamagnetic where T is time period of the applied field.

The fifth chapter explains the crossover of susceptibility by experimental means. The experimental setup for the measurement of susceptibility of the sample was a challenge because it demands two special criteria: weak field (10-20 *Oe*) and high frequency (MHz) measurement. Weak field measurement is prone to noise and high frequency lock-in amplifier is not readily available and is also of high cost. Conventional mutual inductance type susceptometer with long mutual inductance coil requires strong field to measure susceptibility. Because of its strong field application, conventional susceptometer cannot be used. A Self inductance type susceptometer has been specially developed, using a very small coil (2.5 *cm*). Field uniformity in this small coil has been achieved up to 80% by a specially designed shape modified coil. Phase measurement at high frequency is achieved by a simple trigonometric formula implemented in analog hardware combined with computer software. The

susceptibility of the magnetic nano-composites is measured for different frequencies and frequency dependent para-to-dia crossover of susceptibility is observed experimentally.

6.2 Future Outlook

The work described in this thesis contributes to the recent nano-magnetic research and development. This has also relevance in the research field of fish schooling or sperm dynamics. Some improvements may be possible in simulation and experiments also. Some future and outlook are discussed below.

- In the experimental findings, the nature of frequency response has similarity with the simulation results but the frequency at which the crossover of susceptibility takes place is an order higher in simulation than the experiment.
- The crossover frequency depends on the system size. The number of nano-magnets in the simulation is less than 4000 but the number of nano-magnets are more than 10^5 in the particles of the nano-composite samples. So, the simulation is done for an ensemble consisting of a very limited number of nano-magnets with the assumption that the system follows Boltzman-Gibbs extensive statistics.
- The exact dynamic evolution of the moments of the nano-magnets has been calculated *ab-initio* instead of using heuristic Monte-Carlo algorithm.
- In reality, a canonical ensemble with long range interaction follows non-extensive statistics and hence the entropy of the system is not extensive. Such systems cannot be reduced to minimal Hamiltonian model to study the dynamics of the individual nano-magnets in the ensemble. The partition function of the non-extensive system of nano-magnetic ensemble will be different than an ex-

tensive system and hence, the crossover frequency in the simulation is higher than the experimental result.

- The simulation is performed on cobalt nano-magnets, where cobalt has only one easy axis.
- One more simulation could have been done on nickel nano-magnets also. But nickel has three easy axes and it is a complicated problem to solve because it is difficult to get the probable stable axis of the magnetic moment under external magnetic field. The size of the nano-composite particles is of the order of 50-100 μm therefore, number of nano-magnets are $10^5 - 10^6$. In the simulation, less than 4000 nano-magnets are taken because *ab-initio* computation takes a very long time.
- The data storage and magnetoelectronics industries are developing smaller and faster technologies that require sub-hundred-nanometer magnetic structures to operate in the gigahertz regime. New types of spintronic devices with increased functionality and performance are being incorporated into data storage and magnetoelectronic technologies. New techniques are required to characterize these magnetic structures on nanometer scales and over a wide range of time scales varying from picoseconds to years. The response of a 50-nanometer magnetic device, used in a read head or a magnetic random-access memory (MRAM) element, may be determined by a 5-nanometer region that is undergoing thermal fluctuations at frequencies of 1 hertz to 10 gigahertz. These fluctuations give rise to noise, non-ideal sensor response, and long-term memory loss. This crossover of susceptibility in the manufacturing nano-magnetic devices has to be taken care, otherwise along with thermal fluctuations, stray magnetic field will also generate noise in the devices. Crossover of susceptibility is an inevitable trade off between the size minimization and fast response in the development of nano-magnetic devices.

- Spintronic devices and nanomagnetic materials are finding applications in other areas such as homeland security and biomedical imaging. These industries require better low-power magnetic field sensors for weapons detection, chemical detection, and magnetocardiograms, and require novel nanomagnetic materials for MRI contrast agents and defense applications. This frequency dependent negative susceptibility will be useful in high frequency and low magnetic field sensing device development.

Appendix A

Fish School approaching towards a predator

Jonathan Bird has done lot of research on Sailfish at Cancun, Mexico. Sailfish has got a sail and a pointy bill. Sailfish are a genus *Istiophorus* of billfish living in warmer sections of all the oceans in the world. They are predominately blue to gray in color and have a characteristic erectile dorsal fin known as a sail, which often stretches the entire length of the back. Another notable characteristic is the elongated bill, resembling that of the swordfish and other marlins. Sailfish loves to eat Sardines. Sardines, or pilchards, are common names used to refer to various small, oily fish within the herring family of Clupeidae.

Here, Sailfish is the predator and Sardine is the prey. As soon as the predator shows up the sardines form a bait ball. A bait ball, occurs when small fish swarm in a tightly packed spherical formation about a common center. It is a last-ditch defensive measure adopted by small schooling fish when they are threatened by predators. In the Fig. A a negatively susceptible system of fishes is shown.

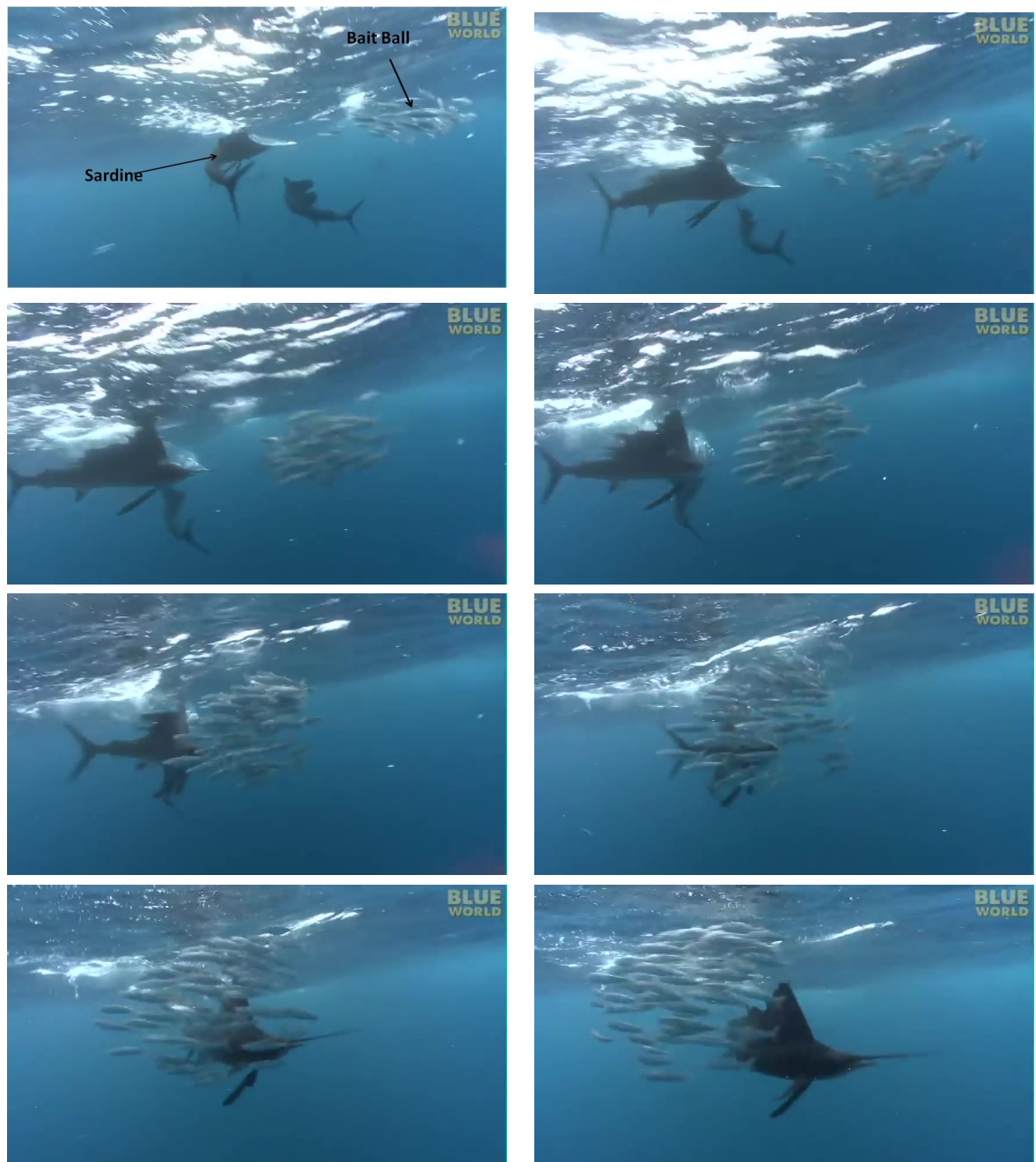


Figure A.1: Sailfish attacks Sardines in all directions. Sardines often come pretty close to the Sailfish for protection. There are incidences when we see the Sardines are heading towards the Sailfish which is very unlikely in nature. This is a condition where the system is susceptible to the external perturbation but opposing the perturbation. This is called diamagnetic susceptibility.

Appendix B

Differential Equation : Dynamics of interacting Dipoles under external perturbation in a dissipative double well potential

Magnetic dipoles of pole-strength μ are scattered on a plane and they are free to rotate about their axis in the same plane. Here, θ is the angular displacement of the dipoles. Let I is the moment of inertia and J is the angular momentum of the dipoles then kinetic energy of the dipole is $\frac{J^2}{2I}$. Dipoles are subjected by a double well potential, where two minima exist at 0° and 180° respectively. The shape of the potential well is sine curve, therefore the potential energy of the dipole in terms of θ is $-\kappa \cos^2 \theta$ where, κ is the depth of the potential well. Let β be the dissipative force of the medium then $\beta\theta$ is the work done by the dipole in the medium. Let $H_0 \sin \omega t$ is the external field, the work done on the system is $\mu H_0 \sin \omega t \cos \theta$. Let r_{ij} represents distance between the i^{th} and j^{th} dipoles, the Hamiltonian of the i^{th} dipole in coupled condition is the sum of potential energy and kinetic energy and is

given in the following Eq. (B.1). Here, the \sum term arises due to collective dipolar interactions.

$$\begin{aligned}
H_i = & J^2/2I - \kappa \cos^2 \theta_i + \mu H_0 \sin \omega t \cos \theta_i - \beta \theta_i \\
& + \mu^2 \sum_{j=1(i \neq j)}^N \frac{1}{r_{ij}^3} (-2 \cos \theta_i \cos \theta_j + \sin \theta_i \sin \theta_j)
\end{aligned} \tag{B.1}$$

The equations of motion are obtained by the properties of Hamiltonian

$$\dot{\theta}_i = \frac{\partial H_i}{\partial J} \text{ and } \dot{J} = -\frac{\partial H_i}{\partial \theta_i}$$

Differentiating the Hamiltonian Eq. (B.1) with respect to J , we get $\frac{\partial H_i}{\partial J} = \frac{J}{I} = \dot{\theta}_i$.

Differentiating the above expression with time, we get $\ddot{\theta} = \frac{\dot{J}}{I}$

Therefore, $\ddot{\theta} = \frac{\dot{J}}{I} = -\frac{1}{I} \frac{\partial H_i}{\partial \theta_i}$ and

$$\frac{\partial H_i}{\partial \theta_i} = \left\{ \begin{array}{c} \kappa \sin 2\theta_i \\ -\mu H_0 \sin \omega t \sin \theta_i \\ +\mu^2 \sum_{j=1(i \neq j)}^N \frac{1}{r_{ij}^3} (2 \sin \theta_i \cos \theta_j + \cos \theta_i \sin \theta_j) \end{array} \right\}$$

The ODE described above finally arrive at the following equation.

$$\begin{aligned}
\frac{d^2 \theta}{dt^2} = & -\frac{\kappa}{I} \sin 2\theta + \frac{\mu H_0}{I} \sin \omega t \sin \theta - \beta \dot{\theta} \\
& + \frac{\mu^2}{I} \sum_{j=1(i \neq j)}^N \frac{1}{r_{ij}^3} (2 \sin \theta_i \sin \theta_j + \cos \theta_i \cos \theta_j)
\end{aligned} \tag{B.2}$$

Appendix C

Dipole-Dipole Interaction Potential

Reference: Griffiths, David J. (2007) Introduction to Electrodynamics, 3rd Edition;
Prentice Hall

We have seen that the potential of a pure dipole with dipole moment \mathbf{p} (that is, a system of charge where only the dipole term in the multipole expansion is non-zero) is, in spherical coordinates:

$$V = \frac{1}{4\pi\epsilon_0 r^2} \mathbf{p} \cdot \hat{\mathbf{r}} = \frac{1}{4\pi\epsilon_0 r^2} p \cos \theta \quad (\text{C.1})$$

By taking the gradient in spherical coordinates, we can find the electric field of a dipole, since $\mathbf{E} = -\nabla V$.

$$\mathbf{E} = -\frac{\partial V}{\partial r} \hat{\mathbf{r}} - \frac{1}{r} \frac{\partial V}{\partial \theta} \hat{\theta} - \frac{1}{r \sin \theta} \frac{\partial V}{\partial \phi} \hat{\phi} = \frac{p}{4\pi\epsilon_0 r^3} \left[2 \cos \theta \hat{\mathbf{r}} + \sin \theta \hat{\theta} \right] \quad (\text{C.2})$$

We can calculate the average field of a dipole over a sphere of radius R but to do this we need to express the spherical unit vectors in terms of rectangular unit

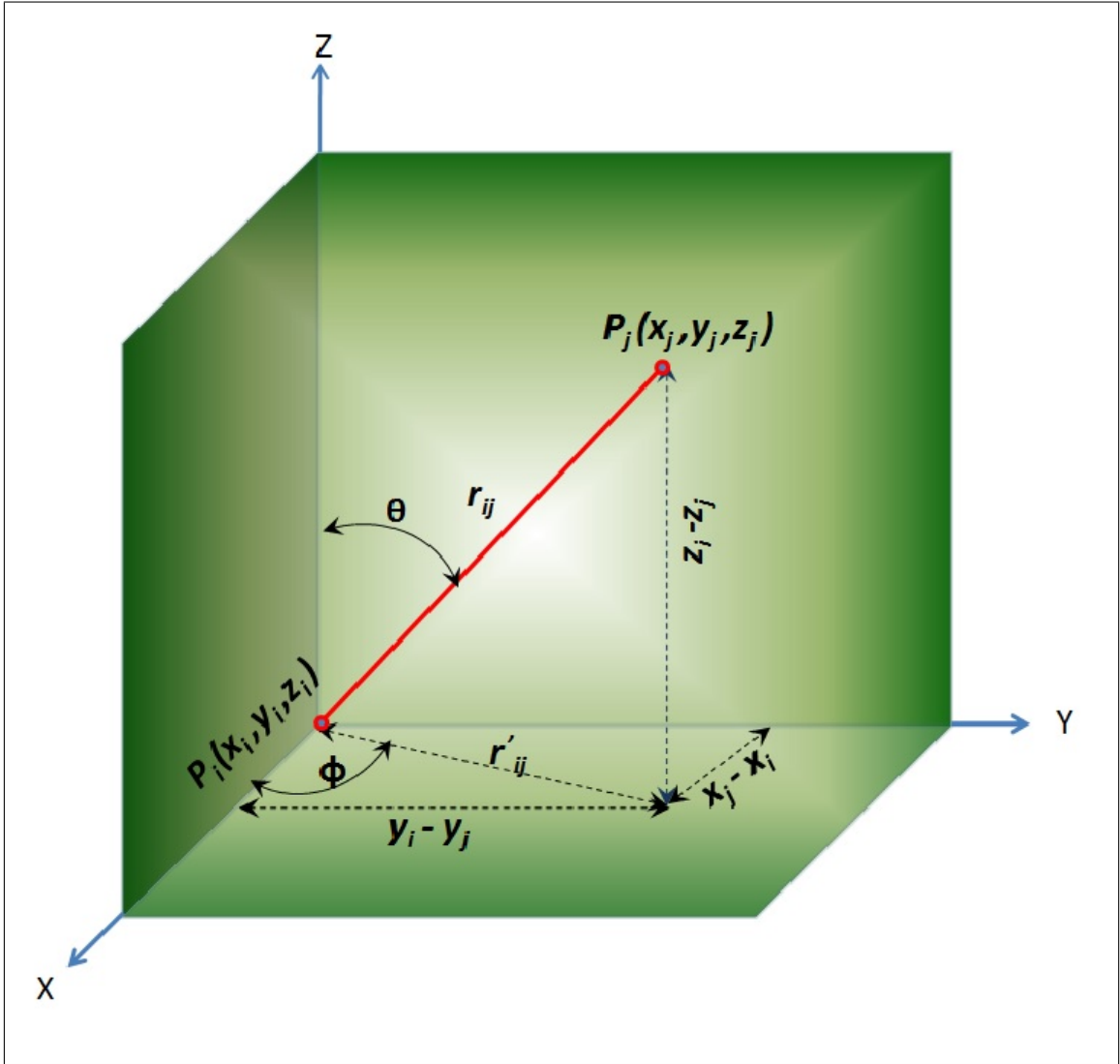


Figure C.1: Dipole dipole interaction.

vectors, since the spherical unit vectors change with position. We have

$$\hat{\mathbf{r}} = \sin \theta \cos \phi \hat{\mathbf{x}} + \sin \theta \sin \phi \hat{\mathbf{y}} + \cos \theta \hat{\mathbf{z}} \quad (\text{C.3})$$

Substituting these into the field and collecting terms we get

$$\mathbf{E} = \frac{p}{4\pi\epsilon_0 r^3} [3 \sin \theta \cos \theta \cos \phi \hat{\mathbf{x}} + 3 \sin \theta \cos \theta \sin \phi \hat{\mathbf{y}} + (3 \cos^2 \theta - 1) \hat{\mathbf{z}}] \quad (\text{C.4})$$

From the Fig. C.1 we get

$$\cos \theta = \frac{z_j - z_i}{r_{ij}}; \sin \theta = \frac{r'_{ij}}{r_{ij}}; \cos \phi = \frac{x_j - x_i}{r'_{ij}}; \cos \phi = \frac{y_j - y_i}{r'_{ij}} \quad (\text{C.5})$$

Replacing the sine and cosine values from Eq. (C.5) to Eq. (C.6) we get

$$\mathbf{E} = \frac{p}{4\pi\epsilon_0 r^3} \left[\frac{3(x_j - x_i)(z_j - z_i)}{r_{ij}^2} \hat{\mathbf{x}} + \frac{3(y_j - y_i)(z_j - z_i)}{r_{ij}^2} \hat{\mathbf{y}} + \left(3 \frac{(z_j - z_i)^2}{r_{ij}^2} - 1 \right) \hat{\mathbf{z}} \right] \quad (\text{C.6})$$

Appendix D

Rodrigues' rotation formula

Rotate a vector $\vec{v} = (x, y, z)$ about a general axis with a direction vector \hat{n} by angle θ as shown in the Fig. D.1. \vec{v} is decomposed into two components: \vec{v}_{\parallel} parallel to \hat{n} and \vec{v}_{\perp} perpendicular to \hat{n} when $\vec{v} = \vec{v}_{\parallel} + \vec{v}_{\perp}$.

Let \vec{T} is the new vector after rotation of θ about \hat{n} . We have to compute $\vec{T}(\vec{v})$. Where, $\vec{T}(\vec{v}) = \vec{T}(\vec{v}_{\parallel} + \vec{v}_{\perp}) = \vec{T}(\vec{v}_{\parallel}) + \vec{T}(\vec{v}_{\perp})$. Also, $\vec{T}(\vec{v}_{\parallel}) = \vec{v}_{\parallel}$ since \vec{v}_{\parallel} has the same direction as \hat{n} . As \vec{v} is rotated around the axis with the direction vector \hat{n} . Therefore, $\vec{T}(\vec{v}) = \vec{v}_{\parallel} + \vec{T}(\vec{v}_{\perp})$.

So, $\vec{T}(\vec{v}_{\perp})$ is the only quantity to be computed. For this a two dimensional basis in the plane of rotation is also shown in the Fig. D.1. The first basis vector is \vec{v}_{\perp} and the second is $\vec{w} = \hat{n} \times \vec{v}_{\perp} = \hat{n} \times \vec{v}$.

Looking at the Fig. D.1, we get

$$\vec{T}(\vec{v}_{\perp}) = \cos \theta \vec{v}_{\perp} + \sin \theta \vec{w} = \cos \theta \vec{v}_{\perp} + \sin \theta (\hat{n} \times \vec{v}_{\perp}).$$

Therefore,

$$\begin{aligned} \vec{T}(\vec{v}) &= \vec{v}_{\parallel} + \vec{T}(\vec{v}_{\perp}) \\ &= (\vec{v} \cdot \hat{n}) \hat{n} + \cos \theta \vec{v}_{\perp} + \sin \theta (\hat{n} \times \vec{v}_{\perp}) \\ &= (\vec{v} \cdot \hat{n}) \hat{n} + \cos \theta [\vec{v} - (\vec{v} \cdot \hat{n}) \hat{n}] + \sin \theta (\hat{n} \times \vec{v}) \end{aligned}$$

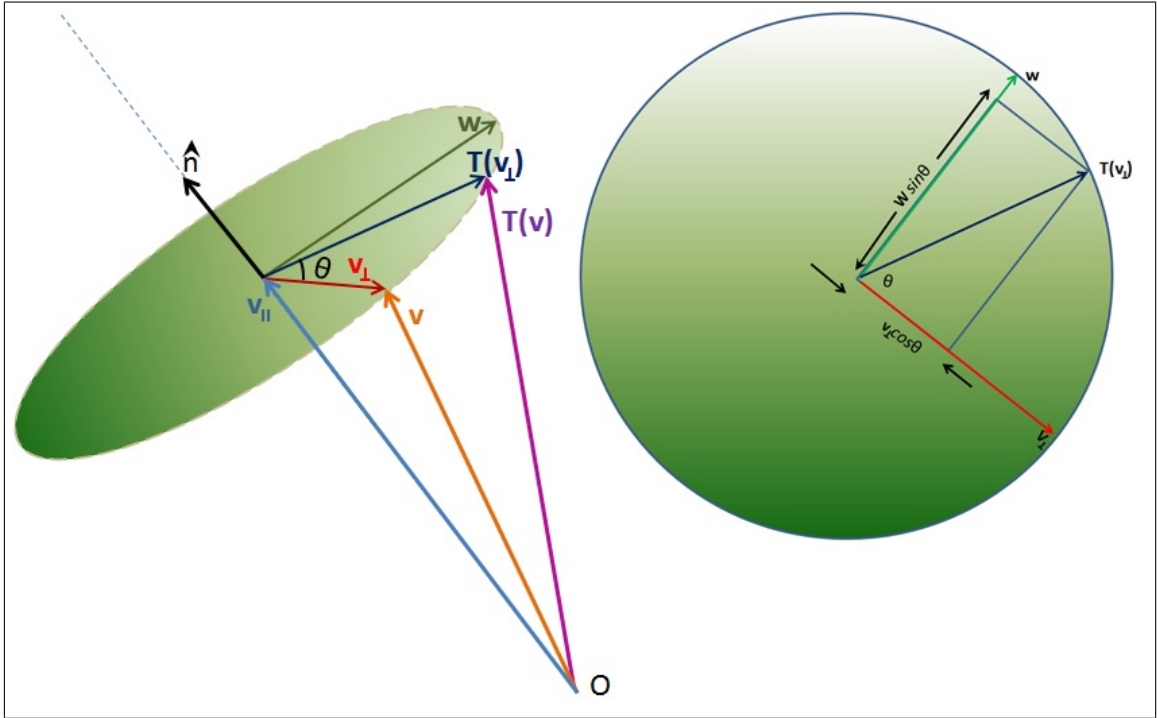


Figure D.1: Rotation about a general axis through the origin, showing the axis of rotation and plane of rotation. Two dimensional basis of the plane of rotation.

$$\begin{aligned}
 &= (\vec{v} \cdot \hat{n})\hat{n} + \cos \theta \vec{v} - \cos \theta (\vec{v} \cdot \hat{n})\hat{n} + \sin \theta (\hat{n} \times \vec{v}) \\
 &= (1 - \cos \theta)(\vec{v} \cdot \hat{n})\hat{n} + \cos \theta \vec{v} + \sin \theta (\hat{n} \times \vec{v})
 \end{aligned}$$

Appendix E

Direction of magnetic moment after turning at an angle ψ from easy axis

The plane in the space is determined by a point and an orthogonal vector \hat{n} that is perpendicular to the plane. Let $P(x_0, y_0, z_0)$ be given point and $\hat{n} = A\hat{i} + B\hat{j} + C\hat{k}$ is the orthogonal vector to the plane. Let $P(x, y, z)$ be any point on the plane where $\hat{r} = x\hat{i} + y\hat{j} + z\hat{k}$ and $\hat{r}_0 = x_0\hat{i} + y_0\hat{j} + z_0\hat{k}$ are the position vectors of P_0 and P respectively. Then the vector equation of the plane is given by $\hat{n} \cdot \hat{r} = \hat{n} \cdot \hat{r}_0$. Hence, the scalar equation of the plane is given by $A(x - x_0) + B(y - y_0) + C(z - z_0) = 0$. The equation of plane can be re-written as $Ax + By + Cz + D = 0$ where $D = -(Ax_0 + By_0 + Cz_0)$. If the plane passes through the origin then $D = 0$ and the scalar equation of the plane is $Ax + By + Cz = 0$. Here, A, B, C are the direction cosines of \hat{n} .

Let $\hat{e} = a_0\hat{i} + b_0\hat{j} + c_0\hat{k}$ is a co-planer vector on the plane and the vector has turned towards west by an angle ψ so that the new vector $\hat{m} = a\hat{i} + b\hat{j} + c\hat{k}$ has different direction cosines. What is the value of a, b, c in terms of a_0, b_0, c_0, A, B, C and ψ ?

The scalar equation of \hat{e} and \hat{m} is $\frac{x}{a_0} = \frac{y}{b_0} = \frac{z}{c_0}$ and $\frac{x}{a} = \frac{y}{b} = \frac{z}{c}$ respectively.

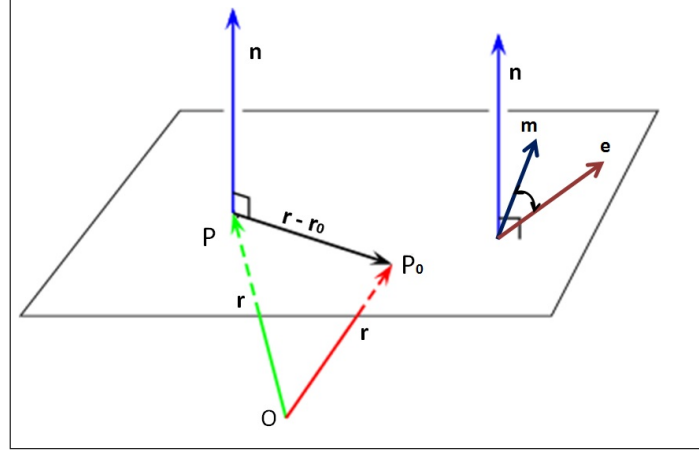


Figure E.1: Direction of magnetic moment after turning at an angle ψ from easy axis.

The dot product of \hat{e} and \hat{m} is given below:

$$\sqrt{a_0^2 + b_0^2 + c_0^2} \sqrt{a^2 + b^2 + c^2} \cos \psi = a_0 a + b_0 b + c_0 c \quad (\text{E.1})$$

The cross product of \hat{e} and \hat{m} is given below:

$$\sqrt{a_0^2 + b_0^2 + c_0^2} \sqrt{a^2 + b^2 + c^2} \sin \psi \hat{n} = (b_0 c - c_0 b) \hat{i} + (c_0 a - a_0 c) \hat{j} + (a_0 b - b_0 a) \hat{k} \quad (\text{E.2})$$

From Eq. (??) and (??) the normal vector of the plane $\hat{n} = A\hat{i} + B\hat{j} + C\hat{k}$ is obtained as given below.

$$\hat{n} = \frac{(b_0 c - c_0 b) \hat{i} + (c_0 a - a_0 c) \hat{j} + (a_0 b - b_0 a) \hat{k}}{(a_0 a + b_0 b + c_0 c) \tan \psi} \quad (\text{E.3})$$

Let $\Gamma = \frac{1}{\tan \psi}$, then

$$b_0 c - c_0 b = A\Gamma(a_0 a + b_0 b + c_0 c) c_0 a - a_0 c = B\Gamma(a_0 a + b_0 b + c_0 c) a_0 b - b_0 a = C\Gamma(a_0 a + b_0 b + c_0 c) \quad (\text{E.4})$$

This Eq. (E.4) leads to a set of homogeneous equations and difficult to solve by computer program. The computation also very time consuming and erroneous. It is better to use Rodrigues' method of computing to get \hat{m} as explained in the Appendix A.

$$\hat{m} = (1 - \cos \psi)(\hat{e} \cdot \hat{n})\hat{n} + \cos \psi \hat{e} + \sin \psi (\hat{n} \times \hat{e}) \quad (\text{E.5})$$

For the computational purpose, Eq. (E.5) is required to represent in matrix notation. Let us define N , the cross product matrix of \hat{n} as given below:

$$\hat{n} \times \hat{e} = N\hat{e} = \begin{bmatrix} 0 & -C & B \\ C & 0 & -A \\ -B & A & 0 \end{bmatrix} \hat{e} \quad (\text{E.6})$$

We know that $\vec{a} \times (\vec{b} \times \vec{c}) = \vec{b}(\vec{a} \cdot \vec{c}) - \vec{c}(\vec{a} \cdot \vec{b})$ and replacing $\vec{a} = \vec{b} = \hat{n}$ and $\vec{c} = \hat{e}$ we get $\hat{n}(\hat{n} \cdot \hat{e}) - \hat{e} = \hat{n} \times (\hat{n} \times \hat{e}) = \hat{n} \times N\hat{e} = N^2\hat{e}$. Therefore, \hat{m} of Eq. (E.6) will be expressed as

$$\hat{m} = [I + (1 - \cos \psi)N^2 + \sin \psi N]\hat{e} \quad (\text{E.7})$$

Appendix F

Angular Dependence of Energy Equation

The energy expression of Eq. (4.2) has the form:

$$E(\psi) = -A \cos^2 \psi - B \cos(\gamma_0 - \psi).$$

E versus ψ plot has two minima E_{min1}, E_{min2} and two maxima E_{max1}, E_{max2} . The positions of minima and maxima depend on the values of A, B, γ_0 . These values are shown in the Fig. F.1. The black curve represents $B = 0$ and $\gamma_0 = 0$ *i.e.*, anisotropic energy variation of the superparamagnetic particle in absence of any external field. Here the two minima are at 0° and 180° respectively and maxima are at 90° and 270° respectively. This holds good even for non-zero B .

Color plots represents the E versus ψ for various γ_0 . The Fig. F.1 shows the maxima and minima are γ_0 dependent.

(Note: In the absence of external field nano-magnets will be on the easy axis at $\psi = 0^\circ$ or 180° . If the applied field direction and easy-axis both are along z-axis direction then also the energy minima stay at 0° to 180° . Here, easy-axis is randomly chosen so there is an angle between H and easy axis. In this case, energy minima

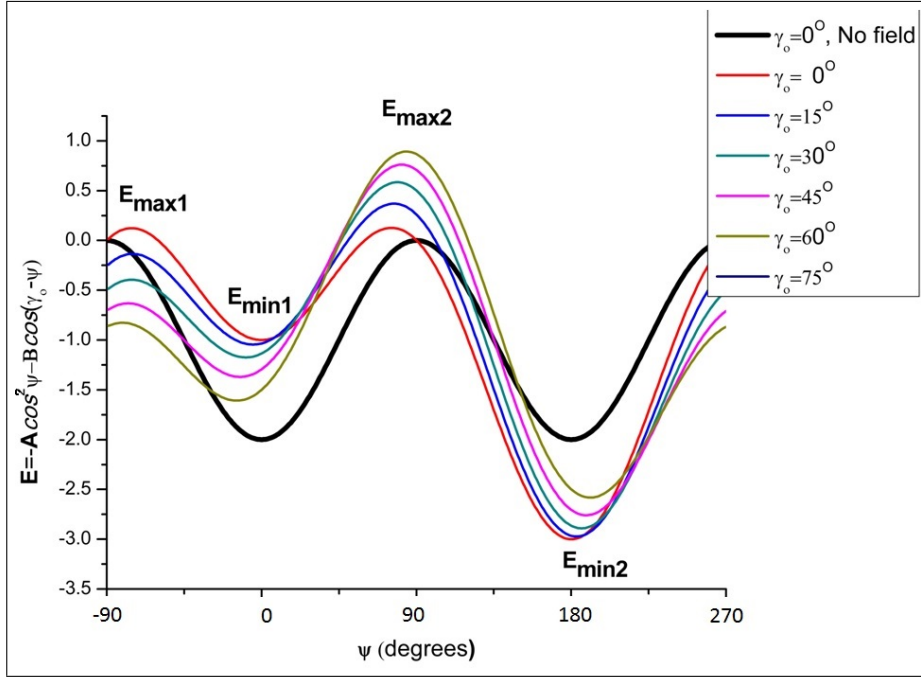


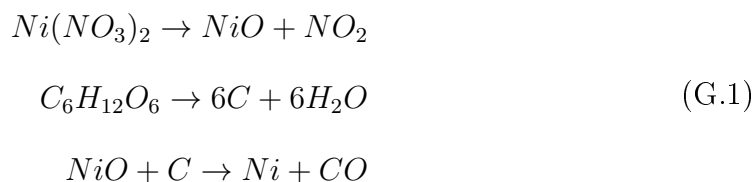
Figure F.1: Energy plots of various γ_0 values

will vary with the instantaneous applied field. It is required to find the angle at which energy minima occurs. This angle is the new location where the nano-magnet will stabilize.)

Appendix G

Stoichiometric Calculations for Ni-silica nano-composites

Following is the stoichiometric calculation for the preparation of Ni-silica nano-composite.



Molecular wt. of $Si(OC_2H_5)_4 = 208$ gm/mol

Molecular wt. of $SiO_2 = 60$ gm/mol

Molecular wt. of $Ni = 58.69$ gm/mol

Molecular wt. of $Ni(NO_3)_2 \cdot 6H_2O = 290.81$ gm/mol

Molecular wt. of $C_6H_{12}O_6 = 180$ gm/mol

$TEOS : H_2O : C_2H_5OH = 1:1:2$ ratio

5ml of TEOS and 5ml of ethyl alcohol mixed thoroughly in a beaker. Density of TEOS is 1gm/c.c. therefore, 5gm of TEOS is taken. In another beaker, 5ml of double distilled water with 5ml of ethyl alcohol is mixed. in this beaker measured

quantity of cobalt nitrate and dextrose are also to be mixed throughly.

One mole of SiO_2 is obtained from one mole of TEOS

Therefore, 208 gm TEOS gives 60 gm SiO_2 and 5gm of TEOS is taken

So, 5 gm TEOS gives $\frac{60 \times 5}{208} = 1.442$ gm SiO_2

For 10% Ni in silica matrix : Amount of $Ni = 10\text{wt}\%$ of SiO_2

= 0.10 x 1.442 gm

= 0.1442 gm nickel is required.

One mole of Ni comes from one mole of NiO . Therefore, 58.69 gm Ni comes from 74.69 gm NiO

Then, 0.1442 gm Ni comes from $\frac{0.1442 \times 74.69}{58.69} = 0.0189$ gm NiO

Calculation to find the required amount of nickel nitrate:

74.69 gm NiO comes from 290.81 gm of $Ni(NO_3)_2 \cdot 6H_2O$

0.0189 gm NiO comes from $\frac{290.81 \times 0.0189}{74.69} = 0.0736$ gm of $Ni(NO_3)_2 \cdot 6H_2O$

Required amount of dextrose:

In this process carbon acts as reducing agent. Dextrose provides the required amount of carbon.

One mole (12 gm) carbon is required to reduce one mole (74.69 gm) of NiO into metallic nickel.

Then, 0.0189 gm NiO is obtained by the reduction process of $\frac{12 \times 0.0189}{74.69} = 0.003$ gm of carbon.

72 gm of carbon comes from 180 gm of $C_6H_{12}O_6$

0.003 gm of carbon comes from $\frac{180 \times 0.003}{72} = 0.0075$ gm of $C_6H_{12}O_6$

Therefore, 0.0075 gm of dextrose is required.

Appendix H

M-H Curve Co-silica nanocomposite

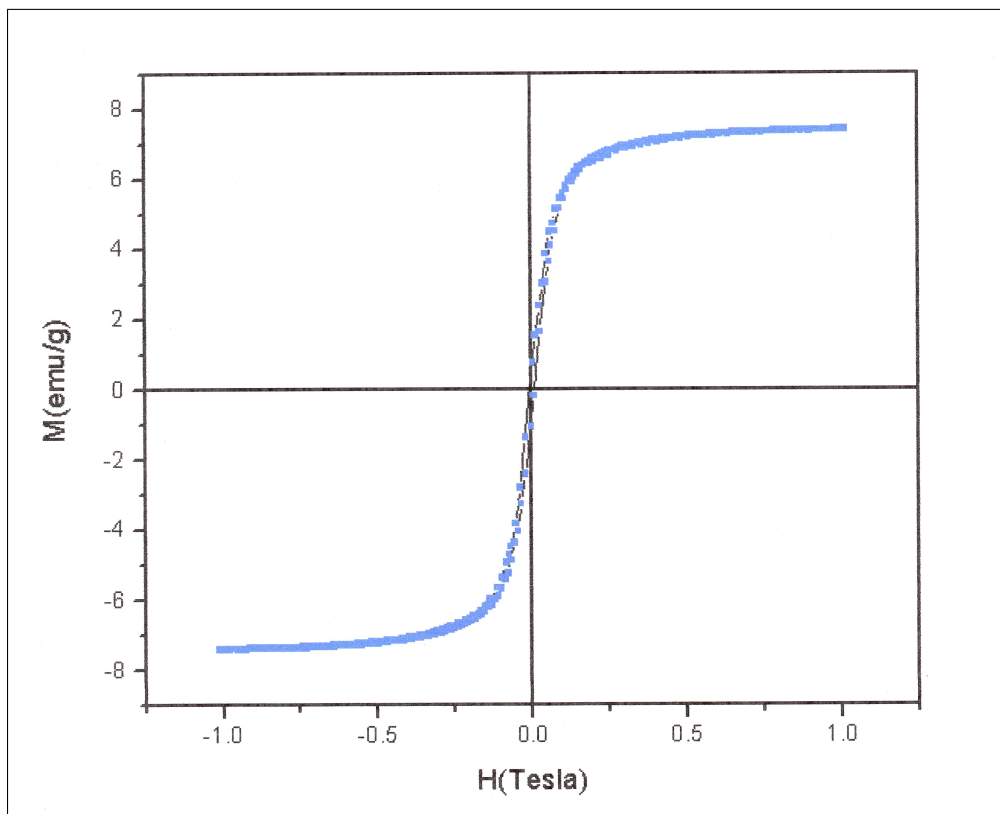


Figure H.1: M-H curve of 20%Co-silica nano-composite at room temperature. Remanence (M_r) is 0.5432 e.m.u per gm and coercivity is 0.00678 T

Appendix I

Low frequency susceptibility plot from simulation data

Software has been developed in this work for the simulation of susceptibility of the magnetic nanoparticles. Susceptibility value reduces as the frequency increases. At lower frequency range, susceptibility is high compared with high frequency susceptibility. After some frequency, this susceptibility falls drastically. Figure I.1 shows susceptibility of cobalt nanoparticles from 5kHz to 100kHz range. This simulation takes very large time because large number of data points is required to get the data in nano-second resolutions. Simulation data and experimental data may not exactly match because we have taken very simple assumptions of the system. But, the order of susceptibility is same in both simulation and experiment in appendix J.

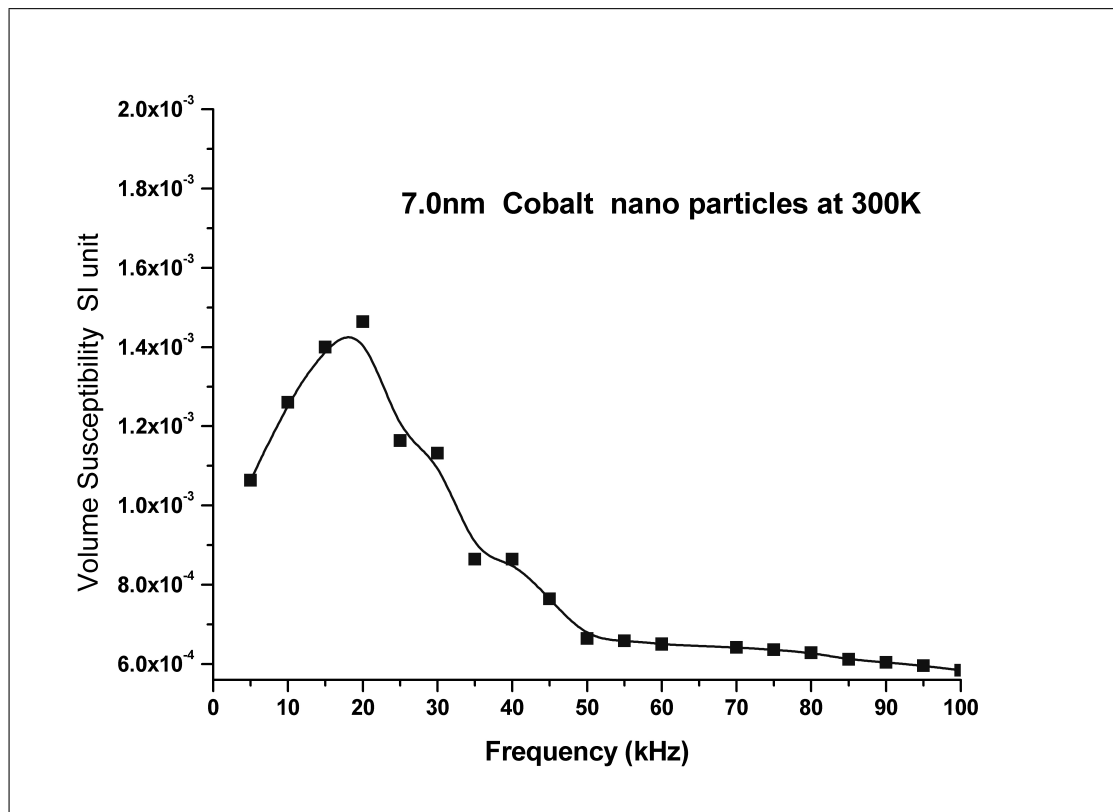


Figure I.1: χ_{ac} of Co-silica nanocomposites at 300K

Appendix J

Low frequency susceptibility plot
from experimental data

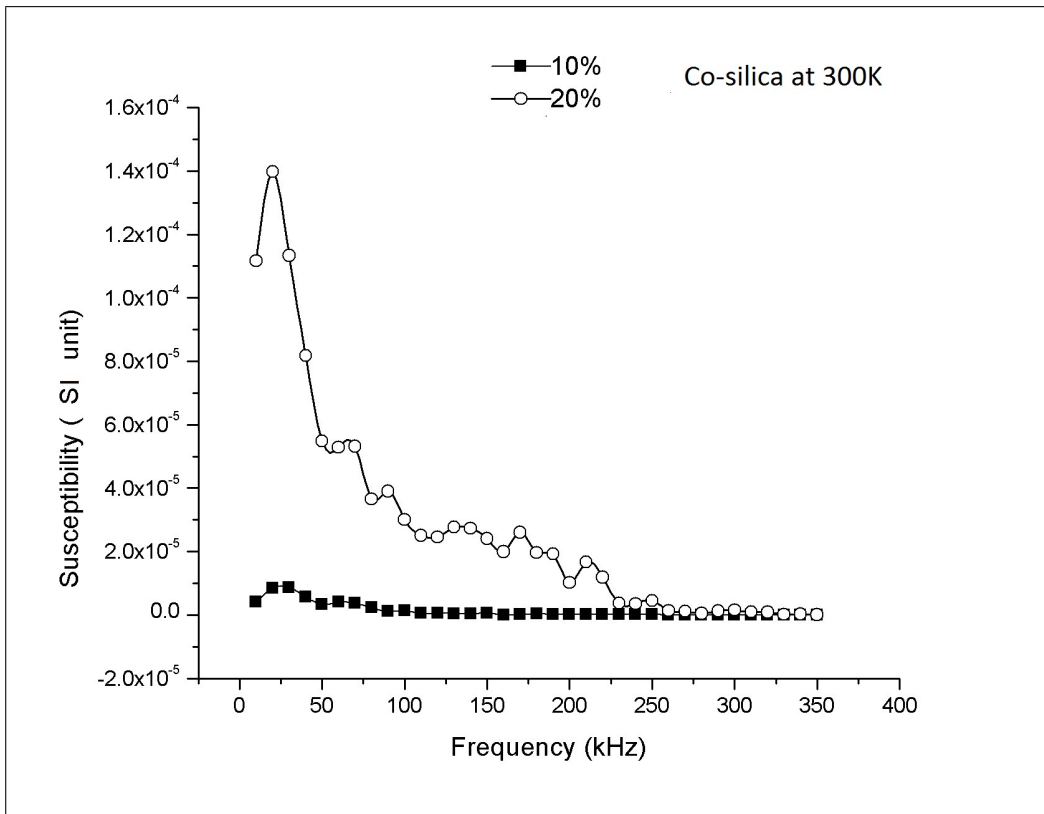


Figure J.1: Real χ_{ac} of Co-silica nanocomposites at 300K

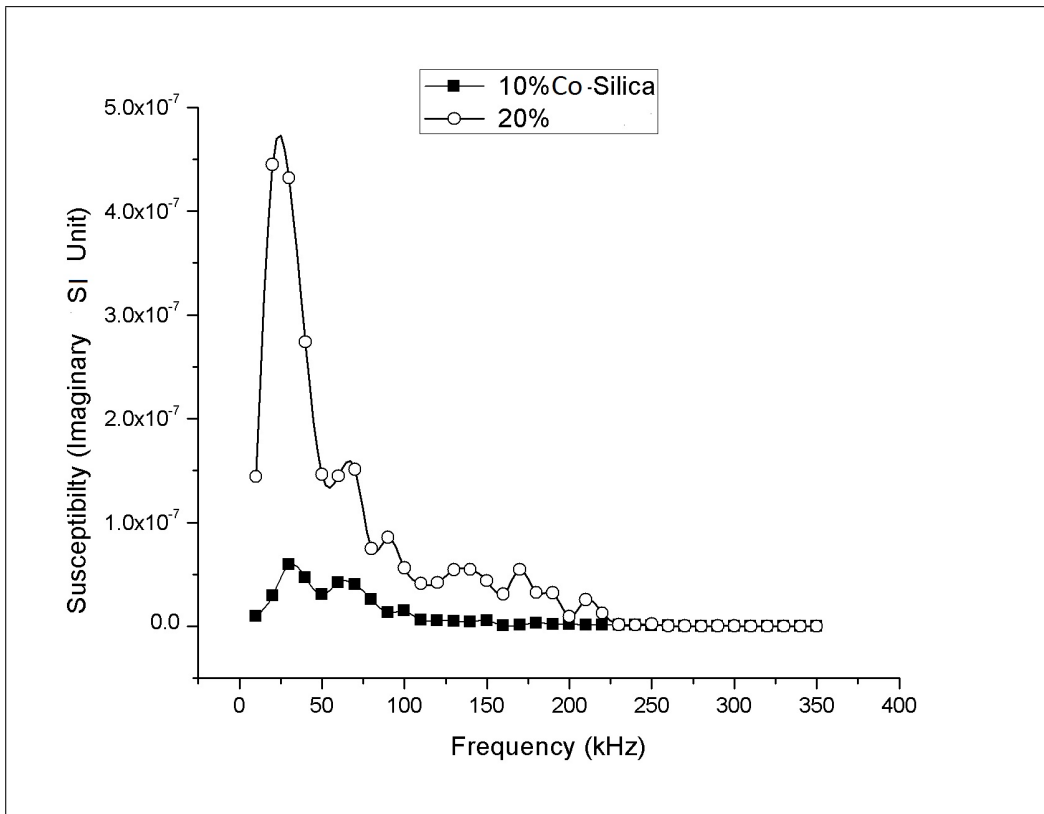


Figure J.2: Imaginary χ_{ac} of Co-silica nanocomposites

Bibliography

References

- [1] A. P. French, "Waves and vibrations", *London: Thomas Nelson*, pp. 121, 1971
- [2] F. S. Crawford, Waves, "The Berkeley physics course", *New York: McGraw-Hill*, pp. 116, 1968
- [3] H. J. Pain, "The physics of vibrations and waves 4th ed.", *Chichester, UK: Wiley*, pp. 80, 1993
- [4] J. Liu, *et.al*, "Complexity of coupled human and natural systems", *Science*. vol. 317, pp. 1513, 2007
- [5] M. J. Luo, "Magnetic susceptibility in strongly coupled systems", *Journal of High Energy Physics*, vol. 11, pp. 142, 2011
- [6] E. Schindling and D. Wilson, "Deterministic nonperiodic flow (1963)", *Gotenborg, Sweden*, 2006
- [7] Y. Nakajima, and S. Naya, "Orientational phase transition and dynamic susceptibility of hindered-rotating dipolar system $\hat{A}\hat{S}$ a librator-rotator model, *J. Phys. Soc. Jpn*, vol. 63, pp. 904, 1994
- [8] H. Meissner and G. Schmidt, "A simple experiment for studying the transition from order to chaos", *Am. J. Phys*, vol. 54, pp. 800, 1986

- [9] Y. Kuramoto, "Chemical Oscillations, Waves, and Turbulence", *Springer-Verlag*, 1984
- [10] R. Fitzpatrick, "Oscillations and Waves: An introduction", *CRC Press. Taylor and Francis Group, NY, USA*, 2013
- [11] J.A.S. Kelso, *et.al.*, "Phase locked modes, phase transition, and component oscillations in biological motion", *Physica Scripta*, vol. 35, pp. 79, 1987
- [12] J. A. Acebron, *et.al.*, "The Kuramoto model: A simple paradigm for synchronization phenomena", *Rev. Mod. Phys.*, vol. 77, pp. 137, 2005
- [13] H. Sakaguchi, "Cooperative phenomena in coupled oscillator systems under external fields", *Progress of Theoretical Physics*, vol. 79, pp. 39, 1988
- [14] E. Oleh, and M. Wolfrum, "Nonuniversal Transitions to Synchrony in the Sakaguchi-Kuramoto Model", *Phys. Rev. Lett.*, vol. 109, pp. 164101, 2012
- [15] C. Huygens, "Horologium Oscillatorium", *Paris, France*, 1973
- [16] I. V. Belykh, *et.al*, "Blinking model and synchronization in small-world networks with a time-varying coupling", *Physica D*, vol. 195, pp. 1, 2004
- [17] A. Pogromsky, *et.al*, "Partial synchronization: from symmetry towards stability", *Physica D*, vol. 172, pp. 65, 2002
- [18] C. W. Wu, *et.al*, "Synchronization in coupled arrays of chaotic oscillators with nonreciprocal coupling", *IEEE Transactions on Circuits and Systems -I: Fundamental Theory and Applications*, vol. 50, pp. 294, 2003
- [19] C. W. Wu and L. O. Chua, "Synchronization in an array of linearly coupled dynamical systems", *IEEE Transactions on Circuits and Systems-I: Fundamental Theory and Applications*, vol. 42, pp. 430, 1995

- [20] S. H. Strogatz, "From Kuramoto to Crawford: exploring the onset of synchronization in populations of coupled oscillators", *Physica D*, vol. 143, pp. 1, 2000
- [21] S. H. Strogatz, "Exploring complex networks", *Nature*, vol. 410, pp. 268, 2001
- [22] J. Alvarez-Ramirez, G. Espinosa-Paredes, H. Puebla, "Chaos control using small amplitude damping signals", *Phys. Lett. A*, vol. 316, pp. 196, 2003
- [23] J. Gautrais, C. Jost, and G. Theraulaz, "Key Behavioral Factors in a Self-organized Fish school Model", *Ann. Zool. Fennici*, vol. 45, pp. 415, 2008
- [24] Nilangshu K. Das, P. Barat, Sounak Dey and T. Jayakumar, "Frequency-adapted crossover from para-to-dia magnetization in an Ising-like dipole-dipole model", *ScienceJet.*, vol. 4: 83, 2015
- [25] J. G. Otero, M. Porto, J. Rivas and A. Bunde, "Influence of dipolar interaction on magnetic properties of ultrafine ferromagnetic particles", *Phys. Rev. Lett.*, vol. 84, pp. 167, 2010
- [26] G. F. Goya, F. C. Fonseca, R. F. Jardim, R. Muccillo, N. L. V. Carreno, E. Longo and E. R. Leite, "Magnetic dynamics of single-domain Ni nanoparticles", *J. Appl. Phys.*, vol. 93, pp. 6531, 2003
- [27] D. W. Abraham, Y. Lu, "Observation of switching of magnetic particle arrays with weak dipole interaction field effects", *J. Appl. Phys.*, vol. 98, pp. 023902, 2005
- [28] M. Osaci, M. Panoiu, T. Heput and Muscalagiu, "Numerical stochastic model for the magnetic relaxation time of the fine particle system with dipolar interactions", *Appl. Math. Model.*, vol. 30, pp. 545, 2006
- [29] A. K. Giri, K. M. Chowdary and S. A. Majetich, "AC magnetic properties of FeCo nanocomposites", *Mater. Phys. Mech.* vol. 1, pp. 1, 2000

- [30] E. C. Stoner and E. P. Wohlfarth, "A mechanism of magnetic hysteresis in heterogeneous alloys", *Philos. Trans. London Ser. A* vol. 240, pp. 599, 1948
- [31] W. F. Brown, "Virtues and weaknesses of the domain concept", *Rev. of Mod. Phys.*, vol. 17, pp. 15, 1945
- [32] S. Morup, F. Bodker, P. V. Hendriksen, S. Linderoth, "Spin-glass-like ordering of the magnetic moments of interacting nanosized maghemite particles", *Phys. Rev. B.*, vol. 52, pp. 287, 1995
- [33] M. El-Hilo, J. Al Saei and R. W. Chantrell, "Distributions of dipolar interaction fields in nano-granular magnetic systems", *IEEE Trans. Mag.*, vol. 47, pp. 3362, 2011
- [34] G. Wang and J. P. Huang, "Nonlinear magnetic susceptibility of ferrofluids", *Chem. Phys. Lett.*, vol. 421, pp. 544, 2006
- [35] M. F. Hansen and S. Morup, "Models for the dynamics of interacting magnetic nanoparticles", *J. Magn. Magn. Mater.*, vol. 184, pp. 262, 1998
- [36] C. Djurberg, P. Svedlinh, P. Nordblad, M. F. Hansen and F. S. Morup, "Dynamics of an interacting particle system: evidence of critical slowing down", *Phys. Rev. Lett.*, vol. 79, pp. 5154, 1997
- [37] H. M. Zhang and H. M. Widom, "Global phase diagrams for dipolar fluids", *Phys. Rev. E.*, vol. 49, pp. R3591, 1994
- [38] S. Morup, M. F. Hansen and C. Frandsen, "Magnetic interactions between nanoparticles", *Beilstein Journal of Nanotech.*, vol. 1, pp. 182, 2010
- [39] J. M. Luttinger and L. Tisza, "Theory of Dipole Interaction in Crystals", *Phys. Rev.*, vol. 70, pp. 954, 1946
- [40] H. Zhang and M. Widom, "Spontaneous magnetic order in random dipolar solids", *Phys. Rev. B.*, vol. 51, pp. 8951, 1995

- [41] L. Hartshorn, "A percision method for the comparison of unequal mutual inductances at telephonic frequencies", *J. Sci. Instrum.*, vol. 2, pp. 145, 1925
- [42] J. Tafur, A. P. Herrera, *et al.*, "Development and validation of a 10kHz-1MHz magnetic susceptometer with a constant excitation field", *J. Appl. Phys.*, vol. 111, pp. 7E349, 2012
- [43] D-X Chen, "High-field ac susceptometer using helmholtz coils as a magnetizer", *Meas, Sc. and Tech.*, vol. 15, pp. 1195, 2004
- [44] S. B. Slade and A. E. Berkowitz, "Ultra-high sensitivity B-H looper/AC susceptometer", *IEEE Magnetics conference, Digests of Intermag'92., International*, pp. 416, 1992
- [45] S. T. P. Boyd *et.al.*, "Miniature thin-film SQUID susceptometer for magnetic microcalorimetry and thermometry, *IEEE Trans. Appl. Superconductivity*, vol. 19, pp. 697, 2009
- [46] K. Park *et.al.* "A miniaturized a.c. magnetic susceptometer for detecting biomolecules tagged to magnetic nanoparticles", *Bioengineering Conference 2009, IEEE 35th Annual Northeast*, pp 1, 2009
- [47] J. R. Kirtley, B. Kalisky, *et al.*, "Scanning SQUID susceptometry of a paramagnetic superconductor", *Phys. Rev. B*, vol. 85, pp. 224518, 2012
- [48] P. C. Fannin, B. K. P. Scaife and S. W. Charles, "New technique for measuring the complex susceptibility of ferrofluids", *J. Phys. E, Sci. Instrum.* vol. 19, pp. 238, 1986
- [49] P. C. Fannin, C. MacOireachtaigh, C. Couper, "An improved technique for the measurement of the complex susceptibility of magnetic colloids in the microwave region", *J. Magn. Magn. Mater.* vol. 322, pp. 2428, 2010

- [50] K. Park, T. Harrah, Ed. B. Goldberg, *et al.*, "Multiplexed sensing based on Brownian Relaxation of magnetic nanoparticles using a compact AC susceptometer", *Nanotechnology*. vol. 22, pp. 85501, 2011
- [51] J. Dho, "A Simple a.c. magnetic susceptometer using self-inductance measurement of a single coil mounted on a cryostat cold head, *Journal of Magnetism*, vol. 13, pp. 177, 2008
- [52] Nilangshu K. Das, T. Jayakumar, and Baldev Raj, Noniterative Digital AC Bridge, *IEEE Trans. Instrum. Meas.*, vol. 59, pp. 3058, 2010
- [53] Nilangshu K. Das, P. Barat, Sounak Dey, and T. Jayakumar, "Design of miniature coil to generate uniform magnetic field" , *Progress In Electromagnetic Research M*, vol. 34, pp. 99, 2014
- [54] S. Sato, S. Sakaguichi, K. Futamata, and K. Katou, "Coil optimization for homogeneous magnetic field with small leakage field," *IEEE Transactions on Magnetism*, vol. 36, pp. 649, 2000
- [55] R. Merritt, C. Purcell, G. Stroink, "Uniform magnetic field produced by three, four, and five square coils", *Review of Scientific Instruments*, vol.54, pp. 879, 1983
- [56] J. L. Kirschvink, "Uniform magnetic fields and double wrapped coil systems: improved techniques for the design of bio-electromagnetic experiments", *Bioelectromagnetics*, vol. 13, pp. 401, 1992
- [57] D. E. Bordelon, R. C. Goldstein, V. S. Nemkov, A. Kumar, J. K. Jackowski, *et al.* , "Modified solenoid coil that efficiently produces high amplitude AC magnetic fields with enhanced uniformity for biomedical applications," *Magnetism, IEEE Transactions on* , vol. 48, pp. 47, 2012

- [58] T. Tadic, B. G. Fallone, "Design and optimization of superconducting MRI magnet systems with magnetic materials," *Applied Superconductivity, IEEE Transactions on* , vol. 22, pp. 4400107, 2012
- [59] N. R. Shaw and R. E. Ansorge, "Genetic algorithms for MRI magnet design," *Applied Superconductivity, IEEE Transactions on* , vol. 12, pp. 733, 2002
- [60] Hao Xu, S. M. Conolly, G. C. Scott, and A. Macovski, "Homogeneous magnet design using linear programming," *Magnetics, IEEE Transactions on* , vol. 36, pp. 476, 2000
- [61] D. Meeker, "Finite Element Method Magnetics" [Online]. Available: www.fwmm.info/wiki/HomePage, Oct. 16, 2010
- [62] Dexin Xie, Xiaowen Sun, Baodong Bai and Shiyong Yang, "Multiobjective Optimization Based on Response Surface Model and Its Application to Engineering Shape Design," *Magnetics, IEEE Transactions on*, vol. 44, pp. 1006, 2008
- [63] A. Stella, F. Trevisan, "Application of the genetic algorithms to the synthesis of the uniform induction gradient in MRI magnets," *Magnetics, IEEE Transactions on*, vol. 36, pp. 1736, 2000
- [64] Edward N. Zalta *et al.*, "Stanford Encyclopedia of Philosophy". *Metaphysics Research Lab, Stanford University*, Spring edition, 2014
- [65] Arthur T. Winfree, "The Geometry of Biological Time". *Springer Study Edition*, 2nd ed, 2001
- [66] T. Yalcinkaya and Y. C. Lai, "Phase characterization of chaos", *Phys. Rev. Lett.* vol. 79, pp. 3885, 1997
- [67] Herbert Goldstein, Charles P. Poole Jr., John L. Safko, "Classical Mechanics (3rd Edition)", *Pearson Education Limited, Edinburgh*, June 25, 2001

- [68] F. C. Moon, "Chaotic Vibrations", *John Wiley & Sons, New York*, 1987
- [69] K. F. Riley, M. P. Hobson and S. J. Bence. "Mathematical methods for Physics and Engineering", *Cambridge University Press, Cambridge, UK*, 1998
- [70] W. H. Press, S. A. Teukolsky, W. T. Vetterling, and B. P. Flannery, "Numerical Recipes in Fortran 77: The Art of Scientific Computing", *Cambridge University Press, Cambridge, UK*, 1992
- [71] D. W. Jordan and P. Smith, "Nonlinear ordinary differential equations", *Oxford University Press, Oxford*, 1990
- [72] Ziya Kalay, "A Review on Synchronization Through the Kuramoto Model, Consortium of Americans for Interdisciplinary Science", *Department of Physics and Astronomy, University of New Mexico, New Mexico*, 2007
- [73] Nilangshu K. Das, P. Barat and T. Jayakumar, "Coupled dynamics of N-body dipoles in a double well potential", *J. Coupled Syst. Multiscale Dyn.*, vol. 2, pp. 74, 2014
- [74] G. Helfman and B. Collette, "Fishes: the animal answer guide", *The Johns Hopkins University Press. 1st Edition*, 2011
- [75] H. Kunz, T. Zublin and C. Hemelrijk, "On prey grouping and predator confusion in artificial fish schools", *10th International Conference on the Simulation and Synthesis of Living System, Bloomington, Indiana, USA*. pp 365, 2006
- [76] School of Fish, Youtube: <https://www.youtube.com/watch?v=sulen9Vxpog>
- [77] A. Cheng Hou Tsang, EvaA Kanso, "Dipole interactions in doubly periodic domains", *Journal of Nonlinear Science*, vol. 23, pp. 971, 2013
- [78] A. A. Tchieu, E. Kanso and P. K. Newton, "The finite-dipole dynamical system", *Proc. R. Soc. A. Mathematical Physics and Engineering Sciences*, vol. 468, pp. 3006, 2012

- [79] J. Bird, "Jonathan Bird's Blue World: Sailfish!", Youtube: <https://www.youtube.com/watch?v=iiQWgeZhmvk>
- [80] N. Borghini, "Topics in nonequilibrium physics", *Fakultat fur Physik, Universitat Bielefeld*, pp. 116, 2014
- [81] A. O. Caldeira and A. J. Leggett, "Path integral approach to quantum brownian motion", *Physica A*, vol. 121, pp. 587, 1983
- [82] R. Moskowitz and E. Della Torre, "Computer Simulation of the Magnetic Dipole Interaction Problem", *J. Appl. Phys.*, vol. 38, pp. 1007, 1967
- [83] J. M. Gonzalez-Miranda, "Synchronization and control of chaos: an introduction for scientists and engineers", *Imperial College Press, London, UK.*, 2004
- [84] F. J. Dyson, "Existence of a phase-transition in a one-dimensional Ising ferromagnet", *Commun. Math. Phys.*, vol. 12, pp. 212, 1969
- [85] J. Frohlich and T. Spencer, "The phase transition in the one-dimensional Ising Model with $1/r^2$ interaction energy", *Communications in Mathematical Physics*, vol. 84, Issue 1, pp. 87, 1982
- [86] S. Giri and S. K. Saha, "Superparamagnetic-to-diamagnetic transition in hydroxo-bridged trinuclear copper(II) complex nanorods", *J. Phys. Chem. C.*, vol. 114, pp. 11723, 2010
- [87] C. Tsallis, "Introduction to Nonextensive Statistical Mechanics (Approaching a Complex World)", *Springer, New York*, 1st ed. 2009
- [88] C. J. Brinker and G. W. Scherer, "Sol-gel science: The physics and chemistry of sol-gel processing", Academic Press Inc., San Deigo, CA, 1990.
- [89] Nilangshu K. Das, Sounak Dey, Sarbajit Pal and P. Barat, "Innovative Instrumentation to Measure Magnetic Susceptibility", *IEEE Trans. Magnetics.*, vol. 49, pp. 4965, 2013

- [90] P. C. Fannin , B. K. P. Scaife and S. W. Charles, "New technique for measuring the complex susceptibility of ferrofluids", *J.Phys. E, Sci. Instrum.*, vol. 19, pp. 238, 1986
- [91] M. A. Azpurua, "A semi-analytical method for the design of coil-systems for homogeneous magnetostatic field generation", *Progress In Electromagnetic Research B*, vol. 37, pp. 171, 2012
- [92] K. Takahiro, S. Ouchi and A. Minoh, "Computational design of solenoid geometry for homogeneous on-axis field", *Jpn. J. Appl. Phys.*, vol. 12, pp. 1572, 1973
- [93] G. Sinha, R. Sundararaman and G. Singh, "Design concepts of optimized MRI magnet", *Magnetics, IEEE Transactions on*, vol. 44, no. 10, pp. 2351, 2008

List of Publications

This thesis gave rise to the following related publications:

1. **Nilangshu K. Das**, T. Jayakumar and Baldev Raj "Noniterative digital AC bridge", *IEEE Trans. Instrum. Meas.*, vol. 59, no. 11, pp. 3058 -3060, 2010
2. **Nilangshu K. Das**, Sounak Dey, Sarbajit Pal and P. Barat, "Innovative Instrumentation to Measure Magnetic Susceptibility", *IEEE Trans. Magnetics.*, vol. 49, no. 9, pp. 4965-4969, 2013
3. **Nilangshu K. Das**, P. Barat, Sounak Dey, and T. Jayakumar, "Design of miniature coil to generate uniform magnetic field" , *Progress In Electromagnetic Research M*, vol. 34, pp. 99, 2014
4. **Nilangshu K. Das**, P. Barat and T. Jayakumar, "Coupled dynamics of N-body dipoles in a double well potential", *J. Coupled Syst. Multiscale Dyn.*, vol. 2, pp. 74, 2014
5. **Nilangshu K. Das**, P. Barat, Sounak Dey and T. Jayakumar, "Frequency-adapted crossover from para-to-dia magnetization in an Ising-like dipole-dipole model, *ScienceJet*, vol. 4: 83, 2015